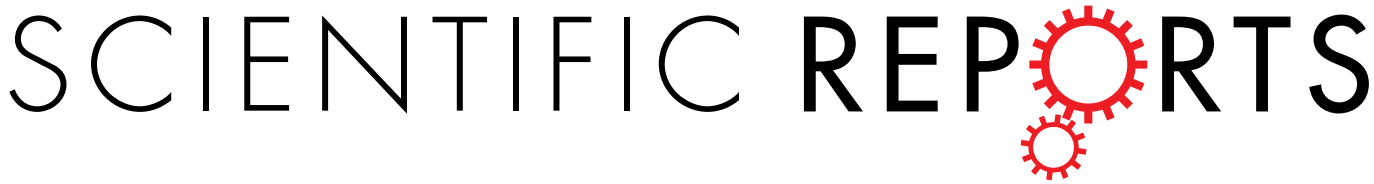

OPEN

Magmatic record of India-Asia collision

Di-Cheng Zhu[1], Qing Wang[1], Zhi-Dan Zhao[1], Sun-Lin Chung[2,3], Peter A. Cawood[4,5], Yaoling Niu[1,6], Sheng-Ao Liu[1], Fu-Yuan Wu[7] & Xuan-Xue Mo[1]

Received: 21 November 2014
Accepted: 24 August 2015
Published: 23 September 2015

New geochronological and geochemical data on magmatic activity from the India-Asia collision zone enables recognition of a distinct magmatic flare-up event that we ascribe to slab breakoff. This tie-point in the collisional record can be used to back-date to the time of initial impingement of the Indian continent with the Asian margin. Continental arc magmatism in southern Tibet during 80–40 Ma migrated from south to north and then back to south with significant mantle input at 70–43 Ma. A pronounced flare up in magmatic intensity (including ignimbrite and mafic rock) at ca. 52–51 Ma corresponds to a sudden decrease in the India-Asia convergence rate. Geological and geochemical data are consistent with mantle input controlled by slab rollback from ca. 70 Ma and slab breakoff at ca. 53 Ma. We propose that the slowdown of the Indian plate at ca. 51 Ma is largely the consequence of slab breakoff of the subducting Neo-Tethyan oceanic lithosphere, rather than the onset of the India-Asia collision as traditionally interpreted, implying that the initial India-Asia collision commenced earlier, likely at ca. 55 Ma.

Continental collision is a dramatic expression of the dynamic nature of the Earth and has long-term impacts on atmosphere and ocean circulation patterns, and on the development and stability of the continental lithosphere. One of the most prominent collisions today is the ongoing interaction between the Indian and Asian continents. However, the timing of the initial India-Asia collision remains uncertain with suggestions ranging from 70 to 34 Ma[1–9]. This uncertainty reflects in part the differing approaches used to define collision.

Continental collision is the natural consequence of plate tectonics involving oceans opening and closing and is driven by a variety of forces most notably the descent of oceanic lithosphere at subduction zones (i.e. slab pull)[10,11]. Such understanding, together with the primary mechanisms of magma generation (i.e., adding fluids, increasing temperature, and decreasing pressure), allows us to place constraints on the relationship between collisional processes and magmatic responses (Fig. 1).

(1) Initial collision, takes place at the initial contact of crust between two continents (Fig. 1a). At this stage, oceanic lithosphere continues to subduct and dehydrates (releasing fluids), resulting in the generation of normal continental arc magmatism dominated by andesitic rocks as seen in the Andes. **(2) Ongoing collision**, involves the thin passive continental lithosphere being dragged by the subducting oceanic lithosphere (slab pull) (Fig. 1b). Minor syn-collisional magmatism during this stage is mostly peraluminous and derived from a metapelite-dominated source within the middle-upper crust due to reduced dehydration of the subducting oceanic lithosphere (releasing fluids), convective heat from small-scale mantle flow[12], and shear heating[13]. **(3) Tectonic transition**, occurs due to the buoyancy of the lower plate continental lithosphere counteracts the effects of slab-pull of the oceanic lithosphere resulting

[1]State Key Laboratory of Geological Processes and Mineral Resources, and School of Earth Science and Resources, China University of Geosciences, Beijing 100083, China. [2]Institute of Earth Sciences, Academia Sinica, Taipei 11529, Taiwan. [3]Department of Geosciences, National Taiwan University, Taipei 10617, Taiwan. [4]Department of Earth Sciences, University of St Andrews, North Street, St Andrews KY16 9AL, UK. [5]Centre for Exploration Targeting, School of Earth and Environment, University of Western Australia, 35 Stirling Hwy., Crawley WA, 6009, Australia. [6]Department of Earth Sciences, Durham University, Durham DH1 3LE, UK. [7]Institute of Geology and Geophysics, Chinese Academy of Sciences, Beijing 100029, China. Correspondence and requests for materials should be addressed to D.-C.Z. (email: dchengzhu@163.com)

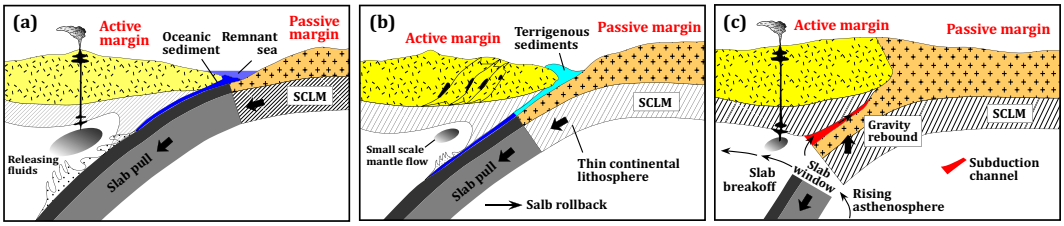

Collisional process:	Initial collision	Ongoing collision	Tectonic tranisition
Magmatic Response:	Normal arc-type magmatism dominated by andesitic rocks	No or only minor peraluminous silicic magmatism with a metapelite-dominated crustal source	a. Intense magmatic activity with compositional diversity, b. Mafic magmatism showing within-plate basalt geochemistry, c. Bimodal magmatism, and d. A2-type felsic magmatism
Primary mechanism of magma generation:	Adding fluids through the dehydration of the subducting oceanic lithosphere	Shear heating, convective heat from small-scale mantle flow, and adding fluids through reduced dehydration of the subducting oceanic lithosphere	Increasing the temperature of lithosphere and decreasing the pressure of asthenosphere
Geodynamic Consequence:	The attached continental plate is thin with less resistance to subduct and may not slow down significantly due to the existence of the slab pull force		The velocity of the attached plate will decrease significantly due to the loss of the slab pull force

Figure 1. Schematic sequence of the relationship between collisional processes and magmatic responses in collision zones. This figure is generated by Di-Cheng Zhu, using Adobe Illustrator CS4 created by the Adobe Illustrator Team under an open license.

in their separation (slab breakoff[14]) (Fig. 1c). After slab breakoff, the collision zone transitions into an intracontinental setting. Slab breakoff will open a slab window and consequently trigger partial melting of differing magma source regions (by increasing the temperature of lithosphere and decreasing the pressure of asthenosphere), producing intense magmatism with compositional diversity (defined here as post-collisional magmatism) (including basaltic magmatism showing within-plate basalt geochemistry, bimodal magmatism, and anorogenic felsic magmatism, etc.)[15,16]. From initial to ongoing collision, the surface plate may not slow down significantly as the attached continental lithosphere is thin with less resistance to subduct due to the descent of the dense oceanic lithosphere (slab pull), whereas after slab breakoff during the tectonic transition the velocity of the surface plate is expected to decrease significantly due to the loss of the slab pull force that is the main driving force of plate motion[10,11].

The evolving magmatic record from ongoing subduction to collision, slab breakoff, and further continental lithospheric interaction provides a framework to evaluate continent-continent collision. This is because slab breakoff will postdate the initial continent-continent collision by several to ten million years, depending on convergence velocity, subducting slab dip[8], and shape of the colliding margins. Thus, defining the timing of slab breakoff, which can be identified on the integration of geological, geochemical, geochronological, and geophysical methods[15–20], provides an important time-stamp on the sequence of collision-related events.

The Gangdese arc in southern Tibet (Fig. 2a), which records the subduction of the Neo-Tethyan oceanic lithosphere and subsequent India-Asia collision[21], allows a direct test of our petrological approach to resolving the timing of India-Asia collision. This is because the voluminous Linzizong volcanic rocks (Fig. 2b,c) and coeval intrusive rocks of the Gangdese arc (Fig. 2d) range in age from 70 to 40 Ma[22], straddling the interpreted timing of collision[1–9]. We provide the first comprehensive dataset on the age and geochemistry of these rocks enabling us to tightly constrain the progressive history of convergence and collision, including redefining the timing of the latter.

Spatial, temporal and compositional changes of the Gangdese arc

The Linzizong volcanic rocks (Fig. 2b) extend for more than 1000 km along the southern Lhasa Terrane and are well exposed in Linzhou Basin (Fig. S1). In this basin, the lower unit of the Linzizong volcanic rocks (Dianzhong Formation) is dominated by thick andesitic rocks (Fig. 2c), which unconformably overlie strongly folded Upper Cretaceous siltstone and mudstone (Fig. S1). The middle unit (Nianbo Formation) is characterized by siltstone, marl, and limestone interbedded with andesitic rocks (Fig. 2c). The upper unit (Pa'na Formation) is characterized by the presence of thick rhyolite and rhyolitic ignimbrite (Fig. 2c) with columnar jointing (Fig. S1). We undertook SIMS (secondary ion mass spectrometry) U-Pb zircon dating[23] of magmatic rocks from the stratigraphic boundaries of each formation (Fig. S1). Sample details, zircon U-Pb age data, and geochemical data are provided in Tables S1 and S2 in the supplementary material. Our new age data are shown in red ovals with numerals in Fig. 2c and S1 and are summarized in Table 1. The SIMS U-Pb zircon age data of two samples (13LZ01-1 and 13LZ17-1) from the lowermost Dianzhong Formation (60.2 ± 0.6 and 60.2 ± 0.8 Ma, respectively) and of one sample (13LZ08-1) from the uppermost Dianzhong Formation (58.3 ± 1.3 Ma) indicate that the Dianzhong andesitic volcanism was most likely active during 60.2–58.3 Ma. One sample (12LZ29-1) from the lowermost Nianbo Formation (55.4 ± 0.5 Ma) and two samples (12LZ27-1 and 13LZ16-1) from the Upper Nianbo Formation (52.6 ± 0.4 and 52.7 ± 1.9 Ma, respectively) provide age constraint on the

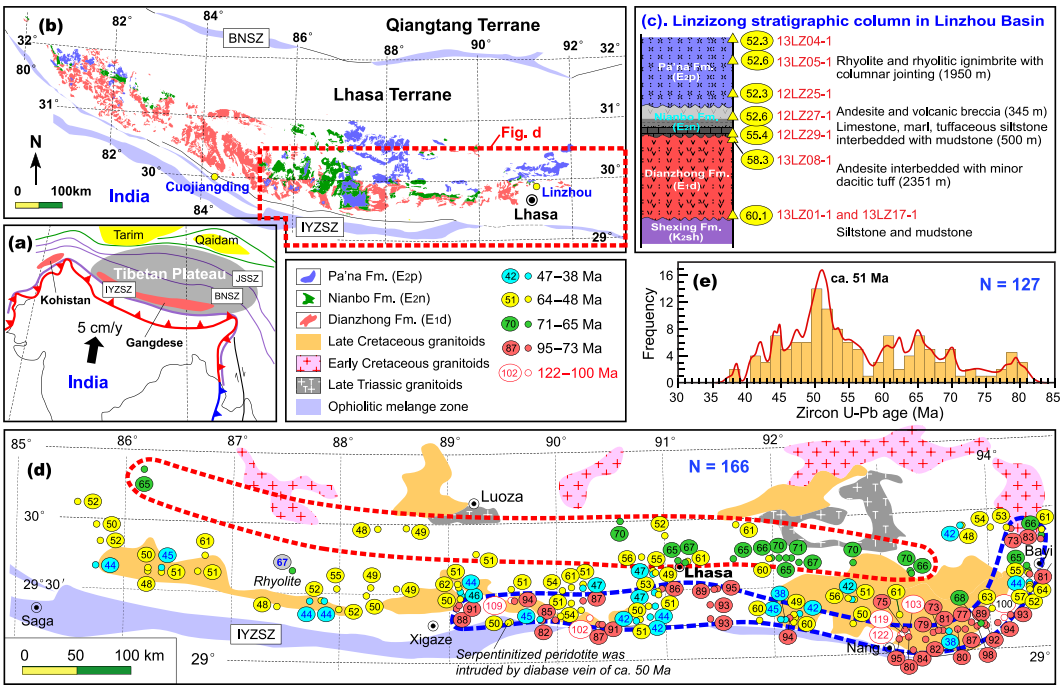

Figure 2. Tectonic framework of the Tibetan Plateau and the Lhasa Terrane. (**a**) Showing the Gangdese arc in the context of the Tibetan Plateau. IYZSZ = Indus-Yarlung Zangbo suture zone, BNSZ = Bangong-Nujiang suture zone, JSSZ = Jinsha suture zone. (**b**) The distribution of the Linzizong volcanic rocks. (**c**) The stratigraphic column of the Linzizong volcanic rocks in Linzhou Basin[4]. The filled ovals with numerals are host-rock crystallization ages in Ma using *in situ* zircon secondary ion mass spectrometry (SIMS) U-Pb dating method (see supplementary Table S1 for sample details). (**d**) The distribution of intrusive rocks in the Gangdese arc. The filled circles indicate sample locations, numerals within ovals are host-rock crystallization ages in Ma using *in situ* zircon LA-ICPMS U-Pb dating method (see supplementary Table S2 for sample details). Five groups of zircon ages are recognized on the basis of spatial variation of magmatism and different magmatic origin[22]. This figure is generated by Di-Cheng Zhu, using Adobe Illustrator CS4 created by the Adobe Illustrator Team under an open license. (**e**) Histogram of crystallization ages (Ma) of the intrusive rocks (85–94°E) from the Gangdese Batholith. The red line represents frequency curve. Age data used in this histogram are the crystallization ages defined by the youngest group of zircon analyses of each sample. The bin width was set at 1.5 Ma to accommodate average age uncertainties of 1.1 Ma (2σ; Table S3). Only one age datum is selected for each pluton if between-sample age difference is lower than 3 Myrs. If this difference is more than 3 Myrs, this pluton is considered to emplace at different pulses and thus the different emplacement ages are used to construct the histogram.

Nianbo Formation of 55.4–52.6 Ma. This is very compatible with the age data obtained from two marl samples (13LZ13-1 and 13LZ14-1) from the lower Nianbo Formation (54.4 ± 0.5 and 54.5 ± 0.7 Ma). Three samples from the Lower (12LZ25-1), Middle (13LZ05-1), and Uppermost (13LZ04-1) Pa'na Formation give SIMS U-Pb zircon ages of 52.3 ± 0.5, 52.6 ± 0.4, and 52.3 ± 0.6 Ma, indistinguishable within analytical errors. These data precisely bracket the duration of each formation of the Linzizong volcanic rocks from the Linzhou Basin: 60.2–58.3 Ma for the Dianzhong Formation, 55.4–52.6 Ma for the Nianbo Formation, and 52.6–52.3 Ma for the Pa'na Formation. Thus the duration of magmatic activity is some 8 m.y. defined by SIMS zircon U-Pb dating and differs significantly from previous estimates of up to 25 m.y. based on laser ablation inductively coupled plasma mass spectrometry (LA-ICPMS) zircon U-Pb and Ar-Ar dating for the Dianzhong (69–61 Ma), Nianbo (61–54 Ma), and Pa'na (54–44 Ma) formations (see ref. 24 for age summary).

The Gangdese Batholith extends over 1500 km along the southern Lhasa Terrane (Fig. 2a). It is composed mainly of diorite and granodiorite, together with abundant mafic enclaves and dykes (Fig. S1). To obtain a comprehensive dataset with adequate spatial coverage, we collected a total of 127 samples with LA-ICPMS U-Pb zircon age data and 213 samples with whole-rock geochemical data on the 80–40 Ma intrusive rocks extending from longitude E85° to E95° along the strike of the batholith (Fig. 2d). Sample details, zircon U-Pb age data, and SiO_2 contents are provided in Tables S3 and S4 in the supplementary material. These age data reveal that the >72 Ma magmatism was confined to a narrow belt in the south (blue dashed line, Fig. 2d), shifting northward at 71–65 Ma (red dashed line), then south at 64–48 Ma, which spread over a relatively broader area than the earlier activity, and is finally (47–38 Ma) largely

Formation	Sample	Rock Type	GPS position	Strata position	Dating method	Analyses	Age (Ma)	MSWD
Pa'na Formation	13LZ04-1	Rhyolitic breccia	N30°00.643′, E91°08.810′	Uppermost Pa'na	SIMS 1280	19	52.29 ± 0.61	2.5
	13LZ05-1[a]	Rhyolitic ignimbrite	N30°00.137′, E91°08.882′	Middle Pa'na	SIMS 1280	16	52.58 ± 0.40	1.3
	13LZ06-1	Rhyolite	N29°59.964′, E91°08.700′	Middle Pa'na	LA-ICPMS	16	50.5 ± 0.4	0.1
	12LZ23-1	Rhyolitic ignimbrite	N29°59.622′, E91°08.415′	Middle Pa'na	LA-ICPMS	16	49.7 ± 0.4	0.2
	12LZ25-1	Rhyolite	N29°59.313′, E91°08.474′	Lower Pa'na	SIMS 1280	13	52.27 ± 0.45	0.8
Nianbo Formation	13LZ16-1	Andesite	N29°59.078′, E91°11.209′	Upper Nianbo	SIMS 1280	4	52.7 ± 1.9	2.0
	12LZ27-1	Rhyolitic tuff	N29°58.557′, E91°08.736′	Upper Nianbo	SIMS 1280	15	52.64 ± 0.42	0.5
	13LZ13-1	Marl	N29°58.812′, E91°11.159′	Lower Nianbo	SIMS 1280	14	54.35 ± 0.47	1.1
	13LZ14-1	Marl	N29°58.815′, E91°11.158′	Lower Nianbo	SIMS 1280	10	54.45 ± 0.68	1.3
	12LZ29-1	Rhyolite	N29°58.231′, E91°08.955′	Lowermost Nianbo	SIMS 1280	14	55.37 ± 0.45	0.4
Dianzhong Formation	13LZ08-1	Andesite	N29°58.708′, E91°11.195′	Uppermost Dianzhong	SIMS 1280	2	58.3 ± 1.3	0.01
	12LZ06-1	Dacite	N29°57.273′, E91°12.107′	Lower Dianzhong	LA-ICPMS	17	58.5 ± 0.5	0.4
	13LZ17-1[b]	Volcanic breccia	N29°57.292′, E91°13.048′	Lowermost Dianzhong	SIMS 1280	13	60.23 ± 0.78	1.8
	13LZ01-1[c]	Andesite	N29°57.117′, E91°11.855′	Lowermost Dianzhong	SIMS 1280	21	60.22 ± 0.61	2.0

Table 1. Summary of new zircon U-Pb age data reported in this study for the Linzizong volcanic rocks in Linzhou Basin, southern Tibet. [a]Rhyolitic ignimbrite with well-developed columnar jointing. [b]ca. 50 cm above the angular unconformity between the Dianzhong and Shexing formations located ca. 78 m east of sample SH530022 that was dated by LA ICP-MS method at 68.7 ± 2.4 Ma (MSWD = 3.6)[25]. [c]ca. 20 cm above the angular unconformity between the Dianzhong and Shexing formations.

restricted to its southern edge. These age data define a pulse of magmatic flare-up event at ca. 51 Ma along the entire length of the arc (Fig. 2e).

Changes in the chemical composition of the Linzizong volcanic rocks available from the Linzhou Basin and the Gangdese Batholith with time are illustrated by SiO_2 variation and zircon saturation temperature[26] against age (Fig. 3). Figure 3a shows that an andesite-dacite association in the Dianzhong Formation was followed by bimodal volcanic suites in both the Nianbo and Pa'na formations. Figure 3b reveals an increase in zircon saturation temperature at ca. 52 Ma documented by the rhyolitic rocks in the Pa'na Formation. Figure 3c illustrates felsic-dominated magmatism in the Gangdese Batholith during 80–73 Ma, followed by significant mafic magmatic activity at 70–43 Ma. It is important to note that bimodal magmatism coeval with or slightly younger than the Nianbo and Pa'na bimodal volcanism is most likely developed within the Gangdese Batholith as indicated by the presence of ca. 52–47 Ma gabbroic dykes that intruded into the coeval granitoid (Fig. S1g). The absence of compositional gap in the whole Gangdese Batholith (Fig. 3c) is probably the consequences of magma mixing between felsic and basaltic melts[27] as indicated by the well-developed coeval mafic enclaves (Figs S1h, S1i, and S1j).

Discussion

Temporal trends for enhanced mafic magmatism and increased zircon saturation temperature within the Linzizong volcanic rocks and Gangdese Batholith indicate an increased mantle heat input. It is emphasized that increased mantle input and coeval magmatic flare-up are difficult to attribute to a large scale change in the stress state of the lithosphere. This is because such change is a shallow response to deep mantle dynamics and is not an effective mechanism that will produce extensive magmatic activity. One possible explanation for higher mantle heat input at 70–43 Ma was the removal of the Asian lithosphere following tectonic shortening between 90 and 69 Ma[28]. However, to account for the southward migration of the magmatism from 72–65 Ma to 64–48 Ma (Fig. 2d), and significantly increased zircon saturation temperature at ca. 52 Ma and peak activity at ca. 51 Ma (Fig. 2e), we argue for slab steepening (Fig. 4a,b) and rollback (Fig. 4c) followed by slab breakoff (Fig. 4d).

We infer that the breakoff of the Neo-Tethyan lithosphere occurred slightly earlier (e.g., ca. 53 Ma; Fig. 4d) than the rapid eruption of ca. 2 km thick rhyolite and rhyolitic ignimbrite (52.5–52.3 Ma) (Fig. 2c) documented by the Linzizong volcanic rocks (Pa'na Formation) and the magmatic flare-up event of ca. 51 Ma shown by the age relationships within the Gangdese Batholith (Fig. 2e). This inference is consistent with numerical modeling that indicates a short duration of slab breakoff (<2 Ma[29]) followed by intense magmatism as a result of the enhanced heat input from rising asthenosphere[30]. Other robust lines of evidence supporting our model of slab breakoff by this time include: (1) the occurrence of abundant 52–47 Ma mafic enclaves and dykes (Fig. S1) that suggest significantly increased contributions from the mantle; (2) the presence of ca. 52.5 Ma bimodal volcanic rocks (Fig. 3a) that points to partial melting of enriched metasomatic layers within lithospheric mantle and to crustal melting caused by thermotectonic effects as a result of slab breakoff[15]; (3) high Zr/Y ratios

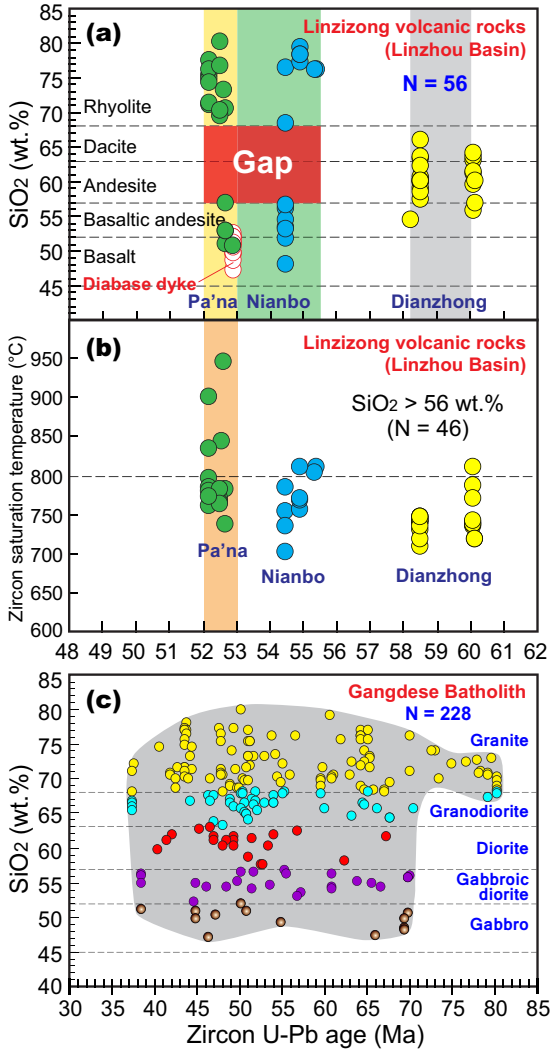

Figure 3. Changes in magmatic compositions with time in the Gangdese arc. (**a**,**b**) Plots of SiO_2 content versus age (Ma) and of zircon saturation temperature (°C) versus age (Ma) for the Linzizong volcanic rocks (see supplementary Table S4 for geochemical data). Zircon saturation temperatures were calculated from whole-rock compositions with SiO_2 >56 wt.% following the method of Watson and Harrison (1983)[26]. (**c**) Plot of SiO_2 content versus age (Ma) for the Gangdese Batholith (E85°–E95°) (see Table S5 for geochemical data). Note that this plot did not show a clear increase of mafic magmatism at ca. 51 Ma as indicated by the presence of well-developed mafic enclaves and dykes (Fig. S1); this inconsistency reflects sampling bias with mafic material underrepresented.

(3.7–6.8) of the basaltic lavas and dykes (ca. 52.9 Ma) in the Linzizong volcanic rocks (Table S2) that suggest input of subslab asthenospheric mantle[16]; and (4) dramatically increased zircon saturation temperature at ca. 52.5 Ma recovered by the rhyolitic rocks of the Pa'na Formation (Fig. 3b) that indicates the anomalously high heat input from the mantle.

The development of magmatic activity at 51–43 Ma in the Gangdese arc (Fig. 3b), as well as ca. 50 Ma diabase dykes that intrude serpentinitized peridotite within the Yarlung-Zangbo suture zone (Fig. 2d), is most likely the consequences of partial melting of differing magma source regions through increasing temperature of lithosphere and decreasing pressure of asthenosphere after slab breakoff. This interpretation is consistent with numerical modeling which indicates that hot asthenosphere continues to ascend and generates melt for several million years after slab breakoff (Fig. 4e)[30]. The shift in the whole-rock Nd and zircon Hf isotopic compositions towards negative values at ca. 50 Ma[6,31,32] most likely reflects a profound change of the source regions associated with the involvement of slab edge materials of the Indian continent that had already been subducted to depths[19,32] (Fig. 4e), rather than indicative of the initial India-Asia collision[6].

The timing of rapid eruption of thick rhyolitic ignimbrite (ca. 52.5 Ma) in the Linzizong volcanic rocks and intense magmatism (ca. 51 Ma) in the Gangdese Batholith matches the sudden drop of the convergence rate of the Indian plate at ca. 51 Ma[33–35]. This synchronicity of events suggests that the slowdown

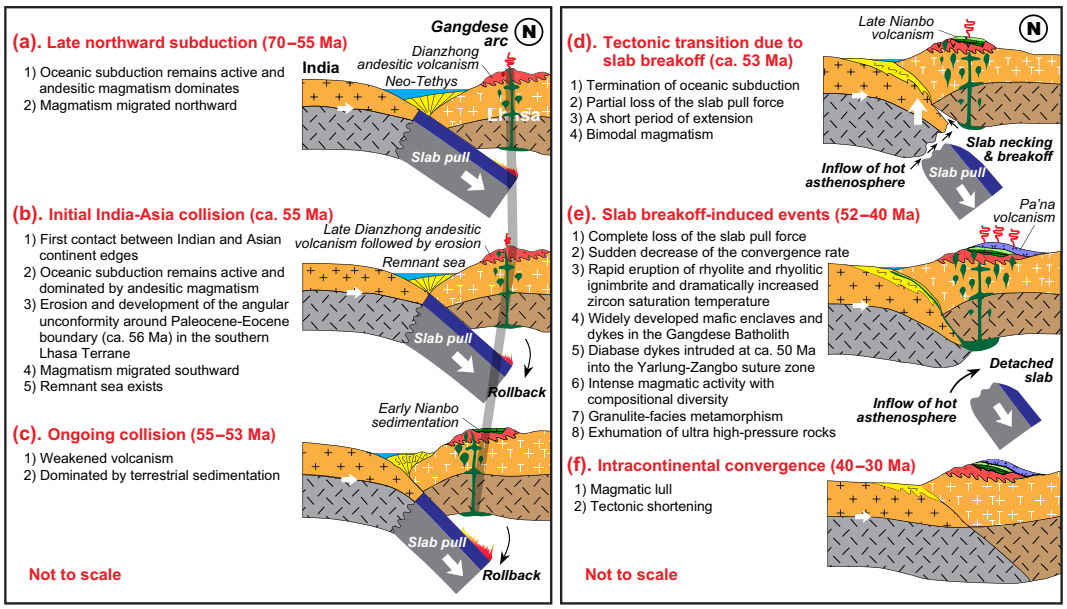

Figure 4. Schematic illustrations showing the India-Asia collisional processes and resultant tectonomagmatic activity over the past 70–40 m.y. (not to scale). This figure is generated by Di-Cheng Zhu, using Adobe Illustrator CS4 created by the Adobe Illustrator Team under an open license.

of the Indian plate is largely the consequence of slab breakoff (Fig. 4e). This is because slab breakoff will result in the loss of the slab pull force[14,29], which exerts a dominant influence on the velocity of the surface plate and cause a drastic change in plate motion[10,11,36,37]. Subsequent intracontinental convergence (Fig. 4f) of the Indian continental lithosphere beneath the Asian lithosphere after slab breakoff is likely driven by the subduction of dense Indian continental lithosphere[38] and slab-pull of oceanic lithosphere on the Indo-Australian plate along the Indonesian segment of the plate margin[39]. Traditionally, the slow-down of the Indian plate at ca. 51 Ma is attributed to the increased resistance to subduction interpreted as a result of the initial India-Asia collision[33,34]. However, we consider this interpretation questionable because (1) under such a collisional regime, no appropriate mechanisms (see Fig. 1b) are available for producing extensive magmatism in southern Tibet as presented in this study (Fig. 2c and S1) and (2) the surface motion of the plate is closely related to or substantially driven by mantle dynamics (i.e., slab pull[10,11,36,37]) and thus if such a driving force disappears, significant slow down would occur.

It is beyond the scope of this article to discuss in detail the problems of each interpreted age (70–34 Ma) proposed for the initiation of the India-Asia collision (see ref. 9, for review). We emphasize that any estimates on the collisional timing must effectively explain all the first-order observations of the spatial, temporal (Fig. 2d), and compositional changes (Fig. 3) of magmatic activities summarized in this study. In particular, we must explain the specific geodynamical processes responsible for the southward migration of magmatism from 72–65 Ma to 64–48 Ma followed by the generation of dramatically enhanced magmatism precisely constrained at ca. 52 Ma in the Gangdese arc, including volumetrically significant ignimbrite in the Linzizong volcanic rocks (Fig. 2c) and widely developed mafic enclaves and dykes (Fig. S1) in the Gangdese Batholith. Such enhanced magmatism requires anomalously high-temperature material and heat supply from the mantle, which are unlikely to be explained by later slab breakoff (at ca. 50–40 Ma[40], 45 Ma[18], 48–44 Ma[41], and 50 Ma[42,43]) that would predate intense magmatism[29,30], or by ca. 50 Ma India-Asia or Tethyan Himalaya-Asia collision[44] that would result in a compression regime without intense magmatism (Fig. 1b).

Eclogite-facies peak metamorphism in the western Himalaya was recently refined at ca. 47–43 Ma and consequently an age of ca. 51–47 Ma was proposed for the initial India-Asia collision[8]. However, this collision age is likely an underestimate because the exhumed ultrahigh-pressure rocks may not represent the materials from the leading edge of subducted Indian continental margin.

Slab breakoff is likely inevitable in all collision zones involving a passive continental margin[14]. It follows that subducted continental crust has reached its maximum depth when slab breakoff occurs. This means that slab breakoff provides a maximal age for continental collision. In the case of the India-Asia collision, if Neo-Tethyan slab breaks off at ca. 53 Ma, the initial India-Asia collision should commence at ca. 55 Ma. This is because the progressively enlarged subducting slab dip revealed by the southward migration of magmatism from 72–65 Ma to 64–48 Ma (Fig. 2d) and high India-Asia convergence velocity[35] point to a time lag of ca. 1–2 Ma (Table S6) between initial collision and slab breakoff.

This timing of the initial India-Asia collision (ca. 55 Ma) obtained from our petrological approach is in good agreement with recent estimates on collision ages from the cessation of Xigaze forearc

sedimentation (ca. 58–54 Ma[45]), the dramatic change of sedimentary environment and the development of an unconformity in the Xigaze forearc basin (>56 Ma[46]), the onset of India-Asia terrestrial faunal exchange (ca. 54 Ma[47]), the reappraisal of existing paleomagnetic data (52.4 ± 4.5 Ma[9]), and the new paleomagnetic data (ca. 54.3 Ma[48]). This collision may account for the angular unconformity between the Dianzhong and Nianbo formations in Linzhou Basin (Fig. 2c) and coeval unconformity found in the Xigaze forearc basin[46] due to the locking of the subduction zone on arrival of the Indian continent at the trench[12]. Therefore, it seems most probable that (1) the Dianzhong andesitic volcanism was generated during the transition from late subduction to initial collision (Fig. 4a,b), (2) the lower Nianbo terrestrial sedimentation represents the ongoing India-Asia collision prior to slab breakoff with a short duration from initial to ongoing collision due to the high India-Asia convergence velocity[35], and (3) the late Nianbo and Pa'na bimodal volcanic rocks (Fig. 3a) are linked to mantle decompression melting and crustal anatexis due to the ascent of hot asthenosphere through slab window after slab breakoff[30] (Fig. 4d,e). Nevertheless, we note that the exact timing of initial impingement of the Indian margin with the subduction zone will depend on the degree of distention of the Asian margin and may vary along the strike of the convergence zone due to irregularities in shape of the margin.

Our work shows that the petrological approach that we employ here can effectively distinguish processes at varying stages of continental collision. This approach may be applied to other continent-continent collision zones also involving a passive continental margin on the down-going plate, such as the Arabia-Eurasia collision zone — where the preserved magmatic record straddles the proposed Arabia-Eurasia collision age[49,50].

References

1. Yin, A. & Harrison, T. M. Geologic evolution of the Himalayan Tibetan Orogen. *Ann. Rev. Earth Planet. Sci.* **28,** 211–280 (2000).
2. Aitchison, J. C., Ali, J. R. & Davis, A. M. When and where did India and Asia collide? *J. Geophys. Res.* **112,** B05423 (2007).
3. Garzanti, E., Baud, A. & Mascle, G. Sedimentary record of the northward flight of India and its collision with Eurasia (Ladakh Himalaya, India). *Geodinamica Acta* **1,** 297–312 (1987).
4. Mo, X. X. *et al.* Mantle contributions to crustal thickening in south Tibet in response to the India–Asia collision. *Lithos* **96,** 225–242 (2007).
5. Najman, Y. *et al.* Timing of India-Asia collision: Geological, biostratigraphic, and palaeomagnetic constraints. *J. Geophys. Res.* **115,** B12416, doi: 10.1029/2010JB007673 (2010).
6. Bouilhol, P., Jagoutz, O., Hanchar, J. M. & Dudas, F. O. Dating the India–Eurasia collision through arc magmatic records. *Earth Planet. Sci. Lett.* **366,** 163–175 (2013).
7. DeCelles, P. G., Kapp, P., Gehrels, G. E. & Ding L. Paleocene-Eocene foreland basin evolution in the Himalaya of southern Tibet and Nepal: Implications for the age of initial India-Asia collision. *Tectonics* **33,** doi: 10.1002/2014TC003522 (2014).
8. Donaldson, D. G. *et al.* Petrochronology of Himalayan ultrahigh-pressure eclogite. *Geology* **41,** 835–838 (2013).
9. Lippert, P. C., van Hinsbergen, D. J. J. & Dupont-Nivet, G. Early Cretaceous to present latitude of the central proto-Tibetan Plateau: A paleomagnetic synthesis with implications for Cenozoic tectonics, paleogeography, and climate of Asia. *Geol. Soc. Am. Spec. Pap.* **507,** 1–21 (2014).
10. Forsyth, D. & Uyeda, S. On the relative importance of the driving forces of plate motions. *Geophys. J. Int.* **43,** 163–200 (1975).
11. Conrad, C. P. & Lithgow-Bertelloni, C. How mantle slabs drive plate tectonics. *Science* **298,** 207–209 (2002).
12. Magni, V. *et al.* Numerical models of slab migration in continental collision zones. *Solid Earth* **3,** 293–306 (2012).
13. Harris, N. B. W., Pearce, J. A. & Tindle, A. G. Geochemical characteristics of collision-zone magmatism. *Geol. Soc. Lond. Spec. Pub.* **19,** 67–81 (1986).
14. Davies, J. H. & von Blanckenburg, F. Slab breakoff: A model of lithosphere detachment and its test in the magmatism and deformation of collisional orogens. *Earth Planet. Sci. Lett.* **129,** 85–102 (1995).
15. von Blanckenburg, F. & Davies, J. H. Slab breakoff: A model for syncollisional magmatism and tectonics in the Alps. *Tectonics* **14,** 120–131 (1995).
16. Ferrari, L. Slab detachment control on mafic volcanic pulse and mantle heterogeneity in central Mexico. *Geology* **32,** 77–80 (2004).
17. van der Voo, R., Spakman, W. & Bijwaard, H. Tethyan subducted slabs under India. *Earth Planet. Sci. Lett.* **171,** 7–20 (1999).
18. Kohn, M. & Parkinson, C. D. Petrologic case for Eocene slab breakoff during the Indo-Asian collision. *Geology* **30,** 591–594 (2002).
19. Leech, M. L., Singh, S., Jain, A. K., Klemperer, S. L. & Manichavasgam, R. M. The onset of India-Asia continental collision: Early, steep subduction required by the timing of UHP metamorphism in the western Himalaya. *Earth Planet. Sci. Lett.* **234,** 83–97 (2005).
20. Lei, J. S. & Zhao, D. P. Teleseismic evidence for a break-off subducting slab under Eastern Turkey. *Earth Planet. Sci. Lett.* **257,** 14–28 (2007).
21. Chung, S. L. *et al.* Tibetan tectonic evolution inferred from spatial and temporal variations in post-collisional magmatism. *Earth-Sci. Rev.* **68,** 173–196 (2005).
22. Zhu, D. C. *et al.* The origin and pre-Cenozoic evolution of the Tibetan Plateau. *Gondwana Res.* **23,** 1429–1454 (2013).
23. Li, X. H. *et al.* Precise determination of Phanerozoic zircon Pb/Pb age by multicollector SIMS without external standardization. *Geochem. Geophys. Geosyst.* **10,** Q04010, doi: 10.1029/2009GC002400 (2009).
24. Huang, W. T. *et al.* Inclination shallowing in Eocene Linzizong sedimentary rocks from Southern Tibet: correction, possible causes and implications for reconstructing the India–Asia collision. *Geophys. J. Int.* **194,** 1390–1411 (2013).
25. He, S. D. *et al.* Cretaceous–Tertiary geology of the Gangdese Arc in the Linzhou area, southern Tibet. *Tectonophysics* **433,** 15–37 (2007).
26. Watson, E. B. & Harrison, T. M. Zircon saturation revisited: temperature and composition effects in a variety of crustal magma types. *Earth Planet. Sci. Lett.* **64,** 295–304 (1983).
27. Mo, X. X. *et al.* Timing of magma mixing in the Gangdise magmatic belt during the India-Asia collision: Zircon SHRIMP U-Pb dating. *Acta Geologica Sinica* **79,** 66–76 (2005).
28. Kapp, P. *et al.* The Gangdese retroarc thrust belt revealed. *GSA Today* **17,** 4–9 (2007).
29. Duretz, T., Schmalholz, S. M. & Gerya, T. V. Dynamics of slab detachment. *Geochem. Geophys. Geosyst.* **13,** Q03020 (2012).
30. van de Zedde, D. M. A. & Wortel, M. J. R. Shallow slab detachment as a transient source of heat at midlithospheric depth. *Tectonics* **20,** 868–882 (2001).

31. Ji, W. Q., Wu, F. Y., Chung, S. L., Li, J. X. & Liu, C. Z. Zircon U-Pb chronology and Hf isotopic constraints on the petrogenesis of Gangdese batholiths, southern Tibet. *Chem. Geol.* **262,** 229–245 (2009).
32. Chu, M. F. *et al.* India's hidden inputs to Tibetan orogeny revealed by Hf isotopes of Transhimalayan zircons and host rocks. *Earth Planet. Sci. Lett.* **307,** 479–486 (2011).
33. Patriat, P. & Achache, J. Indian-Eurasia collision chronology has implications for crustal shortening and driving mechanism of plates. *Nature* **311,** 615–621 (1984).
34. Besse, J. *et al.* Palaeomagnetic estimates of crustal shortening in the Himalayan thrust and Zangbo suture. *Nature* **311,** 621–626 (1984).
35. van Hinsbergen, D. J. J., Steinberger, B., Doubrovine, P. & Gassmöller, R. Acceleration-deceleration cycles of India-Asia convergence: Roles of mantle plumes and continental collision. *J. Geophys. Res.* **116,** B06101 (2011).
36. Niu, Y. L., O'Hara, M. J., Pearce, J. A. Initiation of subduction zones as a consequence of lateral compositional buoyancy contrast within the lithosphere: a petrologic perspective. *J. Petrology* **44,** 851–866 (2003).
37. Austermann, J. *et al.* Quantifying the forces needed for the rapid change of Pacific plate motion at 6 Ma. *Earth Planet. Sci. Lett.* **307,** 289–297 (2011).
38. Capitanio, F. A., Morra, G., Goes, S., Weinberg, R. F., Moresi, L. India-Asia convergence driven by the subduction of the Greater Indian continent. *Nature Geosci*. **3,** 136–139 (2010).
39. Li, C., van der Hilst, R. D., Meltzer, A. S. & Engdahl, E. R. Subduction of the Indian lithosphere beneath the Tibetan Plateau and Burma. *Earth Planet. Sci. Lett.* **274,** 157–168 (2008).
40. Davies, J. H. & von Blanckenburg, F. Thermal controls on slab breakoff and the rise of high-pressure rocks during continental collisions. in When continents collide: Geodynamics and geochemistry of ultrahigh-pressure rocks. (eds Hacker, B. R. & Liou, J. G.) Ch. 4, 97–115 (The Netherlands, 1998).
41. Negredo, A. M., Replumaz, A., Villaseñor, A. & Guillot, S. Modeling the evolution of continental subduction processes in the Pamir-Hindu Kush region. *Earth Planet. Sci. Lett.* **259,** 212–225 (2007).
42. Lee, H. Y., Chung, S. L., Lo, C. H., Ji, J., Lee, T. Y., Qian, Q. & Zhang, Q. Eocene Neotethyan slab breakoff in southern Tibet inferred from the Linzizong volcanic record. *Tectonophysics* **477,** 20–35 (2009).
43. Lee, H. Y. *et al.* Geochemical and Sr-Nd isotopic constraints on the genesis of the Cenozoic Linzizong volcanic successions, southern Tibet. *J. Asian Earth Sci.* **53,** 96–114 (2012).
44. van Hinsbergen, D. J. J. *et al.* Greater India Basin hypothesis and a two-stage Cenozoic collision between India and Asia. *Proc. Natl Acad. Sci. USA* **109,** 7659–7664 (2012).
45. Orme, D. A., Carrapa B. & Kapp, P. Sedimentology, provenance and geochronology of the Upper Cretaceous-Lower Eocene western Xigaze forearc, southern Tibet. *Basin Res.* doi: 10.1111/bre.12080 (2014).
46. Hu, X. M. *et al.* New insights into the timing of the India–Asia collision from the Paleogene Quxia and Jialazi formations of the Xigaze forearc basin, South Tibet. *Gondwana Res.* doi: 10.1016/j.gr.2015.02.007 (2015).
47. Clementz, M. S. *et al.* Early Eocene warming events and the timing of terrestrial faunal exchange between India and Asia. *Geology* **39,** 15–18 (2011).
48. Ma, Y. M. *et al.* Paleomagnetism and U-Pb zircon geochronology of Lower Cretaceous lava flows from the western Lhasa terrane: New constraints on the India-Asia collision process and intracontinental deformation within Asia. *J. of Geophys. Res.: Solid Earth*. doi: 10.1002/2014JB011362 (2014).
49. Keskin, M. Magma generation by slab steepening and breakoff beneath a subduction-accretion complex: An alternative model for collision-related volcanism in Eastern Anatolia, Turkey. *Geophys. Res. Lett.* **30,** 7–10 (2003).
50. Chiu, H. Y. *et al.* Zircon U-Pb age constraints from Iran on the magmatic evolution related to Neotethyan subduction and Zagros orogeny. *Lithos* **162–163,** 70–87 (2013).

Acknowledgements

This work was financially co-supported by Chinese Academy of Sciences (XDB03010301) and other Chinese funding agencies (Project 973: 2011CB403102 and 2015CB452604; NSFC projects: 41225006, 41273044, and 41472061). We thank Xiu-Mian Hu for discussions and comments on the early version of the manuscript. We also thank Xian-Hua Li and Qiu-Li Li, and Zhao-Chu Hu for helping with the SIMS and LA-ICPMS U-Pb zircon dating analyses, respectively.

Author Contributions

D.C.Z., Q.W. and Z.D.Z. were involved in designing the study, collecting and analyzing the data, and writing the manuscript. S.L.C., P.A.C., Y.L.N., S.A.L., F.Y.W. and X.X.M. contributed to discussions, interpretation of results, and manuscript writing and editing. All authors reviewed the manuscript.

Additional Information

Supplementary information accompanies this paper at http://www.nature.com/srep

Competing financial interests: The authors declare no competing financial interests.

How to cite this article: Zhu, D.-C. *et al.* Magmatic record of India-Asia collision. *Sci. Rep.* **5**, 14289; doi: 10.1038/srep14289 (2015).

Online supplementary information

Magmatic record of India-Asia collision

Di-Cheng Zhu*, Qing Wang, Zhi-Dan Zhao, Sun-Lin Chung, Peter A. Cawood, Yaoling Niu, Sheng-Ao Liu, Fu-Yuan Wu, and Xuan-Xue Mo

Corresponding author, Email: dchengzhu@163.com

Includes the following materials:

Magmatic record of India-Asia collision

Di-Cheng Zhu*, Qing Wang, Zhi-Dan Zhao, Sun-Lin Chung, Peter A. Cawood, Yaoling Niu, Sheng-Ao Liu, Fu-Yuan Wu, and Xuan-Xue Mo

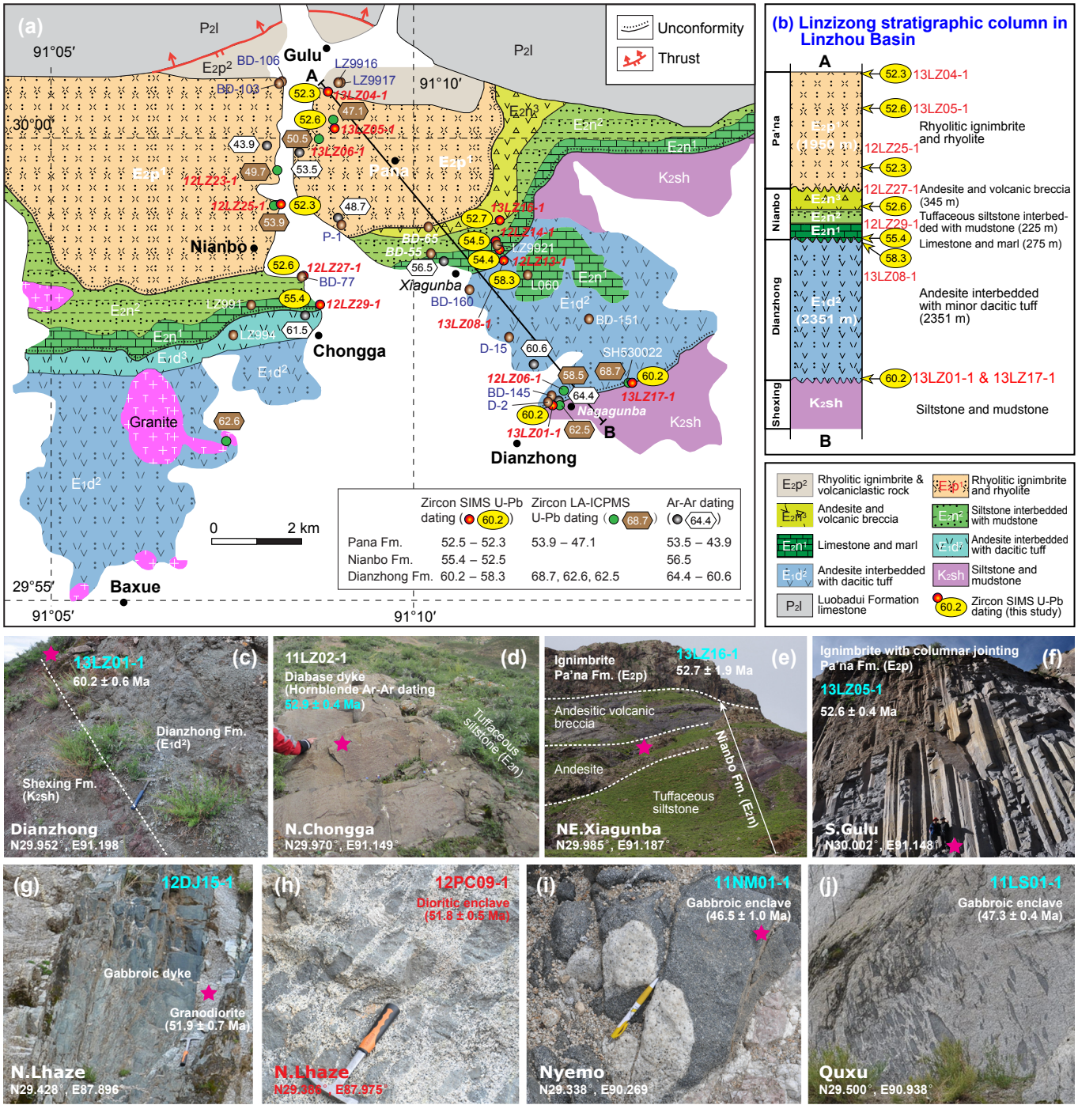

Figure S1 Distributions and field occurrences of the Gangdese arc rocks in southern Tibet

a - Distributions of the Linzizong volcanic rocks in Linzhou Basin (modified from Dong et al., 2005);
b - The stratigraphic column of the Linzizong volcanic rocks in Linzhou Basin (modified from Mo et al., 2007);
c, d, e, and f - Photos of the Linzizong volcanic rocks in Linzhou Basin taken by Di-Cheng Zhu (2011, 2013);
g, h, i, and j - Photos of the granitoids in the Gangdese Batholith taken by Di-Cheng Zhu (2011, 2012). This figure is generated by Di-Cheng Zhu, using Adobe Illustrator CS4 created by the Adobe Illustrator Team under an open license.

References:

Dong, G., Mo, X., Zhao, Z., Wang, L., Zhou, S. A new understanding of the stratigraphic successions of the Linzizong volcanics in the Linzhou Basin, northern Lhasa, Tibet, China. Geol. Bull. China 24, 549–557 (in Chinese with English abstract) (2005).

Mo, X.X. et al. Mantle contributions to crustal thickening in south Tibet in response to the India-Asia collision. Lithos 96, 225–242 (2007).

2. Zircon U-Pb dating methods, data, and Geochemical data

SIMS U-Pb dating:

Samples for U-Pb analysis were processed by conventional magnetic and density techniques to concentrate non-magnetic, heavy fractions. Zircon grains, together with zircon standard 91500 were mounted in epoxy mounts which were then polished to section the crystals in half for analysis. All zircons were documented with transmitted and reflected light micrographs as well as cathodoluminescence (CL) images to reveal their internal structures, and the mount was vacuum-coated with high-purity gold prior to secondary ion mass spectrometry (SIMS) analysis.

Measurements of U, Th and Pb were conducted using the Cameca IMS-1280 SIMS at the Institute of Geology and Geophysics, Chinese Academy of Sciences in Beijing. U-Th-Pb ratios and absolute abundances were determined relative to the standard zircon 91500 (Wiedenbeck et al., 1995), analyses of which were interspersed with those of unknown grains, using operating and data processing procedures similar to those described by Li et al. (2009). A long-term uncertainty of 1.5% (1 RSD) for $^{206}Pb/^{238}U$ measurements of the standard zircons was propagated to the unknowns (Li et al., 2010), despite that the measured $^{206}Pb/^{238}U$ error in a specific session is generally around 1% (1 RSD) or less. Measured isotopic compositions were corrected using the ^{207}Pb-based correction method and were shown as Tera-Wasserburg plots (Li et al., 2010). Uncertainties on individual analyses in data tables are reported at a 1 level; mean ages for pooled U/Pb (and Pb/Pb) analyses are quoted with 95% confidence interval. Data reduction was carried out using the Isoplot/Ex v. 2.49 program (Ludwig, 2001). The lower intercept age in the Tera-Wasserburg plot of the Qinghu standard measured during the sample runs is 160.22 ± 0.86 Ma (46 analyses, 2σ; MSWD = 1.4), identical to the result (159.5 ± 0.7 Ma) reported by Li et al. (2009).

References:

Li, Q.L., Li, X.H., Liu, Y., Tang, G.Q., Yang, J.H., Zhu, W.G., 2010. Precise U-Pb and Pb-Pb dating of Phanerozoic baddeleyite by SIMS with oxygen flooding technique. Journal of Analytical Atomic Spectrometry 25, 1107–1113.

Li, X.H., Liu, Y., Li, Q.L., Guo, C.H., Chamberlain, K.R., 2009. Precise determination of Phanerozoic zircon Pb/Pb ageby multicollector SIMS without external standardization, Geochemistry, Geophysics, Geosystems 10, Q04010, doi: 10.1029/2009GC002400.

Ludwig, K.R., 2001. Users manual for Isoplot/Ex rev. 2.49. Berkeley Geochronology Centre Special Publication. No. 1a, 1–56 pp.

Stacey, J.S., Kramers, J.D., 1975. Approximation of terrestrial lead isotope evolution by a two-stage model. Earth and Planetary Science Letters 26, 207–221.

Wiedenbeck, M., Alle, P., Corfu, F., Griffin, W.L., Meier, M., Oberli, F., Vonquadt, A., Roddick, J.C., Speigel, W., 1995. Three natural zircon standards for U-Th-Pb, Lu-Hf, trace-element and REE analyses. Geostandards Newsletter 19, 1–23.

LA-ICPMS U-Pb dating:

The Zircon U-Pb isotopic analyses were performed using the LA-ICPMS housed at the State Key Laboratory of Geological Processes and Mineral Resources, China University of Geosciences (Wuhan). The detailed operating conditions for the laser ablation system, the ICP-MS instrument, and data reduction followed those described in Liu et al. (2010). ICPMSDataCal (Liu et al., 2010) was used for off-line selection and the integration of background and analyse signals, time-drift correction, U–Pb dating, and quantitative calibration for trace element analyses. The common Pb correction followed the ComPbCorr#3-151 procedure (Andersen, 2002). Age calculations and plotting of concordia diagrams were made using ISOPLOT (ver 3.0) (Ludwig, 2003). Uncertainties of individual analyses are reported as 1σ; mean ages for pooled $^{206}Pb/^{238}U$ results are reported as 2σ.

References:

Andersen, T., 2002. Correction of common lead in U–Pb analyses that do not report ^{204}Pb. Chemical Geology 192, 59–79.

Liu, Y.S., Gao, S., Hu, Z.C., Gao, C.G., Zong, K.Q., Wang, D.B., 2010. Continental and Oceanic Crust Recycling-induced Melt-Peridotite Interactions in the Trans-North China Orogen: U–Pb Dating, Hf Isotopes and Trace Elements in Zircons from Mantle Xenoliths. Journal of Petrology 51, 537–571.

Ludwig, K.R., 2003. Isoplot 3.00: a geochronological toolkit for Microsoft Excel. Berkeley Geochronology Center, Special Publication No. 4, pp. 1–70.

Magmatic record of India-Asia collision

Di-Cheng Zhu*, Qing Wang, Zhi-Dan Zhao, Sun-Lin Chung, Peter A. Cawood, Yaoling Niu, Sheng-Ao Liu, Fu-Yuan Wu, and Xuan-Xue Mo

Concordia plots for single zircon analyzed by SIMS 1280 U–Pb dating

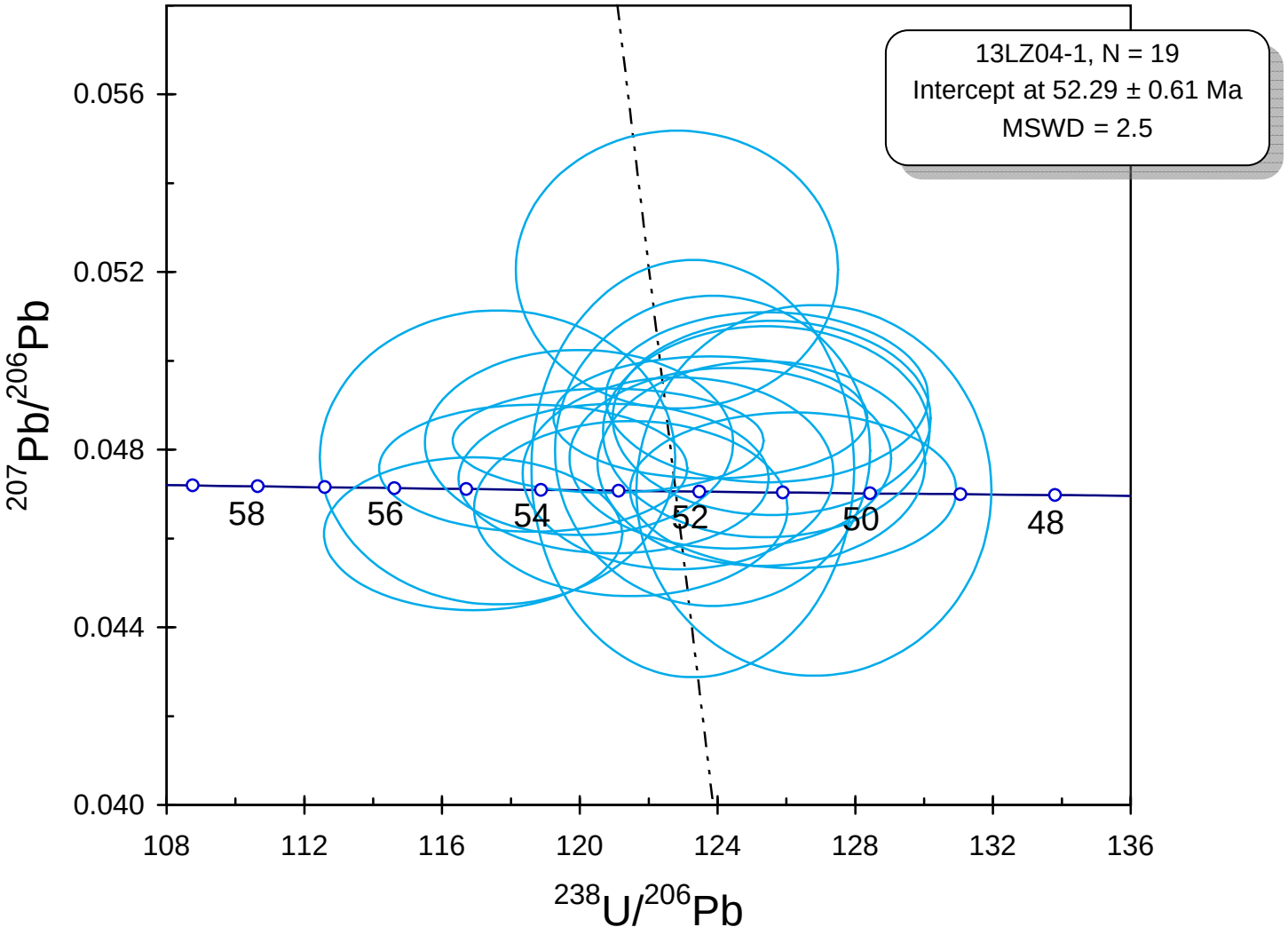

Concordia plots for single zircon analyzed by SIMS 1280 U–Pb dating

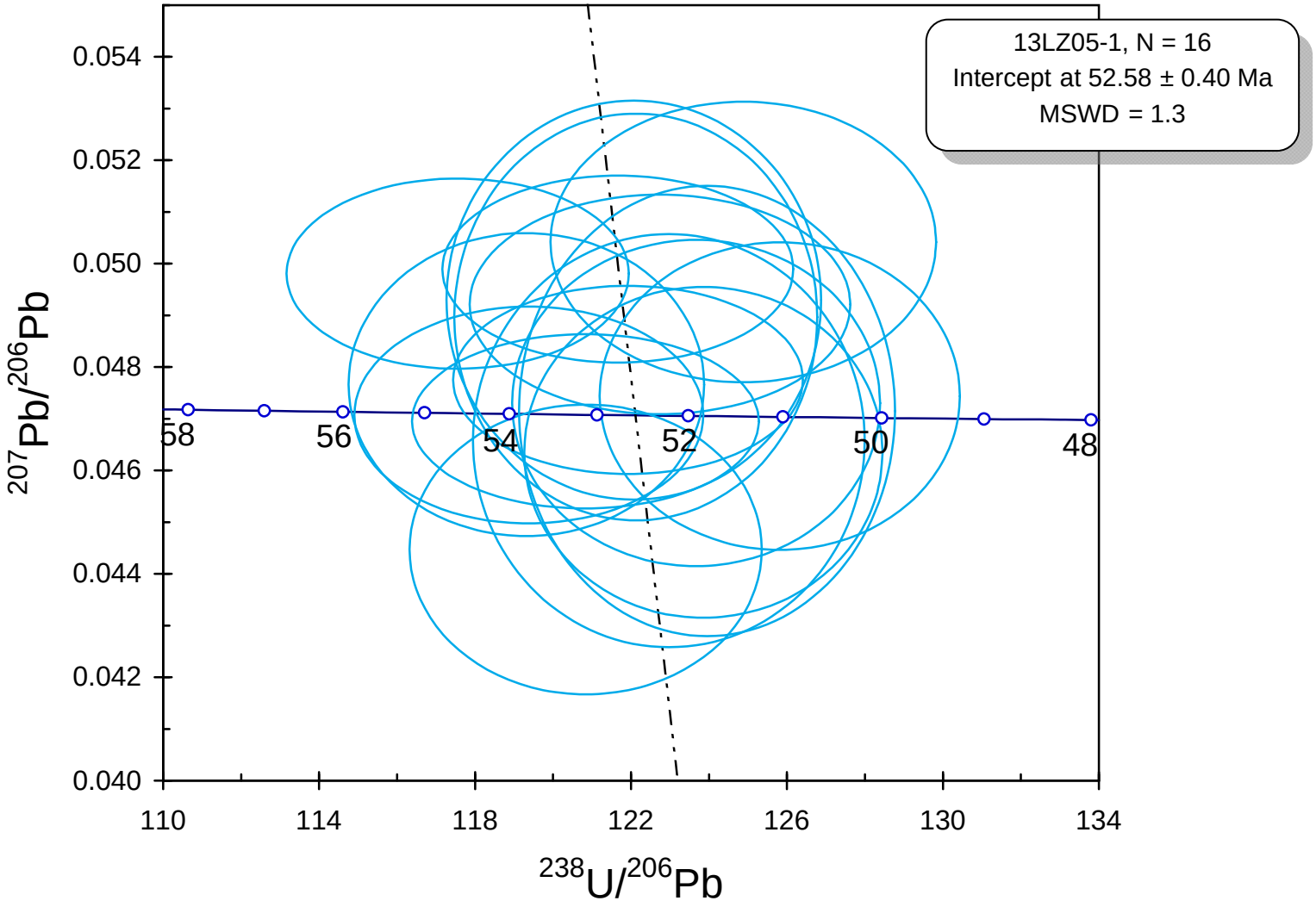

Concordia plots for single zircon analyzed by LA-ICPMS U–Pb dating

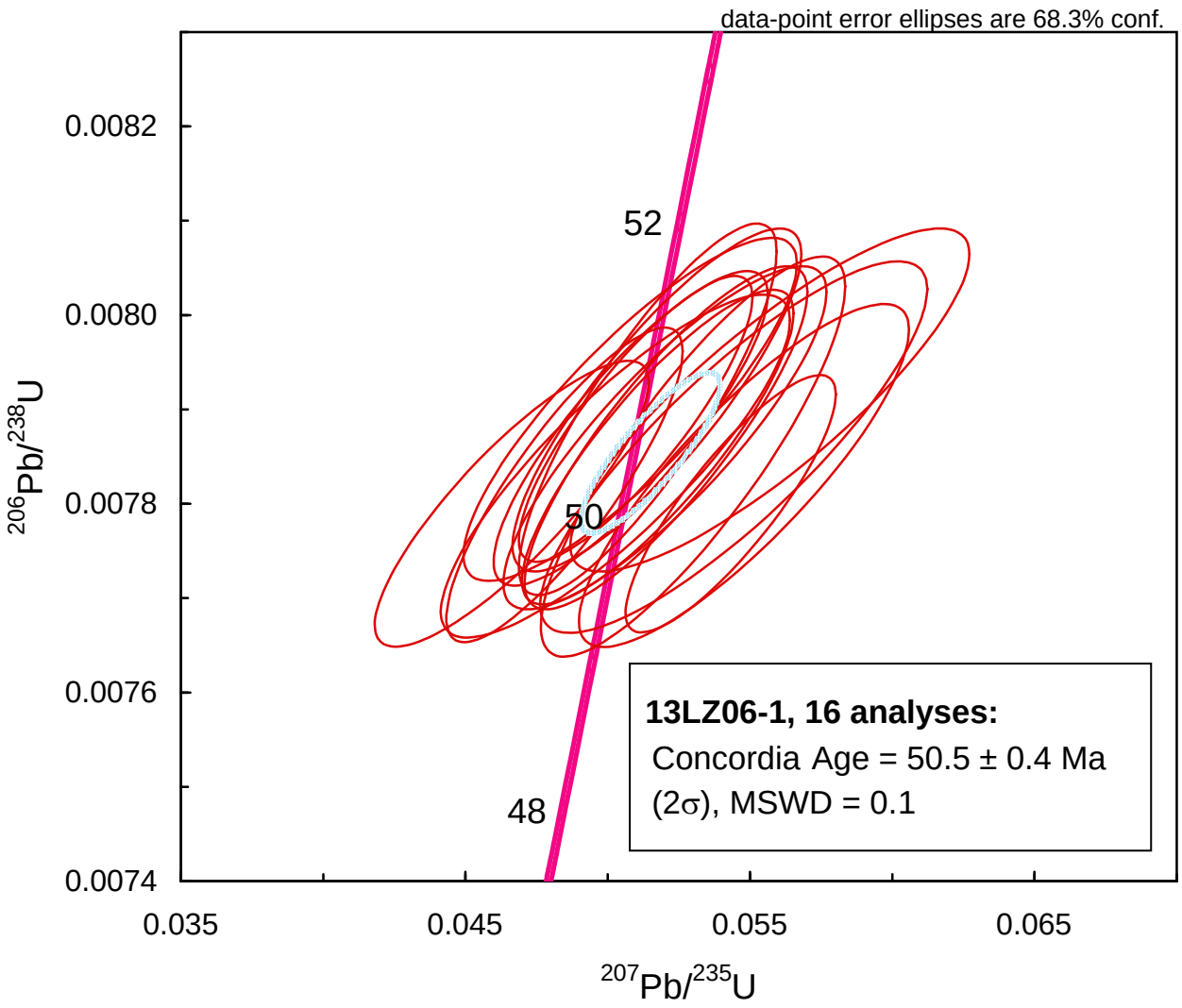

Concordia plots for single zircon analyzed by LA-ICPMS U–Pb dating

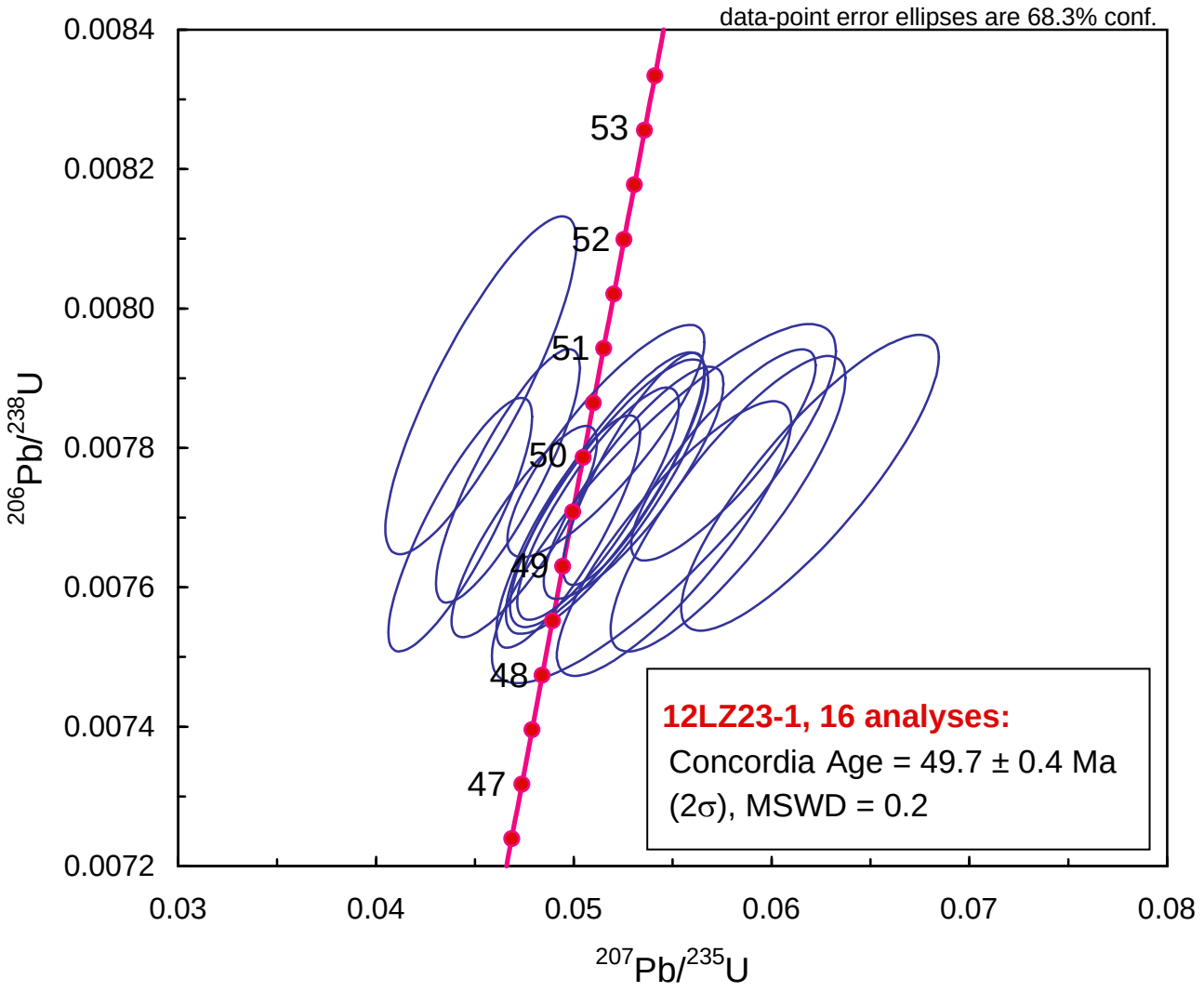

Concordia plots for single zircon analyzed by SIMS 1280 U–Pb dating

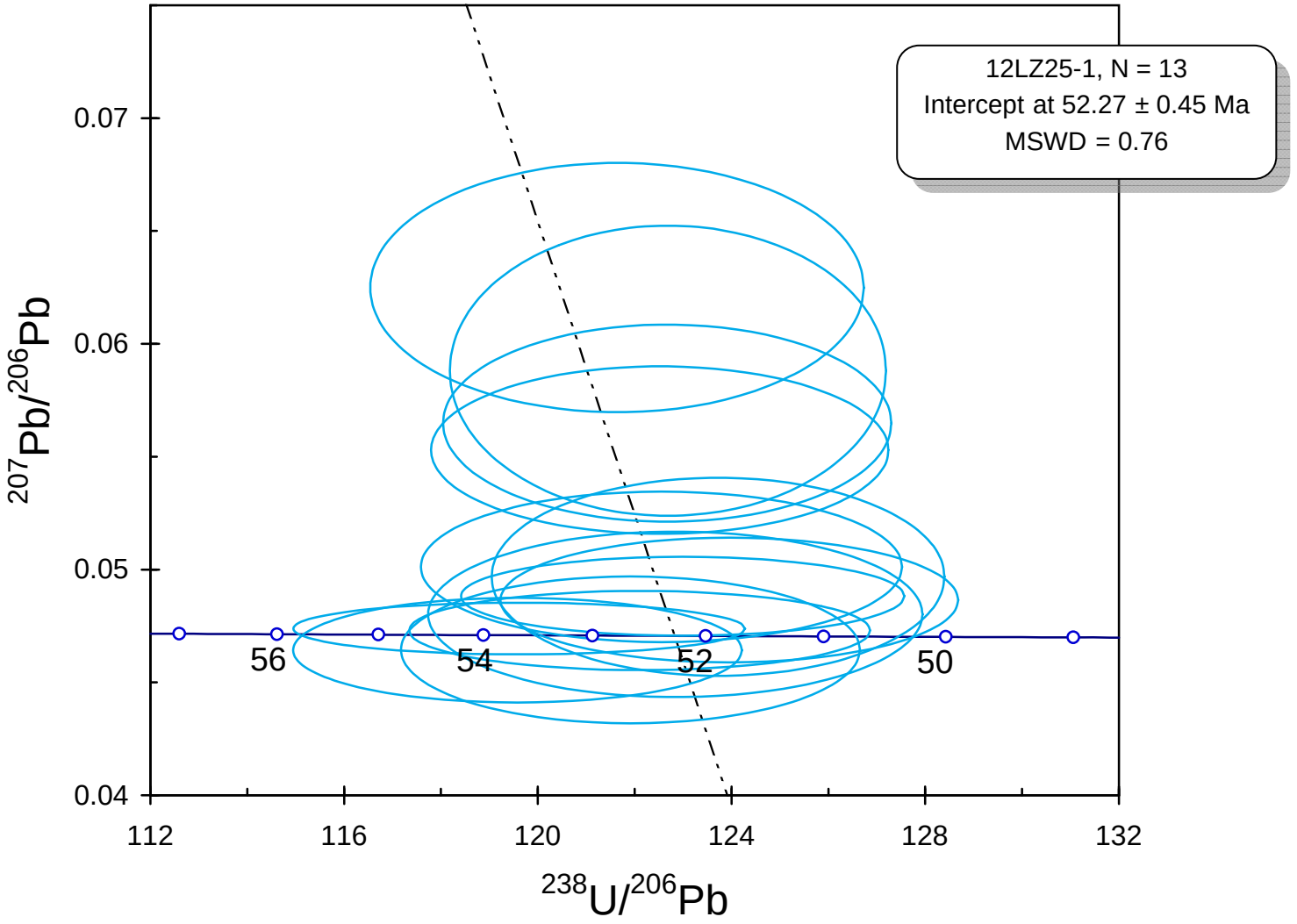

Concordia plots for single zircon analyzed by SIMS 1280 U–Pb dating

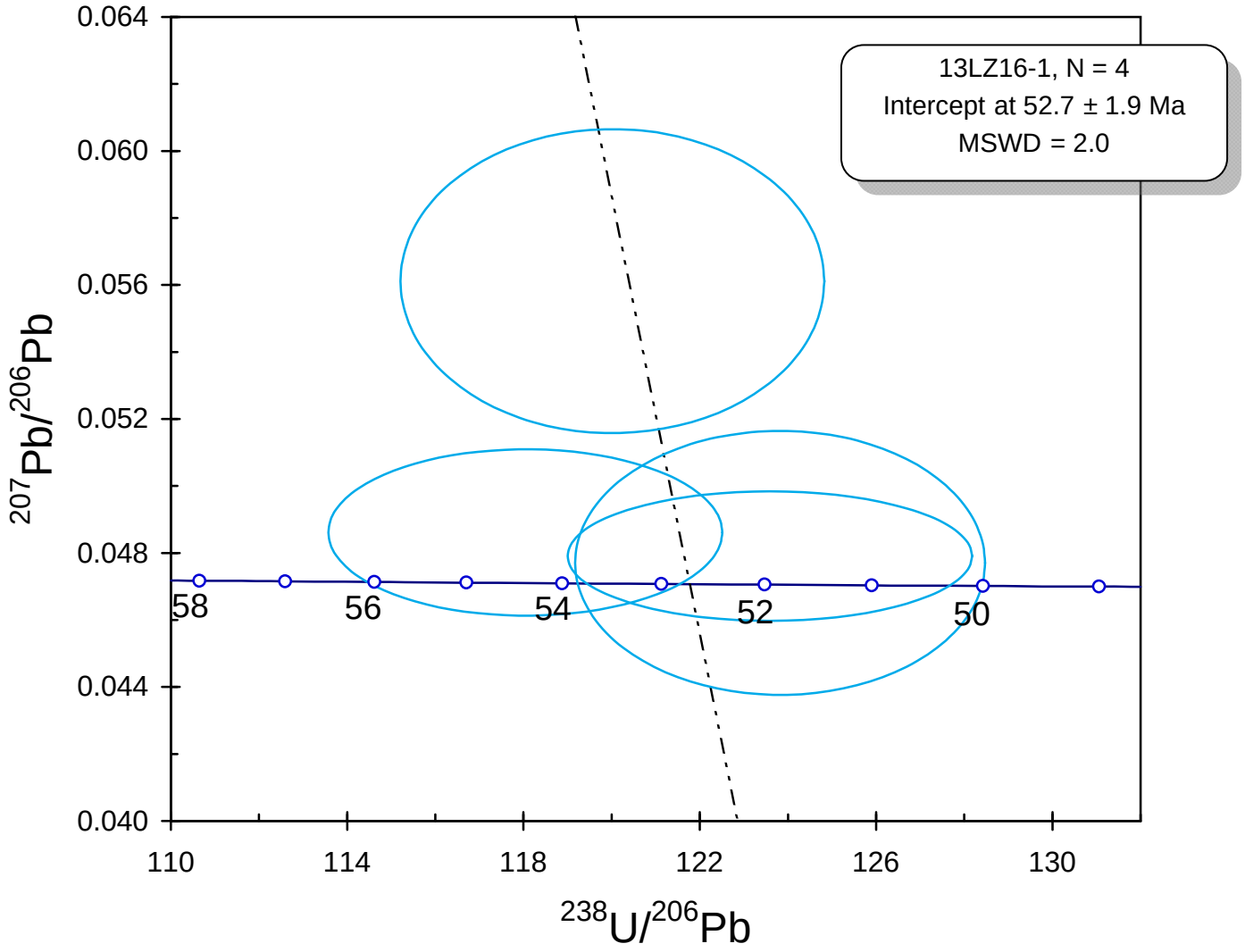

Concordia plots for single zircon analyzed by SIMS 1280 U–Pb dating

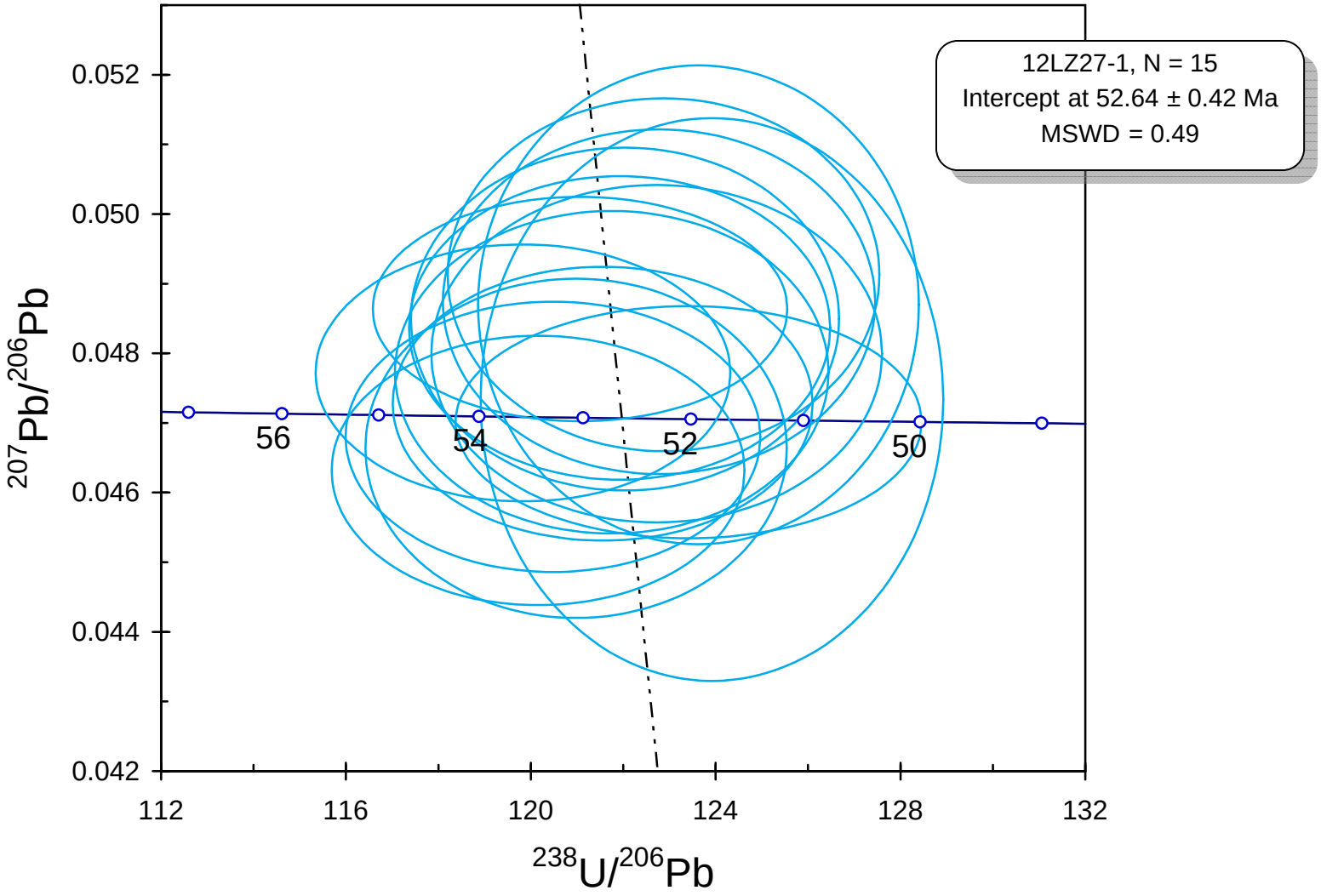

Concordia plots for single zircon analyzed by SIMS 1280 U–Pb dating

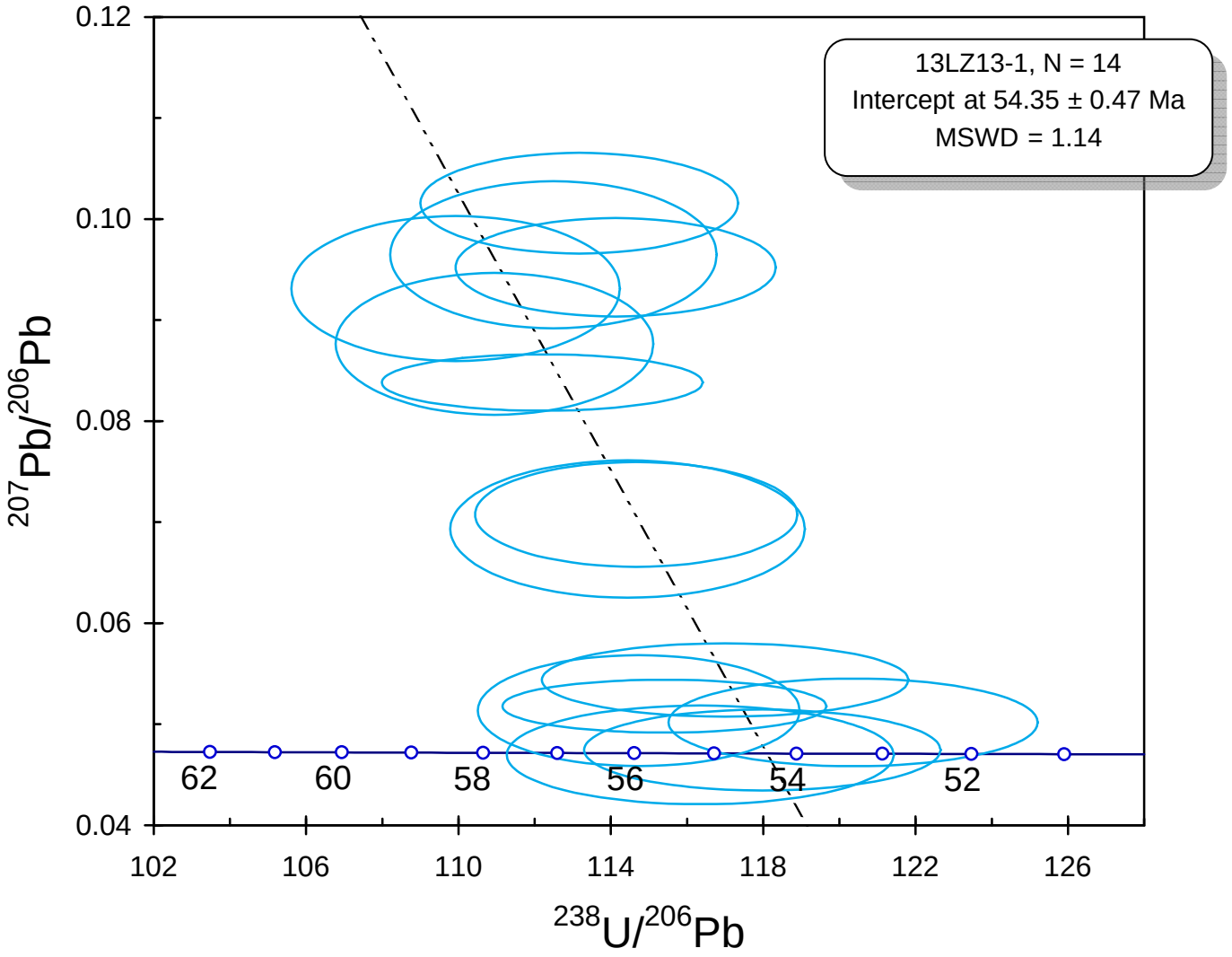

Concordia plots for single zircon analyzed by SIMS 1280 U–Pb dating

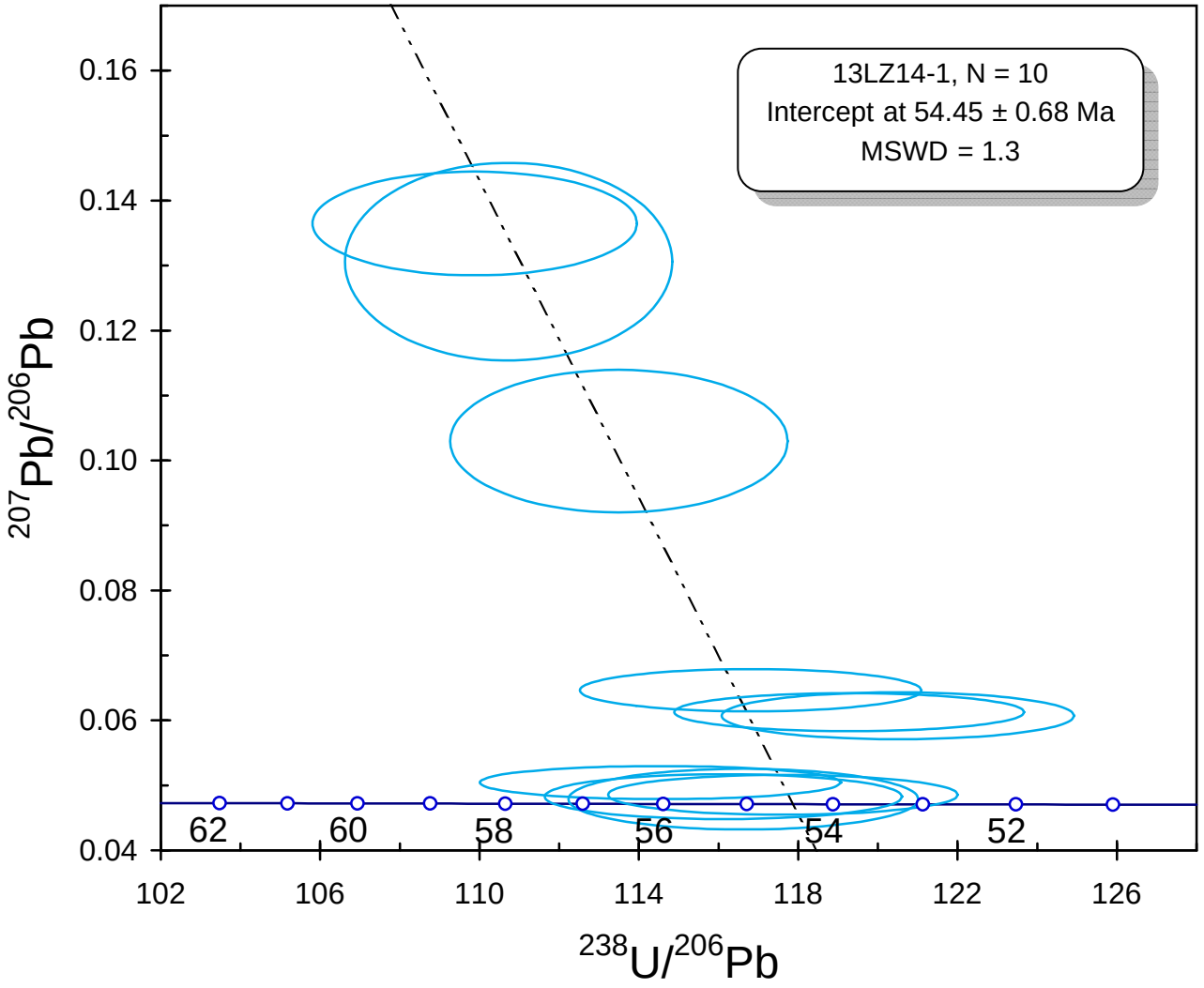

Concordia plots for single zircon analyzed by SIMS 1280 U–Pb dating

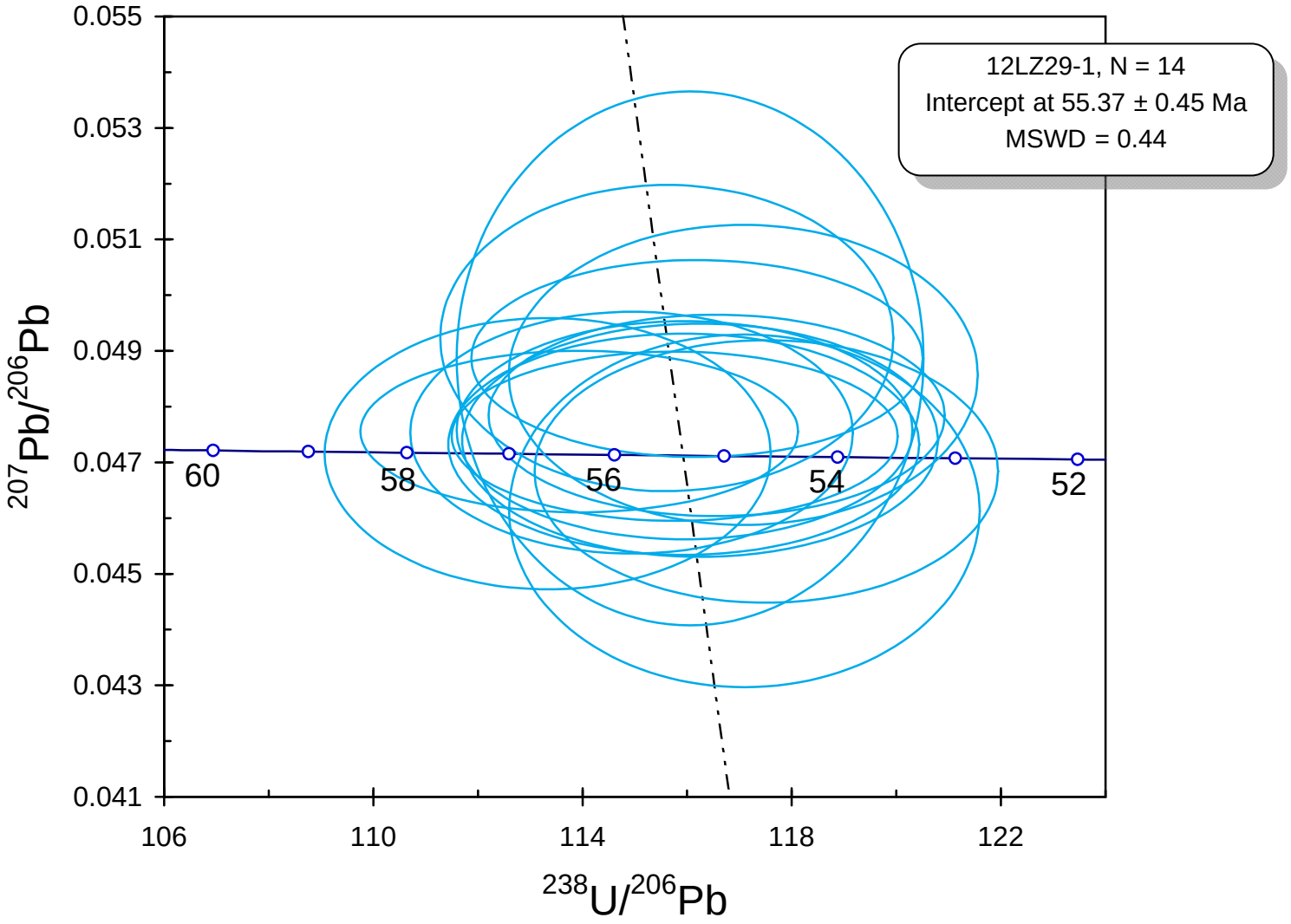

Concordia plots for single zircon analyzed by SIMS 1280 U–Pb dating

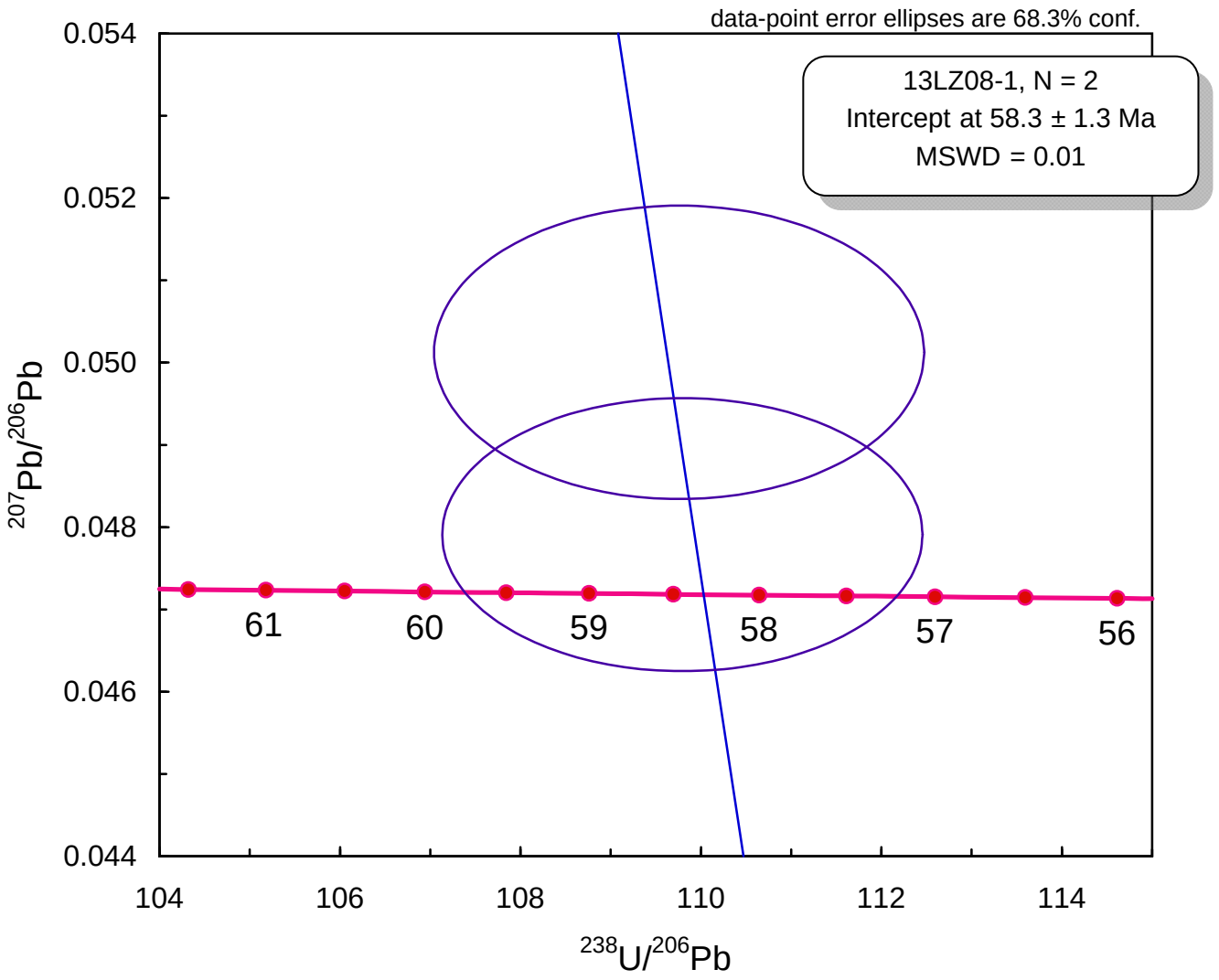

Concordia plots for single zircon analyzed by LA-ICPMS U–Pb dating

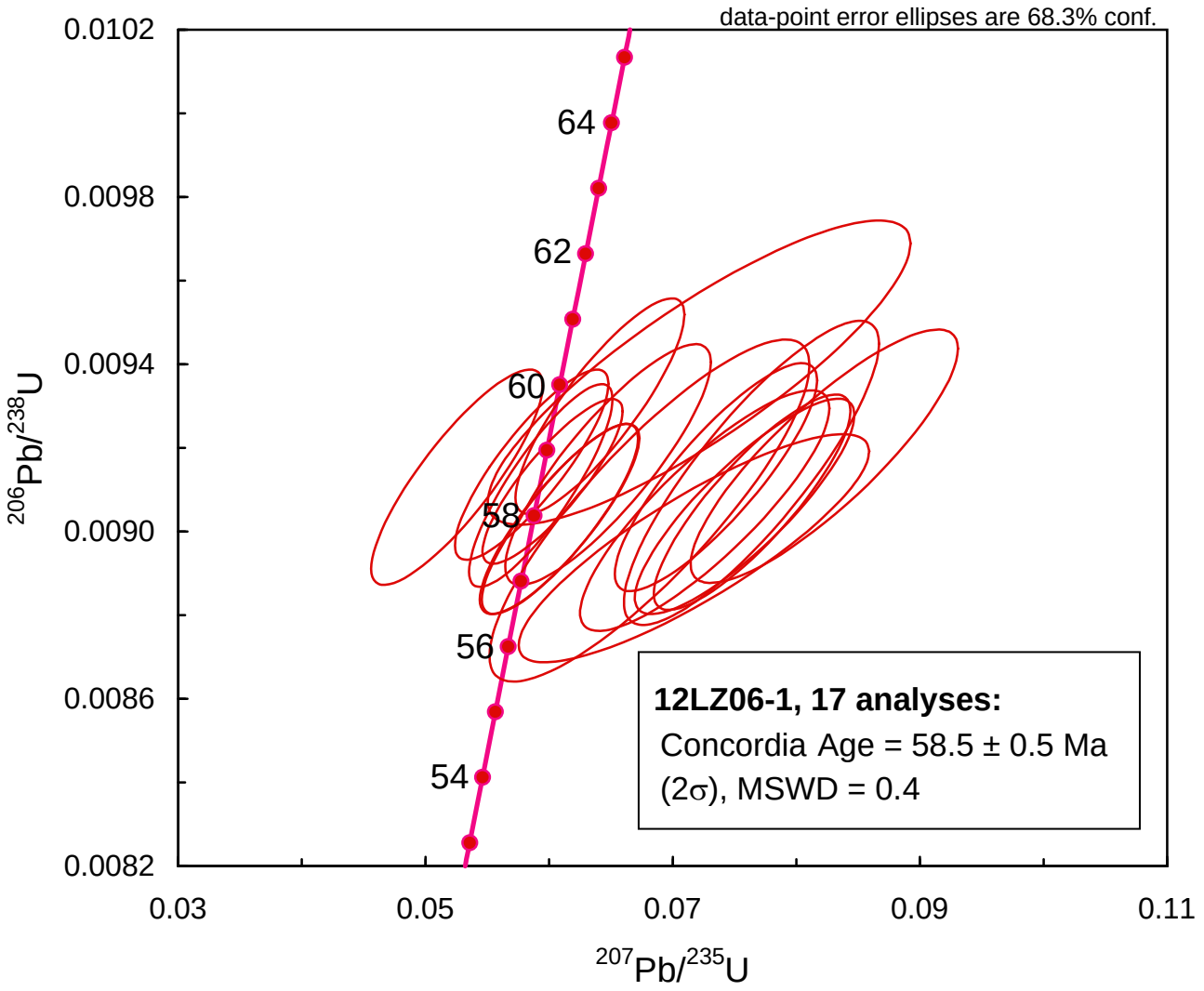

Concordia plots for single zircon analyzed by SIMS 1280 U–Pb dating

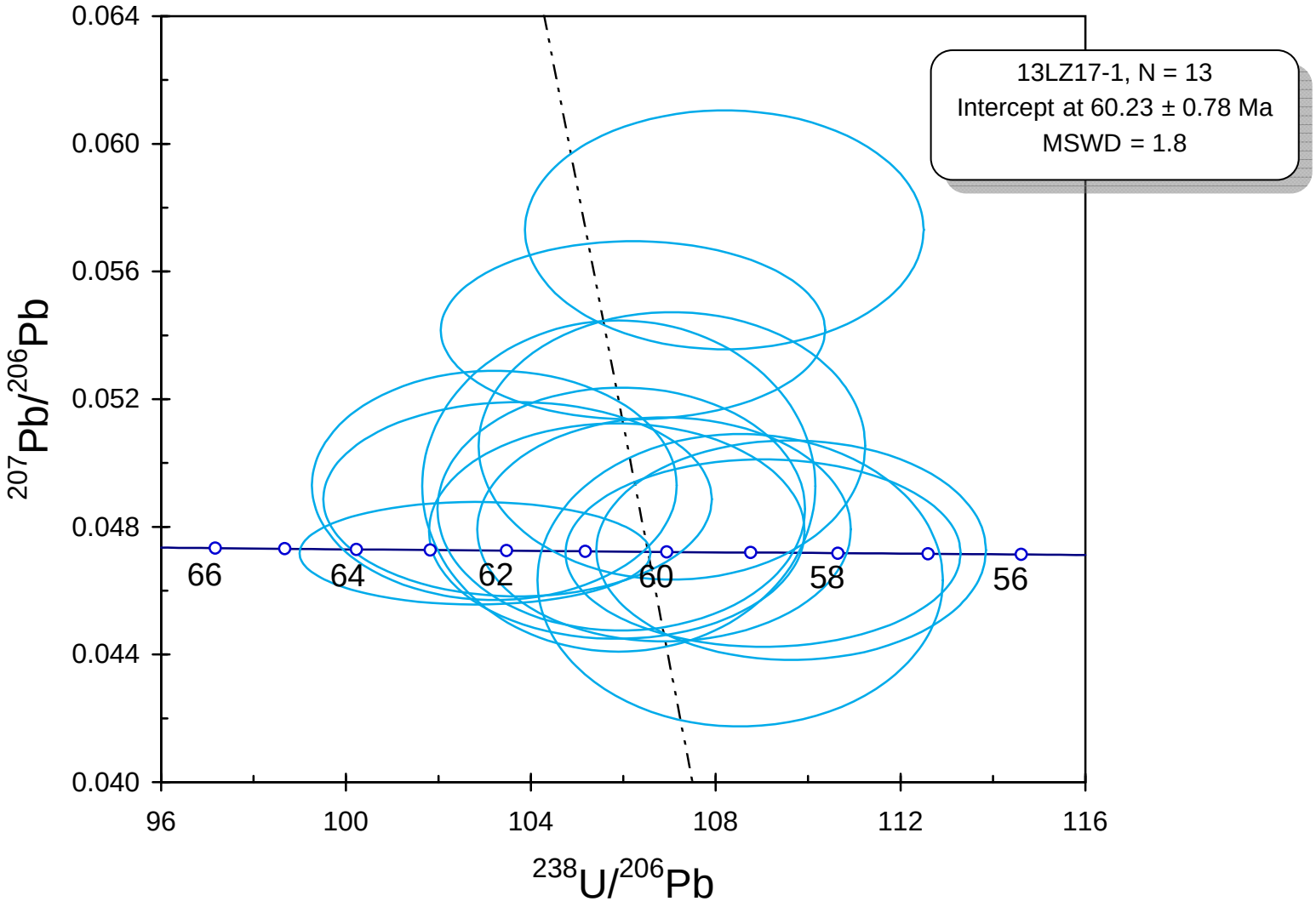

Concordia plots for single zircon analyzed by SIMS 1280 U–Pb dating

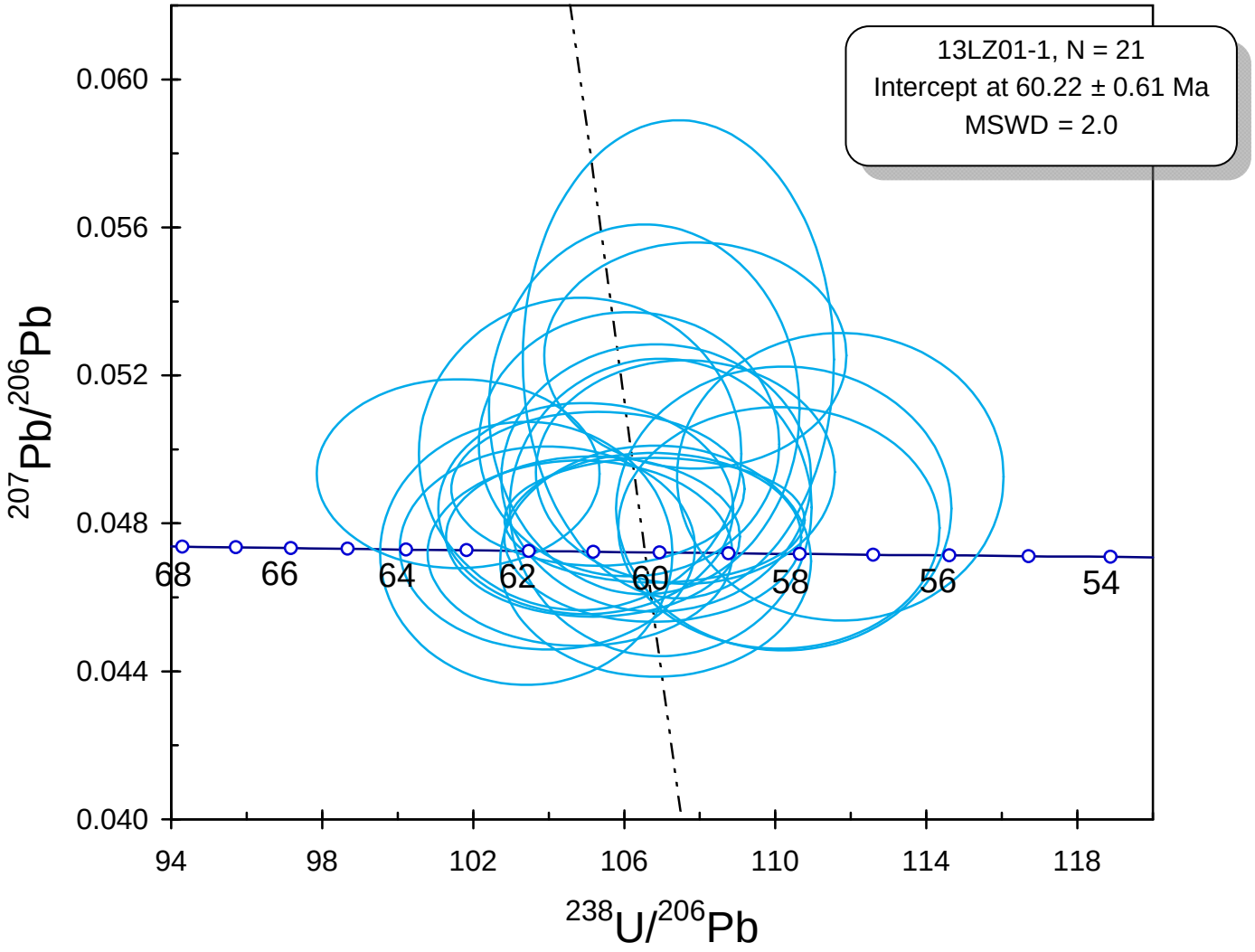

Concordia plots for single zircon analyzed by SIMS 1280 U–Pb dating

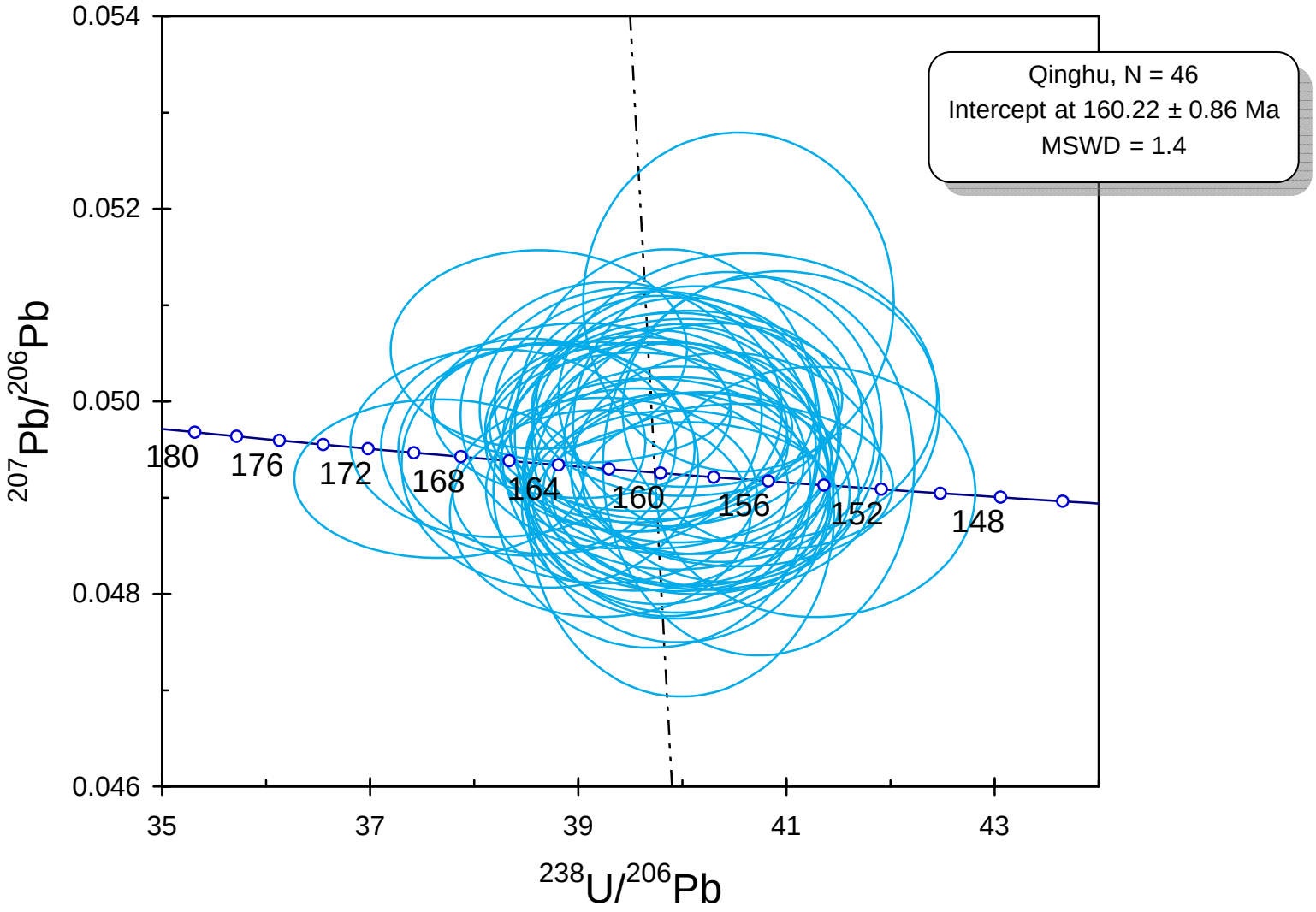

Magmatic record of India-Asia collision

Di-Cheng Zhu*, Qing Wang, Zhi-Dan Zhao, Sun-Lin Chung, Peter A. Cawood, Yaoling Niu, Sheng-Ao Liu, Fu-Yuan Wu, and Xuan-Xue Mo

Table S1 Zircon SIMS U-Pb age data reported in this study for the Linzizong volcanic rocks in Linzhou Basin

					TW concordia columns (Pbc uncorr.)					
Sample/	**[U]**	**[Th]**	**[Pb]**	**Th/U**	**^{238}U**	**±σ**	**^{207}Pb**	**±σ**	**207-corr**	**±σ**
spot #	**ppm**	**ppm**	**ppm**	**meas**	**^{206}Pb**	**%**	**^{206}Pb**	**%**	**age (Ma)**	
13LZ01-1@2	1717	1795	23	1.05	105.301	1.51	0.04894	1.74	60.8	0.9
13LZ01-1@4	475	324	6	0.68	107.433	1.57	0.05243	5.04	59.3	1.0
13LZ01-1@5	1268	1066	16	0.84	103.404	1.53	0.04719	3.08	62.0	1.0
13LZ01-1@6	1396	1487	19	1.06	103.966	1.54	0.04733	2.37	61.7	0.9
13LZ01-1@7	503	314	6	0.63	110.225	1.64	0.04840	3.24	58.1	1.0
13LZ01-1@8	812	715	10	0.88	107.618	1.50	0.04939	2.50	59.5	0.9
13LZ01-1@9	671	321	7	0.48	106.126	1.53	0.05014	2.91	60.2	0.9
13LZ01-1@10	695	491	8	0.71	110.097	1.58	0.04788	2.79	58.2	0.9
13LZ01-1@11	358	217	4	0.61	106.528	1.58	0.05108	4.00	59.9	1.0
13LZ01-1@12	906	918	12	1.01	106.829	1.57	0.04698	2.72	60.1	0.9
13LZ01-1@13	1076	1034	14	0.96	104.978	1.52	0.04840	2.41	61.0	0.9
13LZ01-1@15	889	1417	13	1.59	104.828	1.67	0.04988	3.46	61.0	1.0
13LZ01-1@16	1025	866	13	0.85	106.964	1.53	0.04843	3.39	59.9	0.9
13LZ01-1@17	925	1025	12	1.11	106.847	1.57	0.04923	3.00	59.9	0.9
13LZ01-1@18	2720	4708	41	1.73	106.807	1.52	0.04809	1.43	60.0	0.9
13LZ01-1@21	1643	2454	24	1.49	105.173	1.51	0.04765	1.86	61.0	0.9
13LZ01-1@22	1156	1387	15	1.20	107.880	1.52	0.05254	2.38	59.1	0.9
13LZ01-1@23	1347	1414	18	1.05	106.754	1.50	0.04762	1.96	60.1	0.9
13LZ01-1@24	1085	989	14	0.91	104.827	1.57	0.04719	2.17	61.2	1.0
13LZ01-1@1	644	366	7	0.57	111.719	1.58	0.04926	3.22	57.3	0.9
13LZ01-1@20	2663	4097	40	1.54	101.599	1.51	0.04934	2.11	63.0	0.9
~~13LZ01-1@14~~	~~1535~~	~~1750~~	~~18~~	~~1.14~~	~~114.101~~	~~6.37~~	~~0.05007~~	~~8.96~~	~~56.0~~	~~3.6~~
~~13LZ01-1@3~~	~~2194~~	~~1803~~	~~30~~	~~0.82~~	~~94.779~~	~~1.51~~	~~0.04766~~	~~1.48~~	~~67.6~~	~~1.0~~
~~13LZ01-1@19~~	~~3730~~	~~1639~~	~~210~~	~~0.44~~	~~21.015~~	~~1.50~~	~~0.05270~~	~~0.57~~	~~299.5~~	~~4.4~~
13LZ04-1@1	664	624	7	0.94	125.275	1.55	0.04769	1.97	51.2	0.8
13LZ04-1@2	814	811	9	1.00	125.571	1.50	0.04871	1.83	51.0	0.8
13LZ04-1@3	871	631	9	0.73	123.858	1.51	0.04797	2.97	51.8	0.8
13LZ04-1@4	1860	732	18	0.39	123.791	1.50	0.04872	1.15	51.8	0.8
13LZ04-1@5	1070	726	11	0.68	126.203	1.53	0.04709	1.52	50.9	0.8

13LZ04-1@6	868	710	9	0.82	122.853	1.50	0.04747	1.86	52.2	0.8
13LZ04-1@8	2269	1981	25	0.87	120.824	1.53	0.04820	0.99	53.1	0.8
13LZ04-1@9	739	437	7	0.59	124.374	1.53	0.04781	1.74	51.6	0.8
13LZ04-1@10	1663	3474	24	2.09	120.983	1.52	0.04735	1.45	53.0	0.8
13LZ04-1@11	918	640	9	0.70	125.435	1.53	0.04918	1.59	51.0	0.8
13LZ04-1@13	654	368	6	0.56	125.413	1.54	0.04840	2.01	51.1	0.8
13LZ04-1@18	2337	1661	24	0.71	121.479	1.53	0.04667	1.73	52.9	0.8
13LZ04-1@22	895	675	9	0.75	126.802	1.66	0.04708	3.62	50.6	0.8
13LZ04-1@19	2012	3024	26	1.50	119.980	1.53	0.04816	1.77	53.4	0.8
13LZ04-1@20	993	1350	12	1.36	123.281	1.55	0.04757	4.03	52.0	0.8
13LZ04-1@21	1030	886	11	0.86	122.823	1.56	0.05205	2.46	51.9	0.8
13LZ04-1@12	1523	1019	16	0.67	118.649	1.54	0.04758	1.23	54.1	0.8
13LZ04-1@14	1468	984	16	0.67	116.904	1.51	0.04610	1.52	55.0	0.8
13LZ04-1@15	347	260	4	0.75	117.612	1.79	0.04783	2.83	54.5	1.0
~~13LZ04-1@17~~	~~808~~	~~1065~~	~~9~~	~~1.32~~	~~121.052~~	~~1.56~~	~~0.06371~~	~~3.61~~	~~51.9~~	~~0.8~~
~~13LZ04-1@7~~	~~2258~~	~~3821~~	~~32~~	~~1.69~~	~~111.222~~	~~1.51~~	~~0.06321~~	~~1.81~~	~~56.5~~	~~0.9~~
~~13LZ04-1@16~~	~~3702~~	~~2849~~	~~35~~	~~0.77~~	~~126.016~~	~~1.50~~	~~0.07698~~	~~1.40~~	~~49.0~~	~~0.8~~
13LZ05-1@1	669	472	7	0.71	123.950	1.59	0.04715	3.78	51.8	0.8
13LZ05-1@2	3372	2482	35	0.74	121.663	1.51	0.04989	1.48	52.6	0.8
13LZ05-1@3	3570	6392	47	1.79	120.832	1.50	0.04695	1.47	53.1	0.8
13LZ05-1@4	1087	799	11	0.73	122.072	1.61	0.04930	3.20	52.4	0.8
13LZ05-1@5	2920	2191	32	0.75	117.553	1.53	0.04981	1.51	54.4	0.8
13LZ05-1@6	537	559	6	1.04	122.971	1.67	0.04658	3.50	52.2	0.9
13LZ05-1@7	1430	913	15	0.64	120.838	1.53	0.04447	2.57	53.3	0.8
13LZ05-1@8	1913	2980	25	1.56	119.378	1.53	0.04707	1.82	53.8	0.8
13LZ05-1@9	1116	766	11	0.69	122.124	1.56	0.04897	3.28	52.4	0.8
13LZ05-1@10	917	1318	11	1.44	123.856	1.52	0.04635	2.82	51.9	0.8
13LZ05-1@11	990	808	10	0.82	123.670	1.56	0.04731	2.73	51.9	0.8
13LZ05-1@12	4269	4381	48	1.03	121.921	1.50	0.04775	1.56	52.6	0.8
13LZ05-1@13	1188	948	13	0.80	119.315	1.56	0.04766	2.51	53.8	0.8
13LZ05-1@14	2508	1773	26	0.71	122.744	1.62	0.04921	1.76	52.2	0.8
13LZ05-1@17	1349	1271	14	0.94	124.881	1.62	0.05042	2.20	51.2	0.8
13LZ05-1@18	2333	2276	25	0.98	125.816	1.50	0.04744	2.56	51.0	0.8
~~13LZ05-1@15~~	~~1195~~	~~994~~	~~12~~	~~0.83~~	~~122.167~~	~~1.56~~	~~0.05991~~	~~2.19~~	~~51.7~~	~~0.8~~
~~13LZ05-1@16~~	~~730~~	~~505~~	~~7~~	~~0.69~~	~~126.497~~	~~1.60~~	~~0.06233~~	~~4.65~~	~~49.8~~	~~0.8~~

12LZ13-1@02	395	246	no data	0.62	112.493	1.56	0.09647	3.08	53.5	1.0
12LZ13-1@06	850	996	9	1.17	113.172	1.51	0.10158	2.00	52.8	1.0
12LZ13-1@16	829	636	8	0.77	114.128	1.51	0.09523	2.09	52.8	0.9
12LZ13-1@1	345	198	no data	0.57	114.440	1.66	0.06933	4.00	54.5	0.9
12LZ13-1@21	292	204	3	0.70	109.925	1.60	0.09313	3.15	55.0	1.0
12LZ13-1@23	895	616	10	0.69	112.201	1.53	0.08383	1.36	54.5	0.9
12LZ13-1@05	1272	1323	15	1.04	110.945	1.54	0.08766	3.27	54.9	0.9
12LZ13-1@14	497	351	5	0.71	114.666	1.51	0.07076	2.99	54.3	0.9
12LZ13-1@08	510	406	5	0.80	117.979	1.62	0.04745	3.44	54.4	0.9
12LZ13-1@17	318	251	4	0.79	117.003	1.68	0.05438	2.73	54.4	0.9
12LZ13-1@09	1319	1163	15	0.88	115.406	1.51	0.05179	2.07	55.3	0.8
12LZ13-1@15	526	427	6	0.81	114.732	1.50	0.05135	4.36	55.6	0.9
12LZ13-1@18	221	191	2	0.87	120.363	1.65	0.05019	3.54	53.1	0.9
12LZ13-1@20	209	159	2	0.76	116.348	1.78	0.04697	4.25	55.2	1.0
~~12LZ13-1@19~~	~~1301~~	~~1007~~	~~15~~	~~0.77~~	~~108.954~~	~~1.58~~	~~0.05203~~	~~1.37~~	~~58.5~~	~~0.9~~
~~12LZ13-1@07~~	~~3609~~	~~2187~~	~~40~~	~~0.61~~	~~110.109~~	~~1.51~~	~~0.04854~~	~~1.31~~	~~58.2~~	~~0.9~~
~~12LZ13-1@12~~	~~542~~	~~748~~	~~[5]~~	~~1.38~~	~~67.986~~	~~3.13~~	~~0.41662~~	~~4.29~~	~~49.9~~	~~6.3~~
~~12LZ13-1@11~~	~~628~~	~~466~~	~~6~~	~~0.74~~	~~68.966~~	~~4.92~~	~~0.37724~~	~~7.31~~	~~53.8~~	~~6.5~~
~~12LZ13-1@04~~	~~755~~	~~662~~	~~no data~~	~~0.88~~	~~91.045~~	~~1.64~~	~~0.26516~~	~~1.79~~	~~50.9~~	~~2.7~~
~~12LZ13-1@13~~	~~589~~	~~383~~	~~[5]~~	~~0.65~~	~~101.675~~	~~1.50~~	~~0.20308~~	~~1.65~~	~~50.6~~	~~1.8~~
~~12LZ13-1@22~~	~~799~~	~~601~~	~~14~~	~~0.75~~	~~73.219~~	~~1.53~~	~~0.05134~~	~~1.42~~	~~87.0~~	~~1.3~~
~~12LZ13-1@10~~	~~821~~	~~539~~	~~14~~	~~0.66~~	~~67.910~~	~~1.51~~	~~0.09360~~	~~2.80~~	~~88.8~~	~~1.5~~
~~12LZ13-1@03~~	~~587~~	~~878~~	~~13~~	~~1.50~~	~~68.491~~	~~1.52~~	~~0.05427~~	~~2.48~~	~~92.7~~	~~1.4~~
12LZ14-1@02	1011	333	no data	0.33	109.879	1.51	0.13648	2.39	51.8	1.2
12LZ14-1@07	798	526	8	0.66	110.730	1.52	0.13059	4.76	51.8	1.2
12LZ14-1@15	1475	805	14	0.55	120.503	1.50	0.06070	2.43	52.4	0.8
12LZ14-1@16	904	649	9	0.72	113.498	1.53	0.10297	4.35	52.5	1.0
12LZ14-1@13	1959	961	18	0.49	119.280	1.50	0.06127	1.95	52.8	0.8
12LZ14-1@10	1538	851	15	0.55	116.805	1.50	0.06463	2.06	53.7	0.8
12LZ14-1@12	1067	346	10	0.32	117.616	1.53	0.04854	2.58	54.5	0.8
12LZ14-1@1	828	423	9	0.51	116.628	1.54	0.04786	3.99	55.0	0.9
12LZ14-1@14	853	1460	11	1.71	116.127	1.58	0.04826	2.92	55.2	0.9
12LZ14-1@03	1844	1205	19	0.65	114.543	1.62	0.05044	2.07	55.8	0.9
~~12LZ14-1@11~~	~~420~~	~~227~~	~~[2]~~	~~0.54~~	~~92.538~~	~~4.46~~	~~0.55822~~	~~4.34~~	~~24.1~~	~~6.3~~
~~12LZ14-1@05~~	~~1592~~	~~1292~~	~~[12]~~	~~0.81~~	~~119.331~~	~~1.88~~	~~0.28164~~	~~1.68~~	~~37.7~~	~~2.2~~
~~12LZ14-1@08~~	~~885~~	~~362~~	~~[7]~~	~~0.41~~	~~100.858~~	~~2.42~~	~~0.29904~~	~~3.15~~	~~43.2~~	~~2.9~~
~~12LZ14-1@09~~	~~790~~	~~707~~	~~no data~~	~~0.89~~	~~113.755~~	~~1.50~~	~~0.20301~~	~~3.30~~	~~45.2~~	~~1.7~~

~~12LZ14-1@04~~	~~1792~~	~~1497~~	~~16~~	~~0.84~~	~~95.384~~	~~1.60~~	~~0.26339~~	~~3.00~~	~~48.7~~	~~2.6~~
~~12LZ14-1@06~~	~~763~~	~~217~~	~~48~~	~~0.28~~	~~17.857~~	~~1.54~~	~~0.05584~~	~~1.26~~	~~350.2~~	~~5.3~~
13LZ16-1@1	437	659	6	1.51	118.043	1.55	0.04861	2.09	54.3	0.8
13LZ16-1@15	705	776	8	1.10	123.590	1.52	0.04791	1.65	51.9	0.8
13LZ16-1@16	436	534	5	1.22	123.823	1.53	0.04770	3.37	51.8	0.8
13LZ16-1@17	205	156	2	0.76	120.018	1.64	0.05612	3.30	52.9	0.9
13LZ16-1@4	625	292	8	0.47	93.635	1.53	0.04849	1.55	68.4	1.0
13LZ16-1@5	233	295	4	1.27	92.295	1.62	0.04772	2.64	69.4	1.1
13LZ16-1@6	975	852	13	0.87	97.197	1.67	0.04870	1.31	65.9	1.1
13LZ16-1@7	489	194	6	0.40	92.893	1.51	0.04717	1.77	69.0	1.0
13LZ16-1@8	915	772	13	0.84	93.934	1.51	0.04711	1.95	68.3	1.0
13LZ16-1@10	1380	1471	20	1.07	93.985	1.51	0.04678	1.18	68.3	1.0
13LZ16-1@13	665	436	9	0.66	95.934	1.50	0.04764	2.65	66.8	1.0
13LZ16-1@14	725	342	9	0.47	95.731	1.51	0.04975	1.43	66.8	1.0
13LZ16-1@18	498	226	7	0.45	91.134	1.50	0.04751	1.73	70.3	1.1
~~13LZ16-1@3~~	~~346~~	~~201~~	~~4~~	~~0.58~~	~~97.425~~	~~1.59~~	~~0.05074~~	~~2.08~~	~~65.5~~	~~1.0~~
~~13LZ16-1@11~~	~~1258~~	~~1281~~	~~18~~	~~1.02~~	~~95.173~~	~~1.51~~	~~0.05073~~	~~1.48~~	~~67.1~~	~~1.0~~
~~13LZ16-1@2~~	~~1421~~	~~2137~~	~~23~~	~~1.50~~	~~88.800~~	~~1.74~~	~~0.06841~~	~~17.99~~	~~70.3~~	~~1.7~~
~~13LZ16-1@12~~	~~564~~	~~359~~	~~6~~	~~0.64~~	~~96.311~~	~~2.00~~	~~0.10216~~	~~4.62~~	~~61.9~~	~~1.4~~
~~13LZ16-1@9~~	~~435~~	~~861~~	~~8~~	~~1.98~~	~~58.047~~	~~5.33~~	~~0.32544~~	~~10.40~~	~~71.2~~	~~7.9~~
13LZ17-1@01	306	166	3	0.54	109.633	1.57	0.04727	2.97	58.5	0.9
13LZ17-1@04	298	168	3	0.56	108.188	1.63	0.05731	2.67	58.5	1.0
13LZ17-1@11	429	302	5	0.70	109.025	1.60	0.04718	2.54	58.9	0.9
13LZ17-1@07	176	83	2	0.47	108.529	1.65	0.04633	4.04	59.2	1.0
13LZ17-1@05	229	123	3	0.54	107.053	1.60	0.05054	3.39	59.7	1.0
13LZ17-1@16	600	443	7	0.74	106.210	1.60	0.05416	2.10	59.9	1.0
13LZ17-1@02	402	321	5	0.80	106.882	1.55	0.04792	2.99	60.0	0.9
13LZ17-1@13	198	134	2	0.68	105.902	1.64	0.04928	4.30	60.4	1.0
13LZ17-1@14	755	583	9	0.77	105.957	1.53	0.04856	3.20	60.5	0.9
13LZ17-1@09	407	173	5	0.42	105.860	1.57	0.04787	2.88	60.6	1.0
13LZ17-1@17	465	219	5	0.47	103.713	1.66	0.04886	2.54	61.7	1.0
13LZ17-1@20	324	135	4	0.42	103.210	1.56	0.04930	2.98	62.0	1.0
13LZ17-1@10	1418	1064	18	0.75	102.794	1.51	0.04717	1.39	62.4	0.9
~~13LZ17-1@19~~	~~100~~	~~66~~	~~2~~	~~0.66~~	~~61.630~~	~~1.62~~	~~0.04618~~	~~4.28~~	~~104.0~~	~~1.7~~
~~13LZ17-1@08~~	~~394~~	~~192~~	~~8~~	~~0.49~~	~~60.541~~	~~1.54~~	~~0.04885~~	~~2.11~~	~~105.5~~	~~1.6~~
~~13LZ17-1@12~~	~~121~~	~~168~~	~~4~~	~~1.39~~	~~51.491~~	~~1.56~~	~~0.04850~~	~~3.93~~	~~124.0~~	~~1.9~~

~~13LZ17-1@06~~	~~375~~	~~213~~	~~9~~	~~0.57~~	~~49.593~~	~~1.52~~	~~0.05080~~	~~1.70~~	~~128.3~~	~~1.9~~
~~13LZ17-1@18~~	~~196~~	~~131~~	~~6~~	~~0.67~~	~~40.695~~	~~1.53~~	~~0.04909~~	~~3.00~~	~~156.5~~	~~2.4~~
~~13LZ17-1@03~~	~~349~~	~~133~~	~~20~~	~~0.38~~	~~20.901~~	~~1.50~~	~~0.05267~~	~~1.13~~	~~301.2~~	~~4.5~~
~~13LZ17-1@15~~	~~1074~~	~~742~~	~~67~~	~~0.69~~	~~20.313~~	~~1.50~~	~~0.05213~~	~~0.71~~	~~310.0~~	~~4.6~~
12LZ25-1@16	1255	1526	15	1.22	122.992	1.52	0.04882	1.46	52.1	0.8
12LZ25-1@15	522	531	6	1.02	121.911	1.59	0.04644	2.86	52.7	0.8
12LZ25-1@14	512	515	6	1.01	123.722	1.54	0.04968	3.61	51.7	0.8
12LZ25-1@13	619	732	7	1.18	123.955	1.56	0.04865	2.31	51.7	0.8
12LZ25-1@08	474	518	5	1.09	121.635	1.71	0.06249	3.61	51.7	0.9
12LZ25-1@11	1361	2233	18	1.64	122.104	1.59	0.04730	1.51	52.6	0.8
12LZ25-1@10	3176	870	30	0.27	119.616	1.59	0.04739	0.99	53.6	0.9
12LZ25-1@07	348	315	4	0.91	122.554	1.66	0.05012	2.72	52.2	0.9
12LZ25-1@06	857	863	10	1.01	119.582	1.58	0.04643	2.04	53.7	0.9
12LZ25-1@03	928	1209	11	1.30	122.673	1.54	0.05649	3.16	51.7	0.8
12LZ25-1@05	356	576	4	1.62	122.686	1.50	0.05881	4.46	51.5	0.8
12LZ25-1@04	1290	1797	15	1.39	122.518	1.57	0.05530	2.74	51.9	0.8
12LZ25-1@1	805	1206	9	1.50	122.838	1.70	0.04802	3.12	52.2	0.9
~~12LZ25-1@09~~	~~1830~~	~~1943~~	~~22~~	~~1.06~~	~~115.528~~	~~1.60~~	~~0.06726~~	~~3.53~~	~~54.1~~	~~0.9~~
~~12LZ25-1@02~~	~~687~~	~~1052~~	~~8~~	~~1.53~~	~~126.135~~	~~1.54~~	~~0.05114~~	~~3.32~~	~~50.6~~	~~0.8~~
~~12LZ25-1@12~~	~~580~~	~~767~~	~~7~~	~~1.32~~	~~119.202~~	~~1.58~~	~~0.06250~~	~~9.57~~	~~52.8~~	~~0.9~~
12LZ27-1@15	648	532	7	0.82	122.775	1.56	0.04874	2.07	52.2	0.8
12LZ27-1@14	346	396	4	1.15	123.629	1.58	0.04870	2.88	51.8	0.8
12LZ27-1@13	1540	1124	17	0.73	120.481	1.52	0.04680	1.69	53.3	0.8
12LZ27-1@12	1003	624	11	0.62	120.158	1.52	0.04632	1.71	53.5	0.8
12LZ27-1@11	1547	1586	18	1.03	119.830	1.53	0.04772	1.58	53.5	0.8
12LZ27-1@10	864	888	10	1.03	121.922	1.53	0.04837	1.84	52.6	0.8
12LZ27-1@09	627	748	8	1.19	122.723	1.62	0.04799	2.06	52.3	0.8
12LZ27-1@08	598	725	7	1.21	120.978	1.54	0.04664	2.13	53.1	0.8
12LZ27-1@07	1318	947	14	0.72	123.416	1.67	0.04701	1.45	52.0	0.9
12LZ27-1@06	683	525	7	0.77	121.753	1.57	0.04773	1.98	52.7	0.8
12LZ27-1@05	610	677	7	1.11	122.872	1.55	0.04913	2.11	52.1	0.8
12LZ27-1@04	643	802	8	1.25	122.039	1.55	0.04849	2.07	52.5	0.8
12LZ27-1@03	1472	942	15	0.64	121.065	1.51	0.04864	1.35	52.9	0.8
12LZ27-1@02	228	167	2	0.73	123.920	1.65	0.04734	3.49	51.8	0.9
12LZ27-1@1	981	997	11	1.02	121.556	1.53	0.04728	1.70	52.8	0.8
~~12LZ27-1@17~~	~~159~~	~~114~~	~~2~~	~~0.72~~	~~126.116~~	~~1.73~~	~~0.04523~~	~~4.39~~	~~51.0~~	~~0.9~~

~~12LZ27-1@16~~	~~162~~	~~119~~	~~2~~	~~0.74~~	~~119.454~~	~~1.67~~	~~0.04604~~	~~4.71~~	~~53.8~~	~~0.9~~
12LZ29-1@07	1926	982	21	0.51	113.334	1.54	0.04716	2.11	56.6	0.9
12LZ29-1@05	2185	2082	26	0.95	113.938	1.50	0.04755	1.25	56.3	0.8
12LZ29-1@08	1466	1067	16	0.73	114.938	1.50	0.04753	1.86	55.8	0.8
12LZ29-1@1	1955	1656	22	0.85	115.763	1.50	0.04747	1.31	55.4	0.8
12LZ29-1@04	1277	1822	17	1.43	115.611	1.53	0.04923	2.28	55.4	0.8
12LZ29-1@14	887	576	10	0.65	115.937	1.59	0.04732	1.71	55.4	0.9
12LZ29-1@13	934	538	10	0.58	115.953	1.54	0.04758	1.68	55.3	0.8
12LZ29-1@02	1013	568	11	0.56	116.249	1.60	0.04740	1.80	55.2	0.9
12LZ29-1@10	386	190	4	0.49	116.057	1.57	0.04887	4.00	55.2	0.9
12LZ29-1@06	1369	1036	15	0.76	116.190	1.52	0.04886	1.48	55.1	0.8
12LZ29-1@11	1131	741	12	0.66	116.566	1.53	0.04784	1.54	55.0	0.8
12LZ29-1@12	500	334	5	0.67	117.096	1.57	0.04613	2.80	54.9	0.9
12LZ29-1@03	621	364	7	0.59	117.074	1.56	0.04857	2.26	54.7	0.9
12LZ29-1@15	840	785	10	0.94	117.515	1.54	0.04684	2.05	54.6	0.8
~~12LZ29-1@09~~	~~830~~	~~844~~	~~12~~	~~1.02~~	~~97.539~~	~~1.51~~	~~0.04685~~	~~1.74~~	~~65.8~~	~~1.0~~
13LZ08-1@1	525	391	6	0.74	109.796	1.60	0.04791	2.29	57.9	0.9
13LZ08-1@03	352	262	4	0.74	109.759	1.63	0.05012	2.35	57.7	0.9
13LZ08-1@04	1498	834	20	0.56	92.549	1.62	0.04959	1.02	68.5	1.1
13LZ08-1@12	1797	1518	25	0.85	93.967	1.57	0.05263	1.93	67.8	1.1
13LZ08-1@07	741	936	34	1.26	31.315	1.50	0.05109	1.02	200.6	3.0
13LZ08-1@06	2667	1033	100	0.39	30.949	1.50	0.05093	0.44	203.0	3.0
13LZ08-1@11	927	1094	42	1.18	31.127	1.50	0.05120	0.79	201.8	3.0
13LZ08-1@08	2573	1039	147	0.40	20.533	1.52	0.05248	0.37	303.9	4.6
13LZ08-1@10	935	468	221	0.501	5.236	1.59	0.08027	0.45	1112.7	17.1

TW concordia columns (Pbc uncorr.)

Sample/ spot #	**[U] ppm**	**[Th] ppm**	**[Pb] ppm**	**Th/U meas**	**^{238}U ^{206}Pb**	**±σ %**	**^{207}Pb ^{206}Pb**	**±σ %**	**207-corr age (Ma)**	**±σ**
Qinghu@1	561	321	17	0.57	41.280	1.52	0.04906	1.08	154.3	2.3
Qinghu@2	1065	389	31	0.37	39.561	1.50	0.04958	0.77	160.9	2.4
~~Qinghu@3~~	~~1462~~	~~653~~	~~44~~	~~0.45~~	~~39.164~~	~~1.50~~	~~0.05711~~	~~0.67~~	~~160.9~~	~~2.4~~
Qinghu@4	2587	1458	81	0.56	39.021	1.51	0.04999	0.51	163.0	2.4
Qinghu@5	1132	320	32	0.28	39.600	1.50	0.04973	0.72	160.7	2.4
Qinghu@11	1480	612	44	0.41	39.952	1.50	0.04897	0.78	159.4	2.4

Qinghu@10	1334	699	42	0.52	39.253	1.52	0.04907	0.80	162.2	2.4
Qinghu@8	1344	536	40	0.40	39.556	1.50	0.04971	0.79	160.9	2.4
Qinghu@7	1043	410	31	0.39	39.928	1.51	0.04891	0.98	159.5	2.4
Qinghu@6	2441	1383	74	0.57	39.857	1.51	0.04967	1.57	159.7	2.4
Qinghu@5	2309	1351	70	0.58	40.145	1.61	0.04981	1.14	158.5	2.5
Qinghu@4	1733	837	52	0.48	39.708	1.57	0.04909	1.37	160.4	2.5
Qinghu@3	1664	901	51	0.54	39.943	1.51	0.04921	1.16	159.4	2.4
Qinghu@2	1139	673	34	0.59	40.539	1.50	0.05103	1.41	156.7	2.3
Qinghu@1	1643	803	49	0.49	40.629	1.83	0.05004	1.23	156.6	2.8
Qinghu@1	1836	1083	59	0.59	38.228	1.52	0.04957	0.80	166.4	2.5
Qinghu@3	1743	757	53	0.43	39.032	1.50	0.04990	0.74	163.0	2.4
~~Qinghu@4~~	~~830~~	~~352~~	~~25~~	~~0.42~~	~~37.426~~	~~1.51~~	~~0.08969~~	~~1.30~~	~~161.3~~	~~2.7~~
Qinghu@5	1543	575	45	0.37	39.566	1.50	0.04908	0.87	160.9	2.4
Qinghu@6	1680	798	52	0.47	38.726	1.50	0.04934	1.05	164.3	2.5
Qinghu@7	2310	1137	72	0.49	38.521	1.50	0.04952	0.93	165.2	2.5
Qinghu@8	1751	770	53	0.44	38.694	1.50	0.04950	0.90	164.4	2.5
Qinghu@18	1238	462	36	0.37	40.219	1.50	0.04907	0.86	158.4	2.4
Qinghu@17	1447	587	42	0.41	40.534	1.50	0.04913	0.70	157.1	2.3
Qinghu@16	1801	772	54	0.43	40.036	1.50	0.04893	0.71	159.1	2.4
Qinghu@15	689	279	20	0.41	40.422	1.51	0.04927	1.02	157.5	2.4
Qinghu@14	2473	1854	92	0.75	37.660	1.51	0.04920	0.68	169.0	2.5
Qinghu@13	1764	613	52	0.35	39.708	1.50	0.04935	0.73	160.3	2.4
Qinghu@12	1414	576	41	0.41	40.067	1.50	0.05003	0.75	158.8	2.4
Qinghu@11	1880	962	57	0.51	39.965	1.50	0.04945	0.76	159.3	2.4
Qinghu@10	1320	500	39	0.38	39.931	1.50	0.04925	0.83	159.4	2.4
Qinghu@9	1500	704	45	0.47	40.028	1.51	0.04994	0.75	158.9	2.4
Qinghu@8	1228	494	36	0.40	40.134	1.50	0.04904	0.87	158.7	2.4
Qinghu@7	1676	826	51	0.49	39.834	1.53	0.04966	0.79	159.8	2.4
Qinghu@6	1206	743	38	0.62	39.739	1.59	0.04996	0.97	160.1	2.5
Qinghu@5	1727	971	54	0.56	39.211	1.51	0.04884	0.90	162.4	2.4
Qinghu@4	1094	590	33	0.54	40.356	1.51	0.04957	1.02	157.7	2.4
Qinghu@3	1068	454	31	0.42	40.432	1.50	0.04973	1.32	157.4	2.3
Qinghu@2	1285	679	40	0.53	39.316	1.50	0.04986	1.13	161.8	2.4
Qinghu@1	1164	548	35	0.47	40.026	1.50	0.04959	1.23	159.0	2.4
Qinghu@1	1139	609	35	0.54	39.934	1.62	0.04966	1.03	159.4	2.6
Qinghu@2	2065	905	62	0.44	39.775	1.55	0.04949	1.32	159.6	2.5
Qinghu@3	1948	908	58	0.47	39.989	1.50	0.04885	1.60	158.9	2.4
Qinghu@4	1790	887	52	0.50	40.947	1.52	0.04991	1.18	155.0	2.3

Qinghu@5	736	398	22	0.54	40.732	1.50	0.04933	1.63	155.9	2.3
Qinghu@6	1831	887	55	0.48	39.504	1.50	0.04991	1.04	160.6	2.4
Qinghu@7	2494	1238	78	0.50	38.620	1.51	0.05054	0.83	164.1	2.5
~~Qinghu@8~~	~~735~~	~~332~~	~~22~~	~~0.45~~	~~39.949~~	~~1.53~~	~~0.05475~~	~~1.83~~	~~157.8~~	~~2.4~~
Qinghu@9	1088	356	31	0.33	39.969	1.52	0.04915	1.37	158.9	2.4

Note: Qinghu represents external standardization (Li et al., 2009) during zircon SIMS U-Pb dating

Li, X.H. et al. Precise determination of Phanerozoic zircon Pb/Pb age by multicollector SIMS without external standardization. Geochem. Geophys. Geosyst. 10, Q04010, doi: 10.1029/2009GC002400 (2009).

Magmatic record of India-Asia collision

Di-Cheng Zhu*, Qing Wang, Zhi-Dan Zhao, Sun-Lin Chung, Peter A. Cawood, Yaoling Niu, Sheng-Ao Liu, Fu-Yuan Wu, and Xuan-Xue Mo

Table S2 Zircon LA-ICPMS U-Pb age data reported in this study for the Linzizong volcanic rocks in Linzhou Basin

	CORRECTED RATIOS										CORRECTED AGES (Ma)							
Analyses	$^{207}Pb/^{206}Pb$	1σ	$^{207}Pb/^{235}U$	1σ	$^{206}Pb/^{238}U$	1σ	$^{208}Pb/^{232}Th$	1σ	$^{238}U/^{232}Th$	1σ	$^{207}Pb/^{206}Pb$	1σ	$^{207}Pb/^{235}U$	1σ	$^{206}Pb/^{238}U$	1σ	$^{208}Pb/^{232}Th$	1σ
12LZ06-1-01	0.04161	0.00341	0.05255	0.00458	0.00913	0.00017	0.00289	0.00010	1.03	0.01	-198	142	52	4	59	1	58	2
12LZ06-1-02	0.05038	0.00365	0.06085	0.00426	0.00903	0.00015	0.00281	0.00009	0.91	0.01	213	128	60	4	58	1	57	2
12LZ06-1-03	0.05813	0.00441	0.07350	0.00540	0.00913	0.00018	0.00271	0.00012	1.19	0.01	535	128	72	5	59	1	55	2
12LZ06-1-04	0.06786	0.00693	0.08227	0.00714	0.00918	0.00020	0.00290	0.00013	1.07	0.01	864	145	80	7	59	1	58	3
12LZ06-1-05	0.06452	0.00681	0.07259	0.00666	0.00905	0.00019	0.00271	0.00015	1.43	0.01	759	160	71	6	58	1	55	3
12LZ06-1-06	0.05575	0.00884	0.07214	0.01129	0.00938	0.00024	0.00292	0.00006	1.22	0.01	442	348	71	11	60	2	59	1
12LZ06-1-07	0.05250	0.00563	0.06812	0.00855	0.00905	0.00027	0.00325	0.00022	0.92	0.01	307	228	67	8	58	2	66	5
12LZ06-1-08	0.05209	0.00448	0.06477	0.00549	0.00916	0.00019	0.00287	0.00013	1.18	0.01	289	155	64	5	59	1	58	3
12LZ06-1-09	0.05129	0.00414	0.06088	0.00417	0.00903	0.00015	0.00286	0.00011	1.14	0.01	254	127	60	4	58	0.9	58	2
12LZ06-1-10	0.06441	0.00580	0.07637	0.00681	0.00914	0.00024	0.00300	0.00020	1.8	0.02	755	145	75	6	59	2	61	4
12LZ06-1-11	0.04709	0.00336	0.05859	0.00410	0.00916	0.00015	0.00271	0.00011	1.25	0.01	54	122	58	4	58.8	1	55	2
12LZ06-1-12	0.04732	0.00281	0.06028	0.00374	0.00912	0.00013	0.00278	0.00010	1.45	0.01	65	109	59	4	58.5	0.8	56	2
12LZ06-1-13	0.05215	0.00389	0.06412	0.00451	0.00930	0.00017	0.00308	0.00012	1.18	0.01	292	128	63	4	60	1	62	2
~~12LZ06-1-14~~	~~0.04850~~	~~0.00173~~	~~0.32266~~	~~0.01139~~	~~0.04792~~	~~0.00052~~	~~0.01439~~	~~0.00044~~	~~2.97~~	~~0.03~~	~~124~~	~~62~~	~~284~~	~~9~~	~~302~~	~~3~~	~~289~~	~~9~~
12LZ06-1-15	0.04830	0.00323	0.05933	0.00383	0.00911	0.00016	0.00277	0.00010	1.04	0.01	114	112	59	4	58	1	56	2
12LZ06-1-16	0.06358	0.00547	0.07582	0.00586	0.00906	0.00017	0.00290	0.00012	0.99	0.01	728	133	74	6	58	1	59	2
12LZ06-1-17	0.06301	0.00442	0.07642	0.00525	0.00907	0.00017	0.00285	0.00013	1.09	0.01	708	115	75	5	58	1	57	3
12LZ06-1-18	0.05802	0.00767	0.07171	0.00936	0.00896	0.00018	0.00278	0.00004	1.62	0.02	531	301	70	9	58	1	56.1	0.9
~~12LZ23-1-01~~	~~0.04719~~	~~0.00508~~	~~0.04100~~	~~0.00438~~	~~0.00630~~	~~0.00009~~	~~0.00200~~	~~0.00009~~	~~1.41~~	~~0.01~~	~~59~~	~~226~~	~~41~~	~~4~~	~~40.5~~	~~0.5~~	~~40~~	~~2~~
12LZ23-1-02	0.05175	0.00591	0.05455	0.00574	0.00772	0.00017	0.00199	0.00013	1.6	0.02	275	196	54	6	50	1	40	3
12LZ23-1-03	0.04463	0.00226	0.04750	0.00243	0.00768	0.00010	0.00242	0.00007	1.51	0.02	-38	82	47	2	49.3	0.7	49	2
12LZ23-1-04	0.04795	0.00303	0.05162	0.00329	0.00781	0.00011	0.00267	0.00010	1.91	0.02	97	114	51	3	50.1	0.7	54	2
12LZ23-1-05	0.04927	0.00337	0.05168	0.00338	0.00773	0.00013	0.00258	0.00012	1.95	0.02	161	116	51	3	49.7	0.8	52	2
12LZ23-1-06	0.05853	0.00415	0.06194	0.00430	0.00775	0.00014	0.00241	0.00011	1.26	0.01	550	122	61	4	49.7	0.9	49	2
12LZ23-1-07	0.04249	0.00297	0.04531	0.00319	0.00789	0.00016	0.00235	0.00011	1.68	0.02	-150	118	45	3	51	1	48	2
12LZ23-1-08	0.04917	0.00283	0.05123	0.00270	0.00772	0.00011	0.00227	0.00008	1.18	0.01	156	94	51	3	49.6	0.7	46	2
~~12LZ23-1-09~~	~~0.06359~~	~~0.00657~~	~~0.06958~~	~~0.00724~~	~~0.00790~~	~~0.00022~~	~~0.00223~~	~~0.00015~~	~~1.71~~	~~0.02~~	~~728~~	~~174~~	~~68~~	~~7~~	~~51~~	~~1~~	~~45~~	~~3~~
12LZ23-1-10	0.05340	0.00288	0.05756	0.00308	0.00779	0.00010	0.00240	0.00007	1.34	0.01	346	98	57	3	50	0.6	48	1
12LZ23-1-11	0.05575	0.00388	0.05780	0.00392	0.00772	0.00014	0.00238	0.00010	1.26	0.01	442	120	57	4	49.6	0.9	48	2
12LZ23-1-12	0.05323	0.00382	0.05507	0.00391	0.00767	0.00013	0.00234	0.00010	1.23	0.01	339	130	54	4	49.3	0.9	47	2
12LZ23-1-13	0.04400	0.00231	0.04667	0.00240	0.00776	0.00012	0.00223	0.00007	1.32	0.01	-71	81	46	2	49.8	0.8	45	1

12LZ23-1-14	0.04633	0.00211	0.04972	0.00240	0.00768	0.00011	0.00227	0.00008	1.45	0.01	15	76	49	2	49.3	0.7	46	2
12LZ23-1-15	0.04942	0.00222	0.05302	0.00236	0.00777	0.00011	0.00223	0.00006	1.05	0.01	168	78	52	2	49.9	0.7	45	1
12LZ23-1-16	0.04168	0.00220	0.04426	0.00240	0.00769	0.00012	0.00208	0.00007	1.23	0.01	-194	95	44	2	49.4	0.8	42	1
12LZ23-1-17	0.04982	0.00344	0.05170	0.00325	0.00774	0.00013	0.00227	0.00007	1.07	0.01	187	113	51	3	49.7	0.8	46	1
12LZ23-1-18	0.04987	0.00292	0.05302	0.00300	0.00775	0.00011	0.00224	0.00007	1.03	0.01	189	104	52	3	49.8	0.7	45	1
13LZ06-1-01	0.04654	0.00363	0.05079	0.00387	0.00790	0.00012	0.00265	0.00009	1.64	0.02	26	140	50	4	50.8	0.7	54	2
13LZ06-1-02	0.05084	0.00230	0.05432	0.00244	0.00780	0.00009	0.00243	0.00006	0.99	0.01	234	83	54	2	50.1	0.6	49	1
13LZ06-1-03	0.04989	0.00344	0.05300	0.00353	0.00785	0.00014	0.00233	0.00009	1.32	0.01	190	119	52	3	50.4	0.9	47	2
13LZ06-1-04	0.04688	0.00239	0.05098	0.00271	0.00789	0.00010	0.00247	0.00007	0.99	0.01	43	92	50	3	50.7	0.6	50	1
~~13LZ06-1-05~~	~~0.04390~~	~~0.00398~~	~~0.05186~~	~~0.00467~~	~~0.00869~~	~~0.00012~~	~~0.00298~~	~~0.00009~~	~~1.18~~	~~0.01~~	~~-76~~	~~160~~	~~51~~	~~5~~	~~55.8~~	~~0.8~~	~~60~~	~~2~~
13LZ06-1-06	0.04805	0.00351	0.05201	0.00375	0.00787	0.00012	0.00264	0.00009	1.57	0.02	102	131	51	4	50.5	0.8	53	2
13LZ06-1-07	0.04455	0.00246	0.04848	0.00274	0.00782	0.00011	0.00251	0.00007	1.47	0.01	-42	94	48	3	50.2	0.7	51	2
13LZ06-1-08	0.04756	0.00316	0.05173	0.00335	0.00791	0.00012	0.00257	0.00009	1.37	0.01	77	115	51	3	50.8	0.7	52	2
13LZ06-1-09	0.04728	0.00388	0.05027	0.00405	0.00784	0.00012	0.00239	0.00007	0.86	0.01	63	148	50	4	50.3	0.8	48	1
13LZ06-1-10	0.04332	0.00297	0.04663	0.00318	0.00780	0.00010	0.00244	0.00006	0.66	0.01	-106	126	46	3	50.1	0.6	49	1
~~13LZ06-1-11~~	~~0.05666~~	~~0.00694~~	~~0.06053~~	~~0.00731~~	~~0.00775~~	~~0.00016~~	~~0.00241~~	~~0.00003~~	~~1.2~~	~~0.01~~	~~478~~	~~279~~	~~60~~	~~7~~	~~50~~	~~1~~	~~48.6~~	~~0.7~~
13LZ06-1-12	0.04852	0.00308	0.05205	0.00328	0.00787	0.00012	0.00257	0.00009	1.2	0.01	125	114	52	3	50.6	0.8	52	2
13LZ06-1-13	0.05220	0.00448	0.05443	0.00449	0.00786	0.00013	0.00244	0.00009	1.16	0.01	294	157	54	4	50.4	0.8	49	2
13LZ06-1-14	0.05118	0.00426	0.05570	0.00463	0.00791	0.00012	0.00242	0.00008	1.11	0.01	249	161	55	4	50.8	0.8	49	2
13LZ06-1-15	0.04663	0.00253	0.05141	0.00299	0.00790	0.00013	0.00275	0.00010	1.52	0.02	30	96	51	3	50.7	0.8	55	2
13LZ06-1-16	0.05049	0.00359	0.05479	0.00383	0.00783	0.00012	0.00258	0.00009	0.98	0.01	218	130	54	4	50.3	0.8	52	2
13LZ06-1-17	0.04805	0.00290	0.05176	0.00315	0.00786	0.00011	0.00256	0.00008	1.43	0.01	102	109	51	3	50.5	0.7	52	2
13LZ06-1-18	0.04763	0.00311	0.05081	0.00318	0.00788	0.00011	0.00251	0.00007	0.95	0.01	81	112	50	3	50.6	0.7	51	1

Magmatic record of India-Asia collision

Di-Cheng Zhu*, Qing Wang, Zhi-Dan Zhao, Sun-Lin Chung, Peter A. Cawood, Yaoling Niu, Sheng-Ao Liu, Fu-Yuan Wu, and Xuan-Xue Mo

Table S3 Zircon U-Pb age data of the 80-40 Ma intrusive rocks from the Gangdese Batholith (85–95°E) in southern Tibet

No.	Sample	Longitude	Latitude	Rock Type	SiO_2 (wt%)	Zircon U-Pb age (Ma)	± 2σ	References
1	06FW101	91.11	29.69	Monzogranite	72.29	64.7	1.1	Ji et al., 2012, Journal of Asian Earth Sciences 53, 82–95
2	06FW104	91.08	29.68	Monzogranite	71.71	64.4	0.9	Ji et al., 2012, Journal of Asian Earth Sciences 53, 82–95
3	06FW105	90.93	29.68	Granodiorite	67.62	55.2	1.5	Ji et al., 2012, Journal of Asian Earth Sciences 53, 82–95
4	06FW108	90.78	29.76	Diorite	62.25	56.8	0.7	Ji et al., 2012, Journal of Asian Earth Sciences 53, 82–95
5	06FW110	90.83	29.74	Monzogranite	73.45	54.3	0.9	Ji et al., 2012, Journal of Asian Earth Sciences 53, 82–95
6	06FW111	90.96	29.44	Monzogranite	66.49	50.6	0.7	Ji et al., 2012, Journal of Asian Earth Sciences 53, 82–95
7	06FW112	90.96	29.49	Granodiorite	60.23	53.4	1.0	Ji et al., 2012, Journal of Asian Earth Sciences 53, 82–95
8	06FW119	90.94	29.50	Granodiorite	63.91	51.2	0.7	Ji et al., 2012, Journal of Asian Earth Sciences 53, 82–95
9	06FW126	90.87	29.48	Diorite	56.62	55.3	1.0	Ji et al., 2012, Journal of Asian Earth Sciences 53, 82–95
10	06FW127	90.87	29.48	Granitic dike	77.16	49.5	0.6	Ji et al., 2012, Journal of Asian Earth Sciences 53, 82–95
11	06FW129	90.90	29.46	Diorite	57.43	52.9	0.7	Ji et al., 2012, Journal of Asian Earth Sciences 53, 82–95
12	06FW131	90.91	29.41	Granodiorite	69.90	44.0	0.8	Ji et al., 2012, Journal of Asian Earth Sciences 53, 82–95
13	06FW133	90.87	29.33	Monzonite	67.45	47.1	1.0	Ji et al., 2012, Journal of Asian Earth Sciences 53, 82–95
14	06FW134	90.88	29.36	Monzogranite	70.57	41.9	0.6	Ji et al., 2012, Journal of Asian Earth Sciences 53, 82–95
15	06FW139	90.72	29.38	Diorite	61.01	41.5	0.7	Ji et al., 2012, Journal of Asian Earth Sciences 53, 82–95
16	06FW140	90.72	29.47	Monzogranite	70.99	43.7	0.9	Ji et al., 2012, Journal of Asian Earth Sciences 53, 82–95
17	06FW146	90.72	29.40	Gabbro	52.88	56.9	1.4	Ji et al., 2012, Journal of Asian Earth Sciences 53, 82–95
18	06FW148	90.72	29.37	Monzogranite	71.69	51.3	0.6	Ji et al., 2012, Journal of Asian Earth Sciences 53, 82–95
19	06FW151	90.72	29.36	Diorite	56.09	55.5	1.2	Ji et al., 2012, Journal of Asian Earth Sciences 53, 82–95
20	06FW152-2	90.18	29.40	Diorite	53.49	57.3	0.9	Ji et al., 2012, Journal of Asian Earth Sciences 53, 82–95
21	06FW154	90.27	29.58	Monzogranite	75.43	51.3	0.7	Ji et al., 2012, Journal of Asian Earth Sciences 53, 82–95
22	06FW155	90.18	29.54	Bi-monzogranite	70.33	61.1	1.2	Ji et al., 2012, Journal of Asian Earth Sciences 53, 82–95
23	06FW156	90.27	29.50	Granodiorite	67.99	55.4	0.8	Ji et al., 2012, Journal of Asian Earth Sciences 53, 82–95
24	06FW162	89.62	29.54	Diorite	60.29	50.9	0.8	Ji et al., 2012, Journal of Asian Earth Sciences 53, 82–95
25	06FW174	90.10	29.35	Diorite	56.45	50.2	1.5	Ji et al., 2012, Journal of Asian Earth Sciences 53, 82–95
26	06FW175	90.07	29.35	Diorite	57.57	52.6	1.2	Ji et al., 2012, Journal of Asian Earth Sciences 53, 82–95

27	06FW176	90.25	29.33	Diorite	54.48	53.6	1.0	Ji et al., 2012, Journal of Asian Earth Sciences 53, 82–95
28	08CQ02	85.74	29.63	Monzogranite	78.07	43.9	0.3	Zhu et al., 2011, Earth and Planetary Science Letters 301, 241–255
29	08CQ03	85.76	29.78	Monzogranite	67.92	51.9	0.4	Zhu et al., 2011, Earth and Planetary Science Letters 301, 241–255
30	08CQ09	85.74	29.90	Monzogranite	68.52	50.0	0.4	Zhu et al., 2011, Earth and Planetary Science Letters 301, 241–255
31	08DX01	90.57	30.01	Diorite	55.57	69.8	0.7	Zhu et al., unpublished data
32	08FW50	91.18	29.64	Granodiorite	68.13	67.1	4.1	Ji, W.Q., 2010, Ph.D thesis, p. 1–146
33	08FW54	91.99	29.73	Diorite	54.83	65.6	1.4	Ji, W.Q., 2010, Ph.D thesis, p. 1–146
34	08FW56	92.20	29.71	Monzogranite	65.58	70.5	2.1	Ji, W.Q., 2010, Ph.D thesis, p. 1–146
35	08FW60	93.78	29.81	Monzogranite	77.24	47.6	2.5	Ji, W.Q., 2010, Ph.D thesis, p. 1–146
36	08FW61	94.01	29.76	Bi granite	75.98	53.8	1.4	Ji, W.Q., 2010, Ph.D thesis, p. 1–146
37	08FW62	94.29	29.74	Granodiorite	74.05	72.7	3.8	Ji, W.Q., 2010, Ph.D thesis, p. 1–146
38	08FW63	94.19	29.75	Granodiorite	73.05	53.0	3.8	Ji, W.Q., 2010, Ph.D thesis, p. 1–146
39	08FW66	92.04	29.72	Syenogranite	76.03	70.1	2.7	Ji, W.Q., 2010, Ph.D thesis, p. 1–146
40	09FW10	93.31	29.62	Gneissic granodiorite	65.52	66.2	1.1	Ji, W.Q., 2010, Ph.D thesis, p. 1–146
41	09FW30	93.20	29.15	Two mica monzogranite	72.25	76.7	1.6	Ji, W.Q., 2010, Ph.D thesis, p. 1–146
42	09FW33	93.18	29.12	Two mica monzogranite	79.70	79.7	1.3	Ji, W.Q., 2010, Ph.D thesis, p. 1–146
43	09FW41	92.74	29.42	Monzogranite	70.44	56.1	1.1	Ji, W.Q., 2010, Ph.D thesis, p. 1–146
44	09FW42	92.75	29.41	Granitic gneiss	69.74	50.7	1.1	Ji, W.Q., 2010, Ph.D thesis, p. 1–146
45	09FW43	92.75	29.41	Monzogranite	70.66	42.0	0.7	Ji, W.Q., 2010, Ph.D thesis, p. 1–146
46	09FW50	92.70	29.24	Monzogranite	67.85	50.2	0.9	Ji, W.Q., 2010, Ph.D thesis, p. 1–146
47	10CK-02	86.14	30.37	Granodiorite	68.00	65.2	0.5	Wang et al., 2012, Acta Petrologica Sinica, 28(5), 1647–1662
48	11LS01-1	90.94	29.50	Gabbro	50.13	47.3	0.4	Zhu et al., unpublished data
49	11LS06-1	90.71	29.36	Gabbro	54.35	46.2	1.5	Zhu et al., unpublished data
50	12AM04-2	86.32	29.63	Gabbro	52.03	44.8	0.2	Zhu et al., unpublished data
51	12AM06-2	86.32	29.58	Monzogranite	73.02	51.2	0.6	Zhu et al., unpublished data
52	12CZ15-1	86.75	29.75	Granodiorite	79.14	60.8	0.6	Zhu et al., unpublished data
53	12DJ08-1	87.79	29.44	Gabbro	66.09	51.8	0.5	Zhu et al., unpublished data
54	12DJ12-1	87.87	29.43	Monzogranite	66.72	44.3	0.4	Zhu et al., unpublished data
55	12LY00-1	89.24	29.72	Granodiorite	77.02	51.0	0.5	Zhu et al., unpublished data
56	12PC30-1	87.99	29.36	Granodiorite		52.3	0.6	Zhu et al., unpublished data
57	13WBD	89.55	29.29	Diabase dyke		49.8	1.3	Wang et al., 2013, Personal communication
58	D093TW	92.72	29.63	Granodiorite	68.90	70.4	2.2	Chen et al., 2010, Journal of Mineral and Petrology 30(1), 83–92
59	ET021D	91.63	29.69	Monzogranite	71.60	64.6	2.5	Wen, D.R., 2007, Ph.D thesis, National Taiwan University, p. 1–120
60	GR-20	93.42	29.08	Granite		68.0	4.0	Quidelleur et al., 1997, Journal of Geophysical Research 102(B2), 2659–2679

61	LS2	91.00	29.89	Granite	69.59	51.0	1.2	Huang et al., 2010. Acta Petrologica Sinica 26, 10, 3131–3142
62	LS5	91.24	29.69	Dioritie	56.09	61.0	2.9	Huang et al., 2010. Acta Petrologica Sinica 26, 10, 3131–3142
63	LZ09-2	94.47	29.55	Granite	75.22	51.4	1.4	Ji, W.Q., 2010, Ph.D thesis, p. 1–146
64	LZ11-1	94.46	29.46	Granodiorite	73.11	44.3	0.8	Ji, W.Q., 2010, Ph.D thesis, p. 1–146
65	LZ15-5	94.35	29.63	Dioritic enclave	55.22	64.0	1.2	Ji, W.Q., 2010, Ph.D thesis, p. 1–146
66	LZ16-2	94.37	29.60	Granodiorite	61.56	67.4	1.4	Ji, W.Q., 2010, Ph.D thesis, p. 1–146
67	LZ17-1	94.43	29.46	Two-mica monzogranite	73.23	51.7	1.0	Ji, W.Q., 2010, Ph.D thesis, p. 1–146
68	ML06-1	93.37	29.05	Granodiorite	70.58	79.3	0.4	Zhu et al., 2011, Earth and Planetary Science Letters 301, 241–255
69	ML07-1	93.52	29.17	Granodiorite	69.88	73.5	1.2	Ji, W.Q., 2010, Ph.D thesis, p. 1–146
70	ML08-1	93.47	29.15	Bt monzogranite	74.08	73.0	1.7	Ji, W.Q., 2010, Ph.D thesis, p. 1–146
71	ML09-1	93.38	29.06	Bt monzogranite	72.48	78.0	1.3	Ji, W.Q., 2010, Ph.D thesis, p. 1–146
72	ML11-1	93.12	29.11	Two-mica monzogranite	72.15	75.0	1.3	Ji, W.Q., 2010, Ph.D thesis, p. 1–146
73	ML18-4	93.68	29.15	Diorite	54.80	38.5	0.3	Guan et al., 2012, Gondwana Research 21, 88–99
74	ML19-1	93.75	29.13	Granodiorite	70.68	78.1	0.6	Guan et al., 2010, Acta Petrologica Sinica 26, 2165–2179
75	ML25-1	94.43	29.46	Syenogranite	76.11	56.7	1.0	Zhu et al., unpublished data
76	ML26-1	94.35	29.63	Granodiorite	66.17	64.8	0.5	Zhu et al., unpublished data
77	ML28-1	94.24	29.76	Bi monzogranite	70.23	53.4	0.4	Zhu et al., unpublished data
78	ML30-1	93.78	29.81	Granite	76.60	42.0	0.4	Zhu et al., unpublished data
79	ML37-1	93.30	29.60	Bi monzogranite	70.96	70.1	0.4	Zhu et al., unpublished data
80	ML38-2	93.30	29.60	Gabbroic enclave	48.23	69.5	0.7	Zhu et al., unpublished data
81	NB-159	94.70	29.75	Diorite	58.61	66.0	1.9	Booth et al., 2004, American Journal of Science 304, 889–929
82	NM01	89.08	29.54	Diorite	60.53	44.3	1.1	Cong et al., 2012, Journal of Jilin University 42 (6), 1783–1795
83	NM02	89.10	29.49	Granodiorite	65.28	45.5	1.1	Cong et al., 2012, Journal of Jilin University 42 (6), 1783–1795
84	NML03-1	89.06	29.62	Diorite	58.03	62.4	0.3	Zhu et al., 2011, Earth and Planetary Science Letters 301, 241–255
85	PD2-12	92.24	29.62	Syenogranite	77.26	66.6	0.7	Liu et al., 2012, Mineral Deposits 31, 4, 727–744
86	RB12	89.69	29.36	Diorite	54.73	45.0	1.6	Huang et al., 2010. Acta Petrologica Sinica 26, 10, 3131–3142
87	SR01-1	92.10	29.29	Granodiorite	62.52	45.4	0.7	Ji et al., 2012, Journal of Asian Earth Sciences 53, 82–95
88	SR02-1	92.12	29.29	Granite	72.05	37.7	0.7	Ji et al., 2012, Journal of Asian Earth Sciences 53, 82–95
89	SR03-1	92.22	29.27	Granodiorite	71.48	59.8	0.9	Ji et al., 2012, Journal of Asian Earth Sciences 53, 82–95
90	SR04-1	92.24	29.32	Granodiorite	61.81	42.1	0.7	Ji et al., 2012, Journal of Asian Earth Sciences 53, 82–95
91	ST043A	88.23	29.45	Granodiorite	63.60	50.4	1.2	Wen et al., 2008, Chemical Geology 252, 191–201
92	ST104A	91.81	29.27	Granodiorite	65.58	60.1	1.4	Chu et al., 2006, Geology 34, 745–748
93	ST147A	90.18	29.40	Diorite	53.87	50.6	0.7	Wen et al., 2008, Chemical Geology 252, 191–201
94	ST152A	90.69	29.33	Gabbro	49.75	52.7	1.4	Wen et al., 2008, Chemical Geology 252, 191–201

95	SWYT-1	91.69	29.87	Monzogranite		61.0	1.9	Luo et al., 2011, Mineral Deposits 30(2), 266–278
96	T024	93.75	29.14	Tonalite	69.53	80.4	1.1	Wen, D.R., 2007, Ph.D thesis, National Taiwan University, p. 1–120
97	T044E	89.08	29.49	Gabbro	52.10	48.0	1.2	Wen et al., 2008, Chemical Geology 252, 191–201
98	T076	91.22	29.67	Granodiorite	69.90	59.3	1.6	Wen et al., 2008, Chemical Geology 252, 191–201
99	T10-123-2	94.41	29.61	Two-mica granite	75.57	61.9	0.4	Zhang et al., 2013, Journal of Petrology 54, 12, 2547–2580
100	T10-74-2	94.71	29.64	Grt-Bt-Amp gneiss	55.24	61.3	1.2	Zhang et al., 2013, Journal of Petrology 54, 12, 2547–2580
101	T10-94-10	93.89	29.21	Gabbro	51.75	77.3	2.5	Zhang et al., 2014, Geochimica et Cosmochimica Acta, In press
102	T10-95-2	93.91	29.19	Pegimatite		68.2	1.2	Zhang et al., 2014, Geochimica et Cosmochimica Acta, In press
103	T308	90.93	29.48	Monzogranite	64.95	50.7	0.5	Xu, W.C., 2010. Ph.D thesis, China University of Geosciences (Wuhan), p. 1–172
104	T315	90.87	29.38	Granodiorite	59.77	40.5	0.5	Xu, W.C., 2010. Ph.D thesis, China University of Geosciences (Wuhan), p. 1–172
105	T316	90.87	29.38	Qtz diorite	61.49	47.1	0.7	Xu, W.C., 2010. Ph.D thesis, China University of Geosciences (Wuhan), p. 1–172
106	T364	90.27	29.51	Monzogranite	69.97	46.7	0.7	Xu, W.C., 2010. Ph.D thesis, China University of Geosciences (Wuhan), p. 1–172
107	T377	90.06	29.51	Granodiorite	66.43	54.1	1.3	Xu, W.C., 2010. Ph.D thesis, China University of Geosciences (Wuhan), p. 1–172
108	T390	90.12	29.35	Qtz diorite	61.02	48.5	0.8	Xu, W.C., 2010. Ph.D thesis, China University of Geosciences (Wuhan), p. 1–172
109	T392	88.37	29.95	Monzogranite	70.66	47.9	1.1	Xu, W.C., 2010. Ph.D thesis, China University of Geosciences (Wuhan), p. 1–172
110	T405	88.32	29.56	Monzogranite	68.88	49.0	1.0	Xu, W.C., 2010. Ph.D thesis, China University of Geosciences (Wuhan), p. 1–172
111	T420	87.45	29.38	Granodiorite	63.24	48.1	0.6	Xu, W.C., 2010. Ph.D thesis, China University of Geosciences (Wuhan), p. 1–172
112	T426	86.21	29.6	Monzogranite	67.72	50.5	0.8	Xu, W.C., 2010. Ph.D thesis, China University of Geosciences (Wuhan), p. 1–172
113	T439	89.10	29.46	Granodiorite	65.92	49.4	1.0	Xu, W.C., 2010. Ph.D thesis, China University of Geosciences (Wuhan), p. 1–172
114	T445	89.06	29.62	Monzogranite	74.36	40.7	0.5	Xu, W.C., 2010. Ph.D thesis, China University of Geosciences (Wuhan), p. 1–172
115	T446	89.06	29.63	Granodiorite	64.67	50.9	1.1	Xu, W.C., 2010. Ph.D thesis, China University of Geosciences (Wuhan), p. 1–172
116	T478	90.93	29.67	Monzogranite	67.58	46.4	0.8	Xu, W.C., 2010. Ph.D thesis, China University of Geosciences (Wuhan), p. 1–172
117	T479	90.60	30.04	Two-mica granite	71.22	49.6	0.6	Xu, W.C., 2010. Ph.D thesis, China University of Geosciences (Wuhan), p. 1–172
118	T490	91.98	29.73	Monzogranite	71.45	65.3	1.2	Xu, W.C., 2010. Ph.D thesis, China University of Geosciences (Wuhan), p. 1–172
119	T497	92.15	29.71	Granodiorite	64.12	67.7	1.2	Xu, W.C., 2010. Ph.D thesis, China University of Geosciences (Wuhan), p. 1–172
120	T529	94.43	29.45	Granitic gneiss	73.93	49.1	0.4	Xu, W.C., 2010. Ph.D thesis, China University of Geosciences (Wuhan), p. 1–172
121	T556	92.20	29.30	Monzogranite	69.71	59.7	0.6	Xu, W.C., 2010. Ph.D thesis, China University of Geosciences (Wuhan), p. 1–172
122	T560	93.18	29.26	Granite	70.00	60.9	0.9	Xu, W.C., 2010. Ph.D thesis, China University of Geosciences (Wuhan), p. 1–172
123	T670	94.44	29.55	Granitic gneiss	71.72	80.5	0.7	Guo et al., 2011, Lithos 127, 54–67
124	T8-15-2	94.01	29.30	Granodiorite	70.46	63.0	0.6	Zhang et al., 2013, Journal of Petrology 54, 12, 2547–2580
125	T9-33-5	94.44	29.55	Ep granodiorite	68.42	64.8	1.3	Zhang et al., 2013, Journal of Petrology 54, 12, 2547–2580
126	T9-33-7	94.44	29.55	Grt two-mica granodiorite	69.31	54.9	0.8	Zhang et al., 2013, Journal of Petrology 54, 12, 2547–2580
127	T9-62-1	94.45	29.43	Grt-Bt gneiss	64.27	63.6	1.8	Zhang et al., 2013, Journal of Petrology 54, 12, 2547–2580

Magmatic record of India-Asia collision

Di-Cheng Zhu*, Qing Wang, Zhi-Dan Zhao, Sun-Lin Chung, Peter A. Cawood, Yaoling Niu, Sheng-Ao Liu, Fu-Yuan Wu, and Xuan-Xue Mo

Table S4 Geochemical data of the Linzizong volcanic rocks in Linzhou Basin*

Sample	Rock type	Latitude	Longitude	Strata		Age	$[SiO_2]$	$[TiO_2]$	$[Al_2O_3]$	$[Fe_2O_3]$	[MnO]	[MgO]	[CaO]	$[Na_2O]$	$[K_2O]$	$[P_2O_5]$	LOI	Zr/Y	Zr (ppm)	Zircon saturation temperature (°C)	References
12LZ02-1	Andesite	29.95	91.20	Dianzhong	E1d	60.2	63.15	0.69	16.89	5.79	0.11	2.16	5.51	2.97	2.54	0.19	4.26		122	739	This study
12LZ03-1	Andesite	29.95	91.20	Dianzhong	E1d	60.2	63.45	0.67	16.67	5.56	0.12	2.09	5.69	3.16	2.40	0.19	3.87		122	734	This study
12LZ04-1	Andesite	29.95	91.20	Dianzhong	E1d	60.2	64.12	0.66	16.81	5.22	0.13	1.57	5.44	3.28	2.60	0.19	4.30		123	738	This study
12LZ06-1	Dacite	29.95	91.20	Dianzhong	E1d	58.5	66.01	0.69	16.46	5.85	0.06	1.77	4.62	2.95	1.42	0.19	2.59		103	747	This study
12LZ07-1	Andesite	29.95	91.20	Dianzhong	E1d	58.5	63.23	0.69	17.00	5.68	0.10	1.98	5.16	3.38	2.59	0.19	2.58		126	741	This study
12LZ08-1	Andesite	29.95	91.20	Dianzhong	E1d	58.5	60.21	0.82	17.51	7.14	0.10	1.93	6.35	3.32	2.41	0.22	4.73		133	731	This study
12LZ09-1	Andesite	29.95	91.20	Dianzhong	E1d	58.5	59.86	0.82	17.52	7.36	0.12	2.71	6.14	3.09	2.17	0.22	3.92		135	739	This study
12LZ10-1	Andesite	29.96	91.21	Dianzhong	E1d	58.5	60.58	0.80	17.41	7.17	0.15	2.77	5.40	3.35	2.13	0.22	3.38		138	747	This study
12LZ11-1	Andesite	29.96	91.21	Dianzhong	E1d	58.5	63.52	0.71	17.11	6.01	0.14	2.03	5.02	3.75	1.52	0.19	6.82		119	743	This study
12LZ12-1	Andesite	29.97	91.18	Dianzhong	E1d	58.5	57.41	0.90	18.45	8.39	0.12	1.64	6.26	3.33	3.26	0.24	6.30		105	709	This study
13LZ01-1	Andesite	29.95	91.20	Dianzhong	E1d	60.2	60.21	0.75	17.99	5.64	0.22	2.55	5.52	6.10	0.81	0.20	6.00		126	718	This study
13LZ02-1	Andesite	29.95	91.21	Dianzhong	E1d	60.2	56.78	0.87	19.42	7.14	0.27	2.55	8.50	3.06	1.13	0.27	4.66		122	717	This study
13LZ08-1	Andesite	29.98	91.19	Dianzhong	E1d	58.3	54.41	1.02	19.38	9.28	0.17	3.73	6.10	5.34	0.35	0.23	7.06				This study
D-2	Andesite	29.95	91.13	Dianzhong	E1d	58.5	60.02	0.71	16.25	8.64	0.15	3.71	3.72	4.17	2.42	0.19	3.62		136	746	Mo et al., 2008, Chemical Geology
D-15	Andesite	29.96	91.19	Dianzhong	E1d	58.5	59.04	0.69	16.19	9.89	0.15	2.57	6.60	2.78	1.91	0.17	4.22		118	717	Mo et al., 2008, Chemical Geology
BD-145	Andesite	29.95	91.20	Dianzhong	E1d	58.5	62.32	0.63	16.07	7.78	0.11	1.79	5.69	3.07	2.38	0.17	3.48		129	734	Mo et al., 2008, Chemical Geology
BD-151	Andesite	29.97	91.21	Dianzhong	E1d	58.5	58.38	0.65	18.33	8.49	0.11	1.94	8.05	2.65	1.22	0.18	4.56		156	742	Mo et al., 2008, Chemical Geology
BD-160	Andesite	29.96	91.18	Dianzhong	E1d	58.5	60.20	0.73	17.53	7.88	0.10	1.81	3.21	5.77	2.55	0.23	3.07		134	740	Mo et al., 2008, Chemical Geology
T240B	Andesite	29.91	91.07	Dianzhong	E1d	60.2	61.07	0.86	17.89	6.43	0.11	2.54	5.69	1.77	3.45	0.20	1.93		199	788	Lee et al., 2012, JAES
T239	Andesite	29.91	91.08	Dianzhong	E1d	60.2	59.49	0.94	18.35	6.81	0.10	2.97	7.15	2.44	1.55	0.20	3.16		188	771	Lee et al., 2012, JAES
T238B	Andesite	29.96	91.15	Dianzhong	E1d	60.2	55.77	0.95	19.02	8.54	0.11	3.36	8.95	2.82	0.26	0.22	5.07		161	737	Lee et al., 2012, JAES
T233B	Andesite	29.95	91.20	Dianzhong	E1d	60.2	61.41	0.77	17.55	6.39	0.14	2.54	4.17	4.38	2.47	0.18	2.50		126	742	Lee et al., 2012, JAES
BD-55	Rhyolitic tuff	29.98	91.17	Nianbo	E2n	54.5	76.32	0.12	12.15	1.91	0.09	0.44	2.42	2.49	4.02	0.03	3.09		114	753	Mo et al., 2008, Chemical Geology
BD-65	Basalt	29.98	91.17	Nianbo	E2n	52.7	51.11	0.95	17.57	11.86	0.17	3.36	8.92	2.94	2.67	0.45	5.03	3.8			Mo et al., 2008, Chemical Geology
BD-77	Rhyolitic tuff	29.98	91.14	Nianbo	E2n	52.6	70.22	0.25	18.42	0.90	0.01	0.27	0.29	4.22	5.35	0.06	1.68		234	843	Mo et al., 2008, Chemical Geology
LZ991	Rhyolitic tuff	29.97	91.13	Nianbo	E2n	55.4	76.16	0.13	14.72	2.18	0.02	1.08	0.98	0.57	4.12	0.03	3.54		113	811	Mo et al., 2008, Chemical Geology
LZ9921	Rhyolitic tuff	29.98	91.19	Nianbo	E2n	54.9	77.32	0.13	12.45	2.20	0.03	0.47	2.36	2.39	2.61	0.03	3.68		95.6	757	Mo et al., 2008, Chemical Geology
L060	Rhyolitic tuff	29.98	91.19	Nianbo	E2n	54.9	79.44	0.12	11.68	1.53	0.04	0.21	1.64	3.54	1.76	0.03	2.12		112	769	Mo et al., 2008, Chemical Geology
12LZ27-1	Rhyolitic tuff	29.98	91.15	Nianbo	E2n	52.6	73.31	0.63	17.92	1.70	0.01	0.48	0.22	0.59	5.02	0.12	3.34		380	946	This study
12LZ28-1	Basalt	29.97	91.15	Nianbo	E2n	52.9	50.77	0.98	18.95	9.23	0.20	3.27	7.36	4.17	4.56	0.50	6.36	5.5			This study
12LZ29-1	Rhyolite	29.97	91.15	Nianbo	E2n	55.4	76.05	0.37	13.71	1.40	0.03	0.90	0.65	5.35	1.44	0.09	2.16		165	804	This study
13LZ10-1	Basalt	29.98	91.19	Nianbo	E2n	54.5	48.16	1.14	17.35	10.55	0.54	5.16	10.31	3.62	2.79	0.38	8.17	3.7			This study
13LZ11-1	Basalt	29.98	91.19	Nianbo	E2n	54.5	51.85	1.09	18.24	10.31	0.13	5.30	7.41	3.95	1.27	0.48	8.63	5.3			This study
13LZ12-1	Andesite	29.98	91.19	Nianbo	E2n	54.5	56.00	0.88	15.79	9.90	0.17	5.60	5.55	3.96	1.79	0.35	5.35		114	702	This study
13LZ14-1	Basaltic andesite	29.98	91.19	Nianbo	E2n	54.5	53.36	0.87	17.98	9.49	0.17	2.40	9.24	3.30	2.72	0.48	4.84	5.9			This study
13LZ15-1	Basaltic andesite	29.98	91.19	Nianbo	E2n	54.5	54.50	0.87	17.58	8.85	0.16	3.38	8.53	3.15	2.53	0.44	3.65				This study
13LZ16-1	Andesite	29.98	91.19	Nianbo	E2n	52.7	57.01	0.76	18.43	7.57	0.15	3.01	6.58	3.40	2.66	0.43	6.93		157	737	This study
T235B	Rhyolitic tuff	29.98	91.17	Nianbo	E2n	54.9	78.21	0.12	12.89	1.10	0.04	0.33	1.58	2.82	2.90	0.01	2.67		106	771	Lee et al., 2012, JAES
T235A	Rhyolitic tuff	29.98	91.17	Nianbo	E2n	54.9	78.24	0.12	13.24	1.34	0.02	0.39	0.70	2.71	3.23	0.01	2.23		141	810	Lee et al., 2012, JAES
T234C	Dacite	29.98	91.18	Nianbo	E2n	54.5	68.36	0.57	15.12	5.20	0.07	1.13	2.97	4.31	1.99	0.27	2.35		174	786	Lee et al., 2012, JAES
T234B	Basaltic andesite	29.98	91.18	Nianbo	E2n	54.5	53.07	0.88	18.54	9.39	0.16	3.20	8.78	3.02	2.50	0.44	3.91	6.2			Lee et al., 2012, JAES
T234A	Andesite	29.98	91.18	Nianbo	E2n	54.5	56.72	0.71	18.26	7.53	0.15	2.98	6.78	3.25	3.28	0.37	2.89		168	735	Lee et al., 2012, JAES

12LZ16-1	Basalt	29.98	91.19	Pa'na	E2p	52.7	52.80	0.91	18.74	9.52	0.13	2.93	8.66	3.34	2.49	0.49	4.66	6.7			This study
12LZ17-1	Basalt	29.98	91.19	Pa'na	E2p	52.7	52.73	0.89	18.20	9.33	0.14	3.82	8.54	3.41	2.46	0.48	2.93	6.0			This study
12LZ18-1	Rhyolite	29.98	91.19	Pa'na	E2p	52.7	70.65	0.47	14.46	3.74	0.15	0.98	2.14	3.14	4.15	0.12	4.05		152	781	This study
12LZ23-1	Rhyolitic ignimbrite	29.99	91.14	Pa'na	E2p	52.2	75.45	0.21	14.41	1.22	0.05	0.11	0.22	2.95	5.32	0.07	1.29		136	796	This study
12LZ24-1	Rhyolitic ignimbrite	29.99	91.14	Pa'na	E2p	52.2	74.74	0.19	14.23	1.23	0.07	0.25	0.37	3.31	5.55	0.06	0.89		135	785	This study
12LZ25-1	Rhyolite	29.99	91.14	Pa'na	E2p	52.2	71.11	0.35	15.32	2.27	0.05	0.33	1.49	3.11	5.86	0.12	2.50		270	835	This study
12LZ26-1	Rhyolitic ignimbrite	29.98	91.14	Pa'na	E2p	52.2	77.52	0.34	15.72	0.34	0.01	0.39	0.14	0.31	5.17	0.06	2.74		252	900	This study
13LZ06-1	Rhyolite	30.00	91.15	Pa'na	E2p	52.2	71.34	0.31	14.07	2.62	0.11	0.77	2.60	2.89	5.18	0.09	3.08		140	761	This study
13LZ07-1	Rhyolitic ignimbrite	29.99	91.14	Pa'na	E2p	52.2	76.15	0.19	13.49	1.34	0.02	0.16	0.21	2.82	5.57	0.05	0.89		119	780	This study
LZ9917	Rhyolitic ignimbrite	30.01	91.15	Pa'na	E2p	52.5	76.65	0.30	11.37	3.06	0.03	0.49	0.60	1.73	5.63	0.14	1.77		113	771	Mo et al., 2008, Chemical Geology
LZ9916	Rhyolitic ignimbrite	30.01	91.15	Pa'na	E2p	52.5	80.26	0.31	9.83	2.76	0.02	0.23	0.39	2.32	3.71	0.16	1.12		101	767	Mo et al., 2008, Chemical Geology
BD-103	Rhyolitic ignimbrite	30.01	91.14	Pa'na	E2p	52.5	70.22	0.37	14.02	3.72	0.10	0.87	2.87	2.93	4.76	0.14	3.39		150	764	Mo et al., 2008, Chemical Geology
BD-106	Rhyolitic ignimbrite	30.01	91.14	Pa'na	E2p	52.5	69.35	0.37	14.68	4.05	0.11	0.73	3.21	2.54	4.80	0.16	3.93		176	781	Mo et al., 2008, Chemical Geology
P-1	Rhyolitic ignimbrite	29.99	91.15	Pa'na	E2p	52.2	74.41	0.17	13.39	1.76	0.08	0.28	1.07	3.35	5.46	0.04	0.80		142	774	Mo et al., 2008, Chemical Geology
11LZ01-1	Diabase dyke	29.97	91.15			52.9	51.35	0.94	18.94	9.20	0.15	3.44	8.07	3.15	4.28	0.48	6.15	5.2			Jia et al., 2013
11LZ01-2	Diabase dyke	29.97	91.15			52.9	50.65	0.93	18.25	9.41	0.23	3.21	8.76	4.76	3.34	0.46	7.08	4.6			Jia et al., 2013
11LZ02-1	Diabase dyke	29.97	91.15			52.9	51.92	0.95	18.58	9.55	0.15	4.75	7.41	2.87	3.36	0.47	5.58	5.1			Jia et al., 2013
11LZ02-2	Diabase dyke	29.97	91.15			52.9	49.52	0.95	18.55	10.32	0.28	3.57	9.09	5.46	1.91	0.36	7.77	4.3			Jia et al., 2013
11LZ02-3	Diabase dyke	29.97	91.15			52.9	52.41	0.84	18.91	9.52	0.17	3.34	6.95	3.63	3.77	0.46	5.72	4.9			Jia et al., 2013
11LZ03-1	Diabase dyke	29.97	91.15			52.9	51.16	0.85	19.21	9.81	0.13	3.09	7.05	4.84	3.40	0.47	6.71	4.9			Jia et al., 2013
11LZ03-2	Diabase dyke	29.97	91.15			52.9	51.91	0.87	19.18	9.51	0.17	3.91	7.13	3.69	3.17	0.46	5.99	4.9			Jia et al., 2013
11LZ04-1	Diabase dyke	29.97	91.15			52.9	51.97	0.93	19.22	9.43	0.14	3.89	5.85	4.81	3.36	0.40	5.83	4.8			Jia et al., 2013
2003T320	Diabase dyke					52.9	50.94	1.02	17.82	10.18	0.16	5.29	7.78	2.91	3.44	0.46	4.75	5.2			Yue et al., 2006
2003T324	Diabase dyke					52.9	47.29	0.90	17.21	11.86	0.20	5.42	10.32	3.70	2.61	0.49	0.86	4.1			Yue et al., 2006
2003T348	Diabase dyke					52.9	49.60	1.01	17.86	11.15	0.17	4.39	10.45	2.39	2.56	0.42	7.08	4.6			Yue et al., 2006
2003T350	Diabase dyke					52.9	48.62	1.10	17.32	11.59	0.18	5.51	10.16	2.56	2.45	0.50	6.90	5.1			Yue et al., 2006
2003T353	Diabase dyke					52.9	49.78	1.07	18.62	10.85	0.19	3.04	10.67	2.94	2.37	0.46	6.23	4.8			Yue et al., 2006
2003T363	Diabase dyke					52.9	50.40	1.21	17.32	10.29	0.12	5.23	9.64	3.03	2.31	0.45	5.08	5.3			Yue et al., 2006

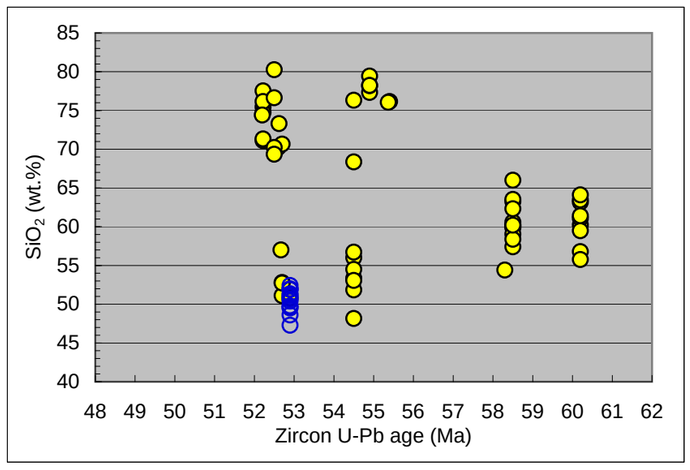

Fig. 3a Plot of SiO2 content versus age (Ma) for the Linzizong volcanic rocks in Linzhou Basin (see Table S4 for data)

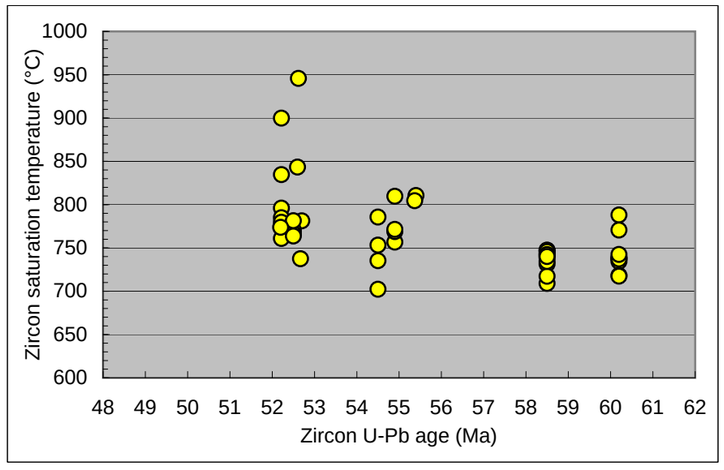

Fig. 3b Plot of zircon saturation temperature (°C) versus age (Ma) for the Linzizong volcanic rocks (see Table S4 for data)

See captions of the Figures 2a and 2b in the text for detrails

*__Note:__ 1) Age data used for this table are from Table 1 and Yue and Ding (2006); 2) Major element contents are recalculated on an anhydrous basis. Zircon saturation temperatures were calculated from whole-rock compositions with SiO_2 > 56 wt.% following the method of Watson and Harrison (1983)

Di-Cheng Zhu*, Qing Wang, Zhi-Dan Zhao, Sun-Lin Chung, Peter A. Cawood, Yaoling Niu, Sheng-Ao Liu, Fu-Yuan Wu, and Xuan-Xue Mo

Table S5 SiO_2 contents of the 80-40 Ma intrusive rocks from the Gangdese Batholith (85–95°E) in southern Tibet

No.	Sample	Longitude	Latitude	Rock Type	Age (Ma)	SiO_2	References
1	06FW101	91.11	29.69	Monzogranite	64.7	72.29	Ji et al., 2012, Journal of Asian Earth Sciences 53, 82–95
2	06FW104	91.08	29.68	Monzogranite	64.4	71.71	Ji et al., 2012, Journal of Asian Earth Sciences 53, 82–95
3	06FW105	90.93	29.68	Monzogranite	55.2	67.62	Ji et al., 2012, Journal of Asian Earth Sciences 53, 82–95
4	06FW108	90.78	29.76	Granodiorite	56.8	62.25	Ji et al., 2012, Journal of Asian Earth Sciences 53, 82–95
5	06FW110	90.83	29.74	Monzogranite	54.3	73.45	Ji et al., 2012, Journal of Asian Earth Sciences 53, 82–95
6	06FW111	90.96	29.44	Monzogranite	50.6	66.49	Ji et al., 2012, Journal of Asian Earth Sciences 53, 82–95
7	06FW112	90.96	29.49	Granodiorite	53.4	60.23	Ji et al., 2012, Journal of Asian Earth Sciences 53, 82–95
8	06FW118	90.94	29.50	Monzogranite	51.0	73.27	Ji et al., 2012, Journal of Asian Earth Sciences 53, 82–95
9	06FW119	90.94	29.50	Granodiorite	51.2	63.91	Ji et al., 2012, Journal of Asian Earth Sciences 53, 82–95
10	06FW120	90.94	29.50	Dioritic enclave	50.3	51.94	Ji et al., 2012, Journal of Asian Earth Sciences 53, 82–95
11	06FW121	90.94	29.50	Graniticdike	51.1	75.29	Ji et al., 2012, Journal of Asian Earth Sciences 53, 82–95
12	06FW126	90.87	29.48	Granodiorite	55.3	56.62	Ji et al., 2012, Journal of Asian Earth Sciences 53, 82–95
13	06FW127	90.87	29.48	Graniticdike	49.5	77.16	Ji et al., 2012, Journal of Asian Earth Sciences 53, 82–95
14	06FW128	90.87	29.48	Doleriticdike	49.9	54.99	Ji et al., 2012, Journal of Asian Earth Sciences 53, 82–95
15	06FW129	90.90	29.46	Granodiorite	52.9	57.43	Ji et al., 2012, Journal of Asian Earth Sciences 53, 82–95
16	06FW131	90.91	29.41	Tonalitic gneiss	44.0	69.90	Ji et al., 2012, Journal of Asian Earth Sciences 53, 82–95
17	06FW133	90.87	29.33	Monzonite	47.1	67.45	Ji et al., 2012, Journal of Asian Earth Sciences 53, 82–95
18	06FW134	90.88	29.36	Monzogranite	41.9	70.57	Ji et al., 2012, Journal of Asian Earth Sciences 53, 82–95
19	06FW139	90.88	29.38	Monzonite	41.5	61.01	Ji et al., 2012, Journal of Asian Earth Sciences 53, 82–95
20	06FW140	90.72	29.47	Monzogranite	43.7	70.99	Ji et al., 2012, Journal of Asian Earth Sciences 53, 82–95
21	06FW146	90.72	29.40	Monzodiorite	56.9	52.88	Ji et al., 2012, Journal of Asian Earth Sciences 53, 82–95
22	06FW147	90.72	29.37	Granodiorite	51.5	61.42	Ji et al., 2012, Journal of Asian Earth Sciences 53, 82–95
23	06FW148	90.72	29.37	Syenogranitic dyke	51.3	71.69	Ji et al., 2012, Journal of Asian Earth Sciences 53, 82–95
24	06FW151	90.72	29.36	Diorite	55.5	56.09	Ji et al., 2012, Journal of Asian Earth Sciences 53, 82–95

25	06FW152-2	90.18	29.40	Diorite	57.3	53.49	Ji et al., 2012, Journal of Asian Earth Sciences 53, 82–95
26	06FW154	90.27	29.58	Syenogranite	51.3	75.43	Ji et al., 2012, Journal of Asian Earth Sciences 53, 82–95
27	06FW155	90.27	29.54	Monzodiorite	61.1	70.33	Ji et al., 2012, Journal of Asian Earth Sciences 53, 82–95
28	06FW156	90.27	29.50	Monzodiorite	55.4	67.99	Ji et al., 2012, Journal of Asian Earth Sciences 53, 82–95
29	06FW162	89.62	29.54	Granodiorite	48.2	60.29	Ji et al., 2012, Journal of Asian Earth Sciences 53, 82–95
30	06FW163	89.62	29.54	Monzogranite	50.9	71.58	Ji et al., 2012, Journal of Asian Earth Sciences 53, 82–95
31	06FW174	90.10	29.35	Diorite	50.2	56.45	Ji et al., 2012, Journal of Asian Earth Sciences 53, 82–95
32	06FW175	90.07	29.35	Diorite	52.6	57.57	Ji et al., 2012, Journal of Asian Earth Sciences 53, 82–95
33	06FW176	90.25	29.34	Diorite	53.6	54.48	Ji et al., 2012, Journal of Asian Earth Sciences 53, 82–95
34	08CQ01	85.74	29.63	Syenogranite	43.9	76.87	Wang and Zhu et al., 2014, To be submitted
35	08CQ02	85.74	29.63	Syenogranite	43.9	78.07	Zhu et al., 2011, Earth and Planetary Science Letters 301, 241–255
36	08CQ03	85.76	29.78	Monzogranite	51.9	67.92	Zhu et al., 2011, Earth and Planetary Science Letters 301, 241–255
37	08CQ09	85.74	29.90	Granodiorite porphyry	50.0	68.52	Zhu et al., 2011, Earth and Planetary Science Letters 301, 241–255
38	08CQ13	85.41	30.14	Diorite	51.5	54.04	Zhu et al., 2011, Earth and Planetary Science Letters 301, 241–255
39	08DX01	90.57	30.01	Diorite	69.8	55.57	Zhu et al., unpublished data
40	08FW50	91.18	29.64	Granodiorite	67.1	68.13	Ji, W.Q., 2010, Ph.D thesis, p. 1–146
41	08FW51	91.16	29.64	Granodiorite	64.5	66.35	Ji et al., 2012, Journal of Asian Earth Sciences 53, 82–95
42	08FW54	91.99	29.73	Diorite	65.6	54.83	Ji, W.Q., 2010, Ph.D thesis, p. 1–146
43	08FW56	92.20	29.71	Monzogranite	70.5	65.58	Ji, W.Q., 2010, Ph.D thesis, p. 1–146
44	08FW60	93.78	29.81	Monzogranite	47.6	77.24	Ji, W.Q., 2010, Ph.D thesis, p. 1–146
45	08FW61	94.01	29.76	Syenogranite	53.8	75.98	Ji, W.Q., 2010, Ph.D thesis, p. 1–146
46	08FW62	94.29	29.74	Monzogranite	72.7	74.05	Ji, W.Q., 2010, Ph.D thesis, p. 1–146
47	08FW63	94.19	29.75	Monzogranite	53.0	73.05	Ji, W.Q., 2010, Ph.D thesis, p. 1–146
48	08FW66	92.04	29.72	Syenogranite	70.1	76.03	Ji, W.Q., 2010, Ph.D thesis, p. 1–146
49	09FW08	93.31	29.62	Gabbro	66.0	47.34	Ji, W.Q., 2010, Ph.D thesis, p. 1–146
50	09FW09	93.31	29.62	Diorite	66.6	54.38	Ji, W.Q., 2010, Ph.D thesis, p. 1–146
51	09FW10	93.31	29.62	Gneissic granodiorite	66.2	65.52	Ji, W.Q., 2010, Ph.D thesis, p. 1–146
52	09FW30	93.20	29.15	Two-mica Monzogranite	76.7	72.25	Ji, W.Q., 2010, Ph.D thesis, p. 1–146
53	09FW33	93.18	29.12	Two-mica Monzogranite	79.7	72.76	Ji, W.Q., 2010, Ph.D thesis, p. 1–146
54	09FW41	92.74	29.42	Monzogranite	56.1	70.44	Ji et al., 2012, Journal of Asian Earth Sciences 53, 82–95

55	09FW42	92.75	29.41	Monzogranite	50.7	69.74	Ji et al., 2012, Journal of Asian Earth Sciences 53, 82–95
56	09FW43	92.75	29.41	Monzogranite	42.0	70.66	Ji et al., 2012, Journal of Asian Earth Sciences 53, 82–95
57	09FW50	92.70	29.24	Granodiorite	50.2	67.85	Ji et al., 2012, Journal of Asian Earth Sciences 53, 82–95
58	10CK-02	86.14	30.37	Granitic porphyry	65.2	68.00	Wang et al., 2012, Acta Petrologica Sinica, 28(5), 1647–1662
59	10CK-03	86.14	30.37	Granitic porphyry	65.2	76.89	Wang et al., 2012, Acta Petrologica Sinica, 28(5), 1647–1662
60	10CK-04	86.14	30.37	Granitic porphyry	65.2	75.49	Wang et al., 2012, Acta Petrologica Sinica, 28(5), 1647–1662
61	10CK-07	86.14	30.37	Granitic porphyry	64.4	75.66	Wang et al., 2012, Acta Petrologica Sinica, 28(5), 1647–1662
62	10CK-08	86.14	30.37	Granitic porphyry	64.4	76.18	Wang et al., 2012, Acta Petrologica Sinica, 28(5), 1647–1662
63	10CK-10	86.14	30.37	Granitic porphyry	64.4	75.98	Wang et al., 2012, Acta Petrologica Sinica, 28(5), 1647–1662
64	10CK-11	86.14	30.37	Granitic porphyry	64.4	77.01	Wang et al., 2012, Acta Petrologica Sinica, 28(5), 1647–1662
65	10CK-14	86.14	30.37	Granitic porphyry	64.4	68.86	Wang et al., 2012, Acta Petrologica Sinica, 28(5), 1647–1662
66	12DJC12-1	85.72	29.63	Syenogranite	42.6	69.79	Wang and Zhu et al., 2014, To be submitted
67	12DJC13-1	85.74	29.63	Syenogranite	42.6	68.66	Wang and Zhu et al., 2014, To be submitted
68	12DJC13-2	85.74	29.63	Syenogranite	42.7	71.49	Wang and Zhu et al., 2014, To be submitted
69	12DJC14-1	85.74	29.63	Syenogranite	43.6	71.59	Wang and Zhu et al., 2014, To be submitted
70	12DJC14-2	85.74	29.63	Monzogranite	43.6	71.62	Wang and Zhu et al., 2014, To be submitted
71	12DJC14-3	85.74	29.63	Syenogranite	43.6	75.59	Wang and Zhu et al., 2014, To be submitted
72	12DJC15-1	85.74	29.63	Monzogranite	43.6	76.85	Wang and Zhu et al., 2014, To be submitted
73	12DJC15-2	85.74	29.63	Syenogranite	43.6	70.08	Wang and Zhu et al., 2014, To be submitted
74	12DJC15-3	85.74	29.63	Syenogranite	43.6	74.72	Wang and Zhu et al., 2014, To be submitted
75	12DJC16-1	85.74	29.62	Syenogranite	43.6	77.01	Wang and Zhu et al., 2014, To be submitted
76	12DJC16-2	85.74	29.62	Monzogranite	43.6	77.25	Wang and Zhu et al., 2014, To be submitted
77	12DJC16-3	85.74	29.62	Monzogranite	43.9	76.33	Wang and Zhu et al., 2014, To be submitted
78	LS2	91.00	29.89	Granodiorite	51.0	69.59	Huang et al., 2010. Acta Petrologica Sinica 26, 10, 3131–3142
79	LS3	91.00	29.89	Dioritic enclave	61.0	54.14	Huang et al., 2010. Acta Petrologica Sinica 26, 10, 3131–3142
80	LS4	91.27	29.68	Dioritie	61.0	54.15	Huang et al., 2010. Acta Petrologica Sinica 26, 10, 3131–3142
81	LS5	91.24	29.69	Dioritie	61.0	56.09	Huang et al., 2010. Acta Petrologica Sinica 26, 10, 3131–3142
82	LZ09-2	94.47	29.55	Granitic gneiss	51.4	75.22	Ji, W.Q., 2010, Ph.D thesis, p. 1–146
83	LZ11-1	94.46	29.46	Gneissic granodiorite	44.3	73.11	Ji, W.Q., 2010, Ph.D thesis, p. 1–146
84	LZ13-1	94.38	29.64	Granodiorite	67.1	68.23	Ji, W.Q., 2010, Ph.D thesis, p. 1–146

85	LZ15-5	94.35	29.63	Dioritic enclave	64.0	55.22	Ji, W.Q., 2010, Ph.D thesis, p. 1–146
86	LZ16-2	94.37	29.60	Granodiorite	67.4	61.56	Ji, W.Q., 2010, Ph.D thesis, p. 1–146
87	LZ17-1	94.43	29.46	Two-mica monzogranite	51.7	73.23	Ji, W.Q., 2010, Ph.D thesis, p. 1–146
88	ML05-1	93.77	29.14	Monzogranite	78.4	70.93	Ji, W.Q., 2010, Ph.D thesis, p. 1–146
89	ML05-1	93.35	29.04	Granodiorite	79.3	67.17	Guan et al., 2010, Acta Petrologica Sinica 26, 2165–2179
90	ML06-1	93.37	29.05	Granodiorite	79.3	70.58	Zhu et al., 2011, Earth and Planetary Science Letters 301, 241–255
91	ML07-1	93.52	29.17	Granodiorite	73.5	69.88	Ji, W.Q., 2010, Ph.D thesis, p. 1–146
92	ML08-1	93.47	29.15	Monzogranite	73.0	74.08	Ji, W.Q., 2010, Ph.D thesis, p. 1–146
93	ML08-1	93.39	29.09	Monzogranite	79.3	70.67	Guan et al., 2010, Acta Petrologica Sinica 26, 2165–2179
94	ML09-1	93.38	29.06	Monzogranite	78.0	72.48	Ji, W.Q., 2010, Ph.D thesis, p. 1–146
95	ML11-1	93.12	29.11	Two-mica granite	75.0	72.15	Ji, W.Q., 2010, Ph.D thesis, p. 1–146
96	ML18-1	93.68	29.15	Gabbroic enclave	38.5	51.08	Guan et al., 2012, Gondwana Research 21, 88–99
97	ML18-10	93.68	29.15	Granodiorite	37.4	65.91	Guan et al., 2012, Gondwana Research 21, 88–99
98	ML18-2	93.68	29.15	Granodiorite	37.4	71.03	Guan et al., 2012, Gondwana Research 21, 88–99
99	ML18-3	93.68	29.15	Granodiorite	37.4	66.59	Guan et al., 2012, Gondwana Research 21, 88–99
100	ML18-4	93.68	29.15	Dioritic enclave	38.5	54.80	Guan et al., 2012, Gondwana Research 21, 88–99
101	ML18-5	93.68	29.15	Dioritic enclave	38.5	56.29	Guan et al., 2012, Gondwana Research 21, 88–99
102	ML18-6	93.68	29.15	Dioritic enclave	38.5	55.97	Guan et al., 2012, Gondwana Research 21, 88–99
103	ML18-7	93.68	29.15	Granodiorite	37.4	66.35	Guan et al., 2012, Gondwana Research 21, 88–99
104	ML18-8	93.68	29.15	Granodiorite	37.4	65.26	Guan et al., 2012, Gondwana Research 21, 88–99
105	ML18-9	93.68	29.15	Granodiorite	37.4	68.07	Guan et al., 2012, Gondwana Research 21, 88–99
106	ML19-1	93.75	29.13	Monzogranite	78.1	70.68	Guan et al., 2010, Acta Petrologica Sinica 26, 2165–2179
107	ML25-1	94.43	29.46	Monzogranite	56.7	76.11	Zhu et al., unpublished data
108	ML26-1	94.35	29.63	Granodiorite	64.8	66.17	Zhu et al., unpublished data
109	ML26-2	94.35	29.63	Monzogranite	64.8	73.82	Zhu et al., unpublished data
110	ML28-1	94.24	29.76	Monzogranite	54.5	70.23	Zhu et al., unpublished data
111	ML37-1	93.30	29.60	Monzogranite	70.1	70.96	Zhu et al., unpublished data
112	ML37-2	93.30	29.60	Dioritic enclave	69.8	55.62	Zhu et al., unpublished data
113	ML37-3	93.30	29.60	Dioritic enclave	70.1	55.79	Zhu et al., unpublished data
114	ML37-5	93.30	29.60	Gabbroic enclave	69.8	50.46	Zhu et al., unpublished data

115	ML38-2	93.30	29.60	Gabbroic enclave	69.5	48.23	Zhu et al., unpublished data
116	ML38-3	93.30	29.60	Gabbroic enclave	69.5	49.57	Zhu et al., unpublished data
117	ML38-6	93.30	29.60	Gabbroic enclave	69.5	47.97	Zhu et al., unpublished data
118	NML03-1	89.06	29.62	Diorite	62.4	58.03	Zhu et al., 2011, Earth and Planetary Science Letters 301, 241–255
119	RB10	89.69	29.36	Gabbro	45.0	50.84	Huang et al., 2010. Acta Petrologica Sinica 26, 10, 3131–3142
120	RB12	89.69	29.36	Diorite	45.0	54.73	Huang et al., 2010. Acta Petrologica Sinica 26, 10, 3131–3142
121	RB15	89.69	29.36	Gabbroic enclave	45.0	49.80	Huang et al., 2010. Acta Petrologica Sinica 26, 10, 3131–3142
122	SR01-1	92.10	29.29	Granodiorite	45.4	62.52	Ji et al., 2012, Journal of Asian Earth Sciences 53, 82–95
123	SR02-1	92.12	29.29	Granite	37.7	72.05	Ji et al., 2012, Journal of Asian Earth Sciences 53, 82–95
124	SR03-1	92.22	29.27	Granodiorite	59.8	71.48	Ji et al., 2012, Journal of Asian Earth Sciences 53, 82–95
125	SR04-1	92.24	29.32	Granodiorite	42.1	61.81	Ji et al., 2012, Journal of Asian Earth Sciences 53, 82–95
126	T024	93.75	29.14	Granodiorite	80.4	69.53	Wen et al., 2008, Lithos 105, 1–11
127	T026	93.44	29.12	Granodiorite	80.4	70.11	Wen et al., 2008, Lithos 105, 1–11
128	T10-113-8	94.44	29.55	Grt two-mica granite	63.3	72.21	Zhang et al., 2013, Journal of Petrology 54, 12, 2547–2580
129	T10-123-2	94.41	29.61	Two-mica granite	61.9	75.57	Zhang et al., 2013, Journal of Petrology 54, 12, 2547–2580
130	T10-72-2	94.79	29.96	Grt two-mica granodiorite	65.9	68.34	Zhang et al., 2013, Journal of Petrology 54, 12, 2547–2580
131	T215	93.41	29.10	Tonalite	80.4	68.28	Wen et al., 2008, Lithos 105, 1–11
132	T216A	93.61	29.17	Tonalite	80.4	67.89	Wen et al., 2008, Lithos 105, 1–11
133	T217	93.64	29.14	Tonalite	80.4	68.78	Wen et al., 2008, Lithos 105, 1–11
134	T218B	93.75	29.14	Tonalite	80.4	67.79	Wen et al., 2008, Lithos 105, 1–11
135	T300	90.95	29.54	Granodiorite	50.3	65.58	Xu, W.C., 2010. Ph.D thesis, China University of Geosciences (Wuhan), p. 1–172
136	T308	90.93	29.48	Granodiorite	50.7	64.95	Xu, W.C., 2010. Ph.D thesis, China University of Geosciences (Wuhan), p. 1–172
137	T315	90.87	29.38	Qtz diorite	40.5	59.77	Xu, W.C., 2010. Ph.D thesis, China University of Geosciences (Wuhan), p. 1–172
138	T316	90.87	29.38	Qtz diorite	47.1	61.49	Xu, W.C., 2010. Ph.D thesis, China University of Geosciences (Wuhan), p. 1–172
139	T318	90.87	29.38	Qtz diorite	47.1	60.91	Xu, W.C., 2010. Ph.D thesis, China University of Geosciences (Wuhan), p. 1–172
140	T319	90.73	29.35	Qtz diorite	47.1	63.72	Xu, W.C., 2010. Ph.D thesis, China University of Geosciences (Wuhan), p. 1–172
141	T364	90.27	29.51	Granodiorite	46.7	69.97	Xu, W.C., 2010. Ph.D thesis, China University of Geosciences (Wuhan), p. 1–172
142	T365	90.27	29.51	Granodiorite	46.7	66.80	Xu, W.C., 2010. Ph.D thesis, China University of Geosciences (Wuhan), p. 1–172
143	T366	90.27	29.51	Granodiorite	46.7	62.78	Xu, W.C., 2010. Ph.D thesis, China University of Geosciences (Wuhan), p. 1–172
144	T375	90.06	29.51	Qtz diorite	54.1	61.85	Xu, W.C., 2010. Ph.D thesis, China University of Geosciences (Wuhan), p. 1–172

145	T376	90.06	29.51	Granodiorite	54.1	66.31	Xu, W.C., 2010. Ph.D thesis, China University of Geosciences (Wuhan), p. 1–172
146	T377	90.06	29.51	Granodiorite	54.1	66.43	Xu, W.C., 2010. Ph.D thesis, China University of Geosciences (Wuhan), p. 1–172
147	T378	90.05	29.52	Granodiorite	54.1	67.46	Xu, W.C., 2010. Ph.D thesis, China University of Geosciences (Wuhan), p. 1–172
148	T390	90.12	29.35	Qtz diorite	48.5	61.02	Xu, W.C., 2010. Ph.D thesis, China University of Geosciences (Wuhan), p. 1–172
149	T391	90.02	29.34	Diorite	48.5	54.18	Xu, W.C., 2010. Ph.D thesis, China University of Geosciences (Wuhan), p. 1–172
150	T392	88.37	29.95	Monzogranite	47.9	70.66	Xu, W.C., 2010. Ph.D thesis, China University of Geosciences (Wuhan), p. 1–172
151	T393	88.37	29.95	Monzogranite	47.9	70.32	Xu, W.C., 2010. Ph.D thesis, China University of Geosciences (Wuhan), p. 1–172
152	T395	88.37	29.95	Monzogranite	47.9	71.35	Xu, W.C., 2010. Ph.D thesis, China University of Geosciences (Wuhan), p. 1–172
153	T396	88.39	29.87	Monzogranite	47.9	76.28	Xu, W.C., 2010. Ph.D thesis, China University of Geosciences (Wuhan), p. 1–172
154	T398	88.39	29.83	Monzogranite	47.9	75.32	Xu, W.C., 2010. Ph.D thesis, China University of Geosciences (Wuhan), p. 1–172
155	T405	88.32	29.56	Monzogranite	49.0	68.88	Xu, W.C., 2010. Ph.D thesis, China University of Geosciences (Wuhan), p. 1–172
156	T406	88.32	29.56	Monzogranite	49.0	66.31	Xu, W.C., 2010. Ph.D thesis, China University of Geosciences (Wuhan), p. 1–172
157	T410	88.32	29.51	Monzogranite	49.0	66.86	Xu, W.C., 2010. Ph.D thesis, China University of Geosciences (Wuhan), p. 1–172
158	T411	88.32	29.48	Monzogranite	49.0	69.13	Xu, W.C., 2010. Ph.D thesis, China University of Geosciences (Wuhan), p. 1–172
159	T420	87.45	29.38	Granodiorite	48.1	63.24	Xu, W.C., 2010. Ph.D thesis, China University of Geosciences (Wuhan), p. 1–172
160	T426	86.21	29.6	Monzogranite	50.5	67.72	Xu, W.C., 2010. Ph.D thesis, China University of Geosciences (Wuhan), p. 1–172
161	T427	86.21	29.58	Monzogranite	50.5	69.93	Xu, W.C., 2010. Ph.D thesis, China University of Geosciences (Wuhan), p. 1–172
162	T430	86.21	29.58	Monzogranite	48.2	68.12	Xu, W.C., 2010. Ph.D thesis, China University of Geosciences (Wuhan), p. 1–172
163	T432	86.22	29.57	Monzogranite	48.2	70.32	Xu, W.C., 2010. Ph.D thesis, China University of Geosciences (Wuhan), p. 1–172
164	T439	89.10	29.46	Granodiorite	49.4	65.92	Xu, W.C., 2010. Ph.D thesis, China University of Geosciences (Wuhan), p. 1–172
165	T440	89.10	29.47	Qtz diorite	49.4	60.28	Xu, W.C., 2010. Ph.D thesis, China University of Geosciences (Wuhan), p. 1–172
166	T442	89.09	29.53	Qtz diorite	49.4	61.65	Xu, W.C., 2010. Ph.D thesis, China University of Geosciences (Wuhan), p. 1–172
167	T443	89.08	29.55	Qtz diorite	49.4	61.10	Xu, W.C., 2010. Ph.D thesis, China University of Geosciences (Wuhan), p. 1–172
168	T445	89.06	29.62	Monzogranite	40.7	74.36	Xu, W.C., 2010. Ph.D thesis, China University of Geosciences (Wuhan), p. 1–172
169	T446	89.06	29.63	Granodiorite	50.9	64.67	Xu, W.C., 2010. Ph.D thesis, China University of Geosciences (Wuhan), p. 1–172
170	T447	89.06	29.63	Granodiorite	50.9	64.88	Xu, W.C., 2010. Ph.D thesis, China University of Geosciences (Wuhan), p. 1–172
171	T477	90.93	29.67	Granodiorite	49.9	68.54	Xu, W.C., 2010. Ph.D thesis, China University of Geosciences (Wuhan), p. 1–172
172	T478	90.93	29.67	Monzogranite	46.4	67.58	Xu, W.C., 2010. Ph.D thesis, China University of Geosciences (Wuhan), p. 1–172
173	T479	90.60	30.04	Monzogranite	49.6	71.22	Xu, W.C., 2010. Ph.D thesis, China University of Geosciences (Wuhan), p. 1–172
174	T490	91.98	29.73	Monzogranite	65.3	71.45	Xu, W.C., 2010. Ph.D thesis, China University of Geosciences (Wuhan), p. 1–172

175	T491	92.02	29.72	Monzogranite	65.3	72.81	Xu, W.C., 2010. Ph.D thesis, China University of Geosciences (Wuhan), p. 1–172
176	T493	92.02	29.72	Monzogranite	65.3	73.13	Xu, W.C., 2010. Ph.D thesis, China University of Geosciences (Wuhan), p. 1–172
177	T497	92.15	29.71	Granodiorite	67.7	64.12	Xu, W.C., 2010. Ph.D thesis, China University of Geosciences (Wuhan), p. 1–172
178	T498	92.15	29.71	Granodiorite	67.7	64.12	Xu, W.C., 2010. Ph.D thesis, China University of Geosciences (Wuhan), p. 1–172
179	T500	92.15	29.71	Granodiorite	67.7	69.31	Xu, W.C., 2010. Ph.D thesis, China University of Geosciences (Wuhan), p. 1–172
180	T529	94.43	29.45	Granitic gneiss	49.1	73.93	Xu, W.C., 2010. Ph.D thesis, China University of Geosciences (Wuhan), p. 1–172
181	T554	92.20	29.30	Monzogranite	59.7	68.71	Xu, W.C., 2010. Ph.D thesis, China University of Geosciences (Wuhan), p. 1–172
182	T555	92.20	29.30	Monzogranite	59.7	70.02	Xu, W.C., 2010. Ph.D thesis, China University of Geosciences (Wuhan), p. 1–172
183	T556	92.20	29.30	Monzogranite	59.7	69.71	Xu, W.C., 2010. Ph.D thesis, China University of Geosciences (Wuhan), p. 1–172
184	T557	92.20	29.30	Monzogranite	59.7	67.69	Xu, W.C., 2010. Ph.D thesis, China University of Geosciences (Wuhan), p. 1–172
185	T560	93.18	29.26	Fine-grained granite	60.9	70.00	Xu, W.C., 2010. Ph.D thesis, China University of Geosciences (Wuhan), p. 1–172
186	T562	93.18	29.26	Fine-grained granite	60.9	70.05	Xu, W.C., 2010. Ph.D thesis, China University of Geosciences (Wuhan), p. 1–172
187	T672	94.47	29.55	Leucosome	50.3	79.89	Guo et al., 2011, Lithos 127, 54–67
188	T8-15-2	94.01	29.30	Ep granodiorite	63.0	70.46	Zhang et al., 2013, Journal of Petrology 54, 12, 2547–2580
189	T9-30-2	94.35	29.63	Ep granodiorite	63.2	64.41	Zhang et al., 2013, Journal of Petrology 54, 12, 2547–2580
190	T9-33-5	94.44	29.55	Ep granodiorite	64.8	68.42	Zhang et al., 2013, Journal of Petrology 54, 12, 2547–2580
191	T9-33-7	94.44	29.55	Grt two-mica granodiorite	54.9	69.31	Zhang et al., 2013, Journal of Petrology 54, 12, 2547–2580
192	11LS01-1	90.94	29.50	Gabbro	47.3	50.13	Zhu et al., unpublished data
193	11LS06-1	90.71	29.36	Gabbroic diorite	46.2	54.35	Zhu et al., unpublished data
194	11NM01-1	90.27	29.34	Gabbro	46.5	46.90	Zhu et al., unpublished data
195	12AM03-1	86.31	29.64	Granodiorite	53.1	66.45	Zhu et al., unpublished data
196	12AM04-2	86.32	29.63	Gabbro	44.8	52.03	Zhu et al., unpublished data
197	12AM06-2	86.32	29.58	Monzogranite	51.2	73.02	Zhu et al., unpublished data
198	12CZ15-1	86.75	29.75	Monzogranite	60.8	79.14	Zhu et al., unpublished data
199	12DJ01-1	87.71	29.42	Granodiorite	55.1	71.99	Zhu et al., unpublished data
200	12DJ04-1	87.73	29.42	Monzogranite	44.4	74.42	Zhu et al., unpublished data
201	12DJ08-1	87.79	29.44	Granodiorite	51.8	66.09	Zhu et al., unpublished data
202	12DJ11-1	87.87	29.43	Monzogranite	44.5	71.28	Zhu et al., unpublished data
203	12DJ12-1	87.87	29.43	Granodiorite	44.3	66.72	Zhu et al., unpublished data
204	12DJ13-2	87.88	29.43	Gabbro	50.9	50.73	Zhu et al., unpublished data

205	12DJ15-1	87.90	29.43	Granodiorite	51.9	66.54	Zhu et al., unpublished data
206	12DJ17-1	87.99	29.39	Granodiorite	52.1	65.23	Zhu et al., unpublished data
207	12DJC09-3	85.79	29.78	Granodiorite	51.5	67.07	Zhu et al., unpublished data
208	12LY00-1	89.24	29.72	Monzogranite	51.0	77.02	Zhu et al., unpublished data
209	12LY01-1	89.24	29.76	Granodiorite	50.4	67.98	Zhu et al., unpublished data
210	12PC02-2	87.97	29.56	Gabbro	55.0	49.26	Zhu et al., unpublished data
211	12PC12-1	87.99	29.38	Diorite	51.8	56.49	Zhu et al., unpublished data
212	12PC12-2	87.99	29.38	Diorite	51.1	58.60	Zhu et al., unpublished data
213	ST104A	91.81	29.27	Granodiorite	60.1	65.58	Chu et al., 2006, Geology 34, 745–748
214	PIII-17	90.57	29.57		46.1	70.29	Ma et al., 2014, Lithos 196–197, 321–338
215	D0175	90.57	29.57		46.1	73.87	Ma et al., 2014, Lithos 196–197, 321–338
216	PIII-03	90.55	29.52		48.2	72.40	Ma et al., 2014, Lithos 196–197, 321–338
217	PIII-04	90.55	29.52		48.2	70.69	Ma et al., 2014, Lithos 196–197, 321–338
218	PIII-05	90.55	29.52		48.2	71.26	Ma et al., 2014, Lithos 196–197, 321–338
219	PIII-06	90.55	29.52		48.2	71.80	Ma et al., 2014, Lithos 196–197, 321–338
220	PIII-07	90.55	29.52		48.2	72.32	Ma et al., 2014, Lithos 196–197, 321–338
221	PIII-08	90.55	29.52		48.2	69.95	Ma et al., 2014, Lithos 196–197, 321–338
222	PIII-16	90.55	29.52		48.2	68.58	Ma et al., 2014, Lithos 196–197, 321–338
223	D0182	90.55	29.52		48.2	66.37	Ma et al., 2014, Lithos 196–197, 321–338
224	PIII-01	90.60	29.58		48.6	75.95	Ma et al., 2014, Lithos 196–197, 321–338
225	PIII-02	90.60	29.58		48.6	74.51	Ma et al., 2014, Lithos 196–197, 321–338
226		91.81	29.33	Quartz diorite (northern)	56.3	64.55	Chen et al., 2015, Lithos 212–215, 379–396
227		91.81	29.33	Quartz diorite (northern)	56.3	64.09	Chen et al., 2015, Lithos 212–215, 379–396
228		91.80	29.30	Monzogranite	52.4	66.01	Chen et al., 2015, Lithos 212–215, 379–396

Magmatic record of India-Asia collision

Di-Cheng Zhu*, Qing Wang, Zhi-Dan Zhao, Sun-Lin Chung, Peter A. Cawood, Yaoling Niu, Sheng-Ao Liu, Fu-Yuan Wu, and Xuan-Xue Mo

Table S6: Calculation for the timing of collision

The timing of collision is calculated using the following equation similar to the ideas of Leech et al. (2005) and Donaldson et al. (2013), giving the timing as a function of depth of slab breakoff, age of slab breakoff, convergence rate, and slab dip.

$$\textbf{Timing of Collision} = \frac{\text{Depth of Slab Breakoff}}{(\text{Convergence Rate} \times \text{Sin}(\text{Slab Dip}))} + \textbf{Age of Slab Breakoff}$$

where, (1) the depth of slab breakoff is assumed to be occurred at 110, 120, 130, 140, and 150 km, given that the exhumed ultrahigh-pressure rocks at ca. 46 Ma (100 km in depth) may not represent the materials from the leading edge of subducted Indian continental margin, (2) the age of slab breakoff is the favored age in this study (ca. 53 Ma), (3) the convergence rates used here are changed from 170 to 150 mm/yr between 67 Ma and 51 Ma (van Hinsbergen et al., 2011), and (4) the slab dip is assumed to be changed from 30°, 45°, and 60° assuming that it increases with depth.

Calculated results indicate that the initial India-Asia collision **was just 1–2 Ma** before the slab breakoff, corresponding to a collision age of ca. 55 Ma.

Table S6 Calculation for the timing of collision

Depth of crust subducted	Convergence rate	Slab dip	Timing of slab breakoff	Initial collision age
100	90	30	53	**55.2**
110	150	30	53	**54.5**
110	160	45	53	**54.0**
110	170	60	53	**53.7**
120	150	30	53	**54.6**
120	160	45	53	**54.1**
120	170	60	53	**53.8**
130	150	30	53	**54.7**

130	160	45	53	**54.1**
130	170	60	53	**53.9**
140	150	30	53	**54.9**
140	160	45	53	**54.2**
140	170	60	53	**54.0**
150	150	30	53	**55.0**
150	160	45	53	**54.3**
150	170	60	53	**54.0**

References:

Donaldson, D.G., Webb. A.A.G., Menold. C.A., Kylander-Clark, A.R.C., Hacker, B.R., 2013. Petrochronology of Himalayan ultrahigh-pressure eclogite. Geology 41, 835–838.

Leech, M.L., Singh, S., Jain, A.K., Klemperer, S.L., Manichavasgam, R.M., 2005. The onset of India-Asia continental collision: Early, steep subduction required by the timing of UHP metamorphism in the western Himalaya. Earth and Planetary Science Letters 234, 83–97.

van Hinsbergen, D.J.J., Steinberger, B., Doubrovine, P., Gassmöller, R., 2011. Acceleration and deceleration of India-Asia convergence since the Cretaceous: Roles of mantle plumes and continental collision. Journal of Geophysical Research 116, B06101, doi: 10.1029/2010JB008051.#

3. References Cited in Tables S3, S4, and S5

Booth, A.L., Zeitler, P.K., Kidd, W.S.F., Wooden, J., Liu, Y.P., Idleman, B., Hren, M., Chamberlain, C.P., 2004. U-Pb zircon constraints on the tectonic evolution of Southeastern Tibet, Namche Barwa area. American Journal of Science 304, 889–929.

Chen, L., Qin, K.Z., Li, G.M., Li, J.X., Xiao, B., Zhao, J.X., Fan, X., 2014. Zircon U–Pb ages, geochemistry and Sr-Nd-Pb-Hf isotopes of Nuri intrusive rocks in Gangdese area, southern Tibet: Constraints on timing, petrogenesis and tectonic transformation. Lithos 212–215, 379–396.

Chen, W., Ma, C.Q., Bian, Q.J., Zhou, R.J., Long, T.C., Yu, S.L., Chen, D.M., Tu, J.H., 2010. Subduction-related late Cretaceous granitoids in Demingding area, east of middle Gangdese, Tibet: Evidences from zircon U-Pb geochronology and geochemistry. Journal of Mineral and Petrology 30, 83–92.

Chu, M.F., Chung, S.L., O'Reilly, S.Y., Pearson, N.J., Wu, F.Y., Li, X.H., Liu, D.Y., Ji, J.Q., Chu, C.H., Lee, H.Y., 2011. India's hidden inputs to Tibetan orogeny revealed by Hf isotopes of Transhimalayan zircons and host rocks. Earth and Planetary Science Letters 307, 479–486.

Chu, M.F., Chung, S.L., Song, B., Liu, D.Y., O'Reilly, S.Y., Pearson, N.J., Ji, J.Q., Wen, D.J., 2006. Zircon U-Pb and Hf isotope constraints on the Mesozoic tectonics and crustal evolution of southern Tibet. Geology 34, 745–748.

Cong, Y., Xiao, K.Y., Zhai, Q.G., Dong, Q.J., 2012. LA-ICP-MS dating and Hf isotopic analysis of zircon from the Puluogang granite in Namulin County, Tibet, and its geological significance. Journal of Jilin University 42, 1783–1795.

Guan, Q., Zhu, D.C., Zhao, Z.D., Dong, G.C., Mo, X.X., Liu, Y.S., Hu, Z.C., Yuan, H.L., 2011. Zircon U-Pb chronology, geochemistry of the Late Cretaceous mafic magmatism in the southern Lhasa terrane and its implications. Acta Petrologica Sinica 27, 2083–2094 (in Chinese with English abstract).

Guan, Q., Zhu, D.C., Zhao, Z.D., Dong, G.C., Zhang, L.L., Li, X.W., Liu, M., Liu, M.H., Mo, X.X., Liu, Y.S., Yuan, H.L., 2012. Crustal thickening prior to 38 Ma in southern Tibet: evidence from lower crust-derived adakitic magmatism in the Gangdese Batholith. Gondwana Research 21, 88–99.

Guan, Q., Zhu, D.C., Zhao, Z.D., Zhang, L.L., Liu, M., Li, X.W., Yu, F., Mo, X.X., 2010. Late Cretaceous adakites in the eastern segment of the Gangdese Belt, southern Tibet: Products

of Neo-Tethyan ridge subduction? Acta Petrologica Sinica 26, 2165–2179 (in Chinese with English abstract).

Guo, L., 2012. The tectono-magma events in the western margin of the eastern Himalayan syntaxis and their geodynamic implications. Ph.D thesis, China University of Geosciences (Wuhan), p. 1–139.

Guo, L., Zhang, H.F., Harris, N., Pan, F.B., Xu, W.C., 2011. Origin and evolution of multi-stage felsic melts in eastern Gangdese belt: Constraints from U-Pb zircon dating and Hf isotopic composition. Lithos 127, 54–67.

Huang, Y., Zhao, Z.D., Zhang, F.Q., Zhu, D.C., Dong, G.C., Mo, X.X., 2010. Geochemistry and implication of the Gangdese batholiths from Renbu and Lhasa areas in southern Gangdese, Tibet. Acta Petrologica Sinica 26, 3131–3142 (in Chinese with English abstract).

Ji, W. Q., Wu, F. Y., Liu, C. Z., Chung, S. L., 2012. Early Eocene crustal thickening in southern Tibet: New age and geochemical constraints from the Gangdese batholith. Journal of Asian Earth Sciences 53, 82–95.

Ji, W.Q., 2010. Geochronology and petrogenesis of granitic rocks from east segment of the Gangdese Batholith, southern Tibet. Ph.D thesis, Chinese Academy of Sciences, p. 1–146.

Ji, W.Q., Wu, F.Y., Chung, S.L., Li, J.X., Liu, C.Z., 2009. Zircon U-Pb chronology and Hf isotopic constraints on the petrogenesis of Gangdese batholiths, southern Tibet. Chemical Geology 262, 229–245.

Jia, L.L., Wang, Q., Zhu, D.C., Chen, Y., Wu, X.Y., Liu, S.A., Zheng, J.P., Zhao, T.P., 2013. Rethinking the geodynamical implications of the basic rocks from Linzhou basin, Tibet. Acta Petrologica Sinica 29, 3671–3680 (in Chinese with English abstract).

Jiang, Z.Q., Wang, Q., Li, Z.X., Wyman, D.A., Tang, G.J., Jia, X.H., Yang, Y.H., 2012. Late Cretaceous (ca. 90 Ma) adakitic intrusive rocks in the Kelu area, Gangdese belt (southern Tibet): Slab melting and implications for Cu–Au mineralization. Journal of Asian Earth Sciences 53, 67–81.

Lee, H.Y., Chung, S.L., Ji, J.Q., Qian, Q., Gallet, S., Lo, C.H., Lee, T.Y., Zhang, Q., 2012. Geochemical and Sr-Nd isotopic constraints on the genesis of the Cenozoic Linzizong volcanic successions, southern Tibet. Journal of Asian Earth Sciences 53, 96–114.

Liu, Y.F., Yang, Z.M., Xie, Y.L., Zhou, P., Du, D.H., Li, Y.X., Li, Q.Y., Qu, H.C., Xu, B., 2012. Zircon SHRIMP U-Pb age and geochemistry of intrusive rocks from Nongruri gold deposit, Gangdese, Tibet. Mineral Deposits 31, 727–744 (in Chinese with English abstract).

Luo, M.C., Wang, L.Q., Leng, Q.F., Chen, W., 2011. Zircon Hf isotope and Ce^{4+}/Ce^{3+} ratio of the monzogranite porphyry and biotite monzonitic granite in Bangpu Mo(Cu) deposit, Tibet. Mineral Deposits 30, 266–278 (in Chinese with English abstract).

Ma, L., Wang, B.D., Jiang, Z.Q., Wang, Q., Li, Z.X., Wyman, D.A., Zhao, S.R., Yang, J.H., Gou, G.N., Guo, H.F., 2014. Petrogenesis of the Early Eocene adakitic rocks in the Napuri area, southern Lhasa: Partial melting of thickened lower crust during slab break-off and implications for crustal thickening in southern Tibet. Lithos 196–197, 321–338.

Ma, L., Wang, Q., Li, Z.X., Wyman, D.A., Jiang. Z.Q., Yang. J.H., Gou, G.N., Guo, H.F., 2013. Early Late Cretaceous (ca. 93 Ma) norites and hornblendites in the Milin area, eastern Gangdese: Lithosphere–asthenosphere interaction during slab roll-back and an insight into early Late Cretaceous (ca. 100–80 Ma) magmatic "flare-up" in southern Lhasa (Tibet). Lithos 172–173, 17–30.

Ma, L., Wang, Q., Wyman, D.A., Jiang, Z.Q., Yang, J.H., Li, Q.L., Gou, G.N., Guo, H.F., 2013. Late Cretaceous crustal growth in the Gangdese area, southern Tibet: Petrological and Sr–Nd–Hf–O isotopic evidence from Zhengga diorite–gabbro. Chemical Geology 349–350, 54–70.

Ma, L., Wang, Q., Wyman, D.A., Li, Z.X., Jiang, Z.Q., Yang, J.H., Gou, G.N., Guo, H.F., 2013. Late Cretaceous (100–89 Ma) magnesian charnockites with adakitic affinities in the Milin area, eastern Gangdese: Partial melting of subducted oceanic crust and implications for crustal growth in southern Tibet. Lithos 175–176, 315–332.

Mo, X.X., Niu, Y.L., Dong, G.C., Zhao, Z.D., Hou, Z.Q., Zhou, S., Ke, S., 2008. Contribution of syncollisional felsic magmatism to continental crust growth: A case study of the Paleocene Linzizong Volcanic Succession in southern Tibet. Chemical Geology 250, 49–67.

Quidelleur, X., Grove, M., Lovera, O.M., Harrison, T.M., Yin, A., Ryerson, F.J., 1997. Thermal evolution and slip history of the Renbu Zedong Thrust, southeastern Tibet. Journal of Geophysical Research 102(B2): 2659–2679.

Wang, B.D., Wang, L.Q., Li, B., Huang, H.X., Chen, F.Q., Duan, Z.M., Zeng, Q.G., 2012. Geochronology and petrogenesis of the ore-bearing pluton in Chagele deposit in middle of the Gangdese metallogenic belt. Acta Petrologica Sinica 28, 1647–1662.

Wang, L., Zeng, L.S., Gao, L.E., Chen, Z.Y.m 2013. Early Cretaceous high Mg# and high Sr/Y clinopyroxene-bearing diorite in the southeast Gangdese batholith, southern Tibet. Acta Petrologica Sinica 29, 1977–1994.

Watson, E.B., Harrison, T.M., 1983. Zircon saturation revisited: temperature and composition effects in a variety of crustal magma types. Earth and Planetary Science Letters 64, 295–304.

Wen, D.R., Chung, S.L., Song, B., Iizuka, Y., Yang, H.J., Ji, J., Liu, D., Gallet, S., 2008b. Late Cretaceous Gangdese intrusions of adakitic geochemical characteristics, SE Tibet: Petrogenesis and tectonic implications. Lithos 105, 1–11.

Wen, D.R., Liu, D.Y., Chung, S.L., Chu, M.F., Ji, J.Q., Zhang, Q., Song, B., Lee, T.Y., Yeh, M.W., Lo, C.H., 2008. Zircon SHRIMP U–Pb ages of the Gangdese batholith and implications for Neotethyan subduction in southern Tibet. Chemical Geology 252, 191–201.

Wen, D.W., 2007. The Gangdese Batholith, southern Tibet: Ages, geochemical characteristics and petrogenesis. Ph.D thesis, National Taiwan University, p. 1–120.

Xu, W.C., 2010. Spatial variation of zircon U-Pb ages and Hf isotopic compositions of the Gangdese granitoids and its geologic implications. Ph.D thesis, China University of Geosciences (Wuhan), p. 1–172.

Yue, Y.H., Ding, L., 2006. $^{40}Ar/^{39}Ar$ Geochronology, geochemical characteristics and genesis of the Linzhou basic dikes, Tibet. Acta Petrologica Sinica, 22(4): 855–866 (in Chinese with English abstract).

Zhang, Z.M., Dong, X., Xiang, H., He, Z.Y., Liou, J.G., 2014. Metagabbros of the Gangdese arc root, south Tibet: Implications for the growth of continental crust. Geochimica et Cosmochimica Acta, doi: 10.1016/j.gca.2014.01.045.

Zhang, Z.M., Dong, X., Xiang, H., Liou, J.G., Santosh, M., 2013. Building of the Deep Gangdese Arc, South Tibet: Paleocene Plutonism and Granulite-Facies Metamorphism. Journal of Petrology 54, 2547–2580.

Zhang, Z.M., Zhao, G.C., Santosh, M., Wang, J.L., Dong, X., Shen, K., 2010. Late Cretaceous charnockite with adakitic affinities from the Gangdese batholith, southeastern Tibet: Evidence for Neo-Tethyan mid-ocean ridge subduction? Gondwana Research 17, 615–631.

Zhu, D.C., Zhao, Z.D., Niu, Y.L., Dilek, Y., Hou, Z.Q., Mo, X.X., 2013. The origin and pre-Cenozoic evolution of the Tibetan Plateau. Gondwana Research 23, 1429–1454.

Zhu, D.C., Zhao, Z.D., Niu, Y.L., Mo, X.X., Chung, S.L., Hou, Z.Q., Wang, L.Q., Wu, F.Y., 2011. The Lhasa Terrane: Record of a microcontinent and its histories of drift and growth. Earth and Planetary Science Letters 301, 241–255.

#